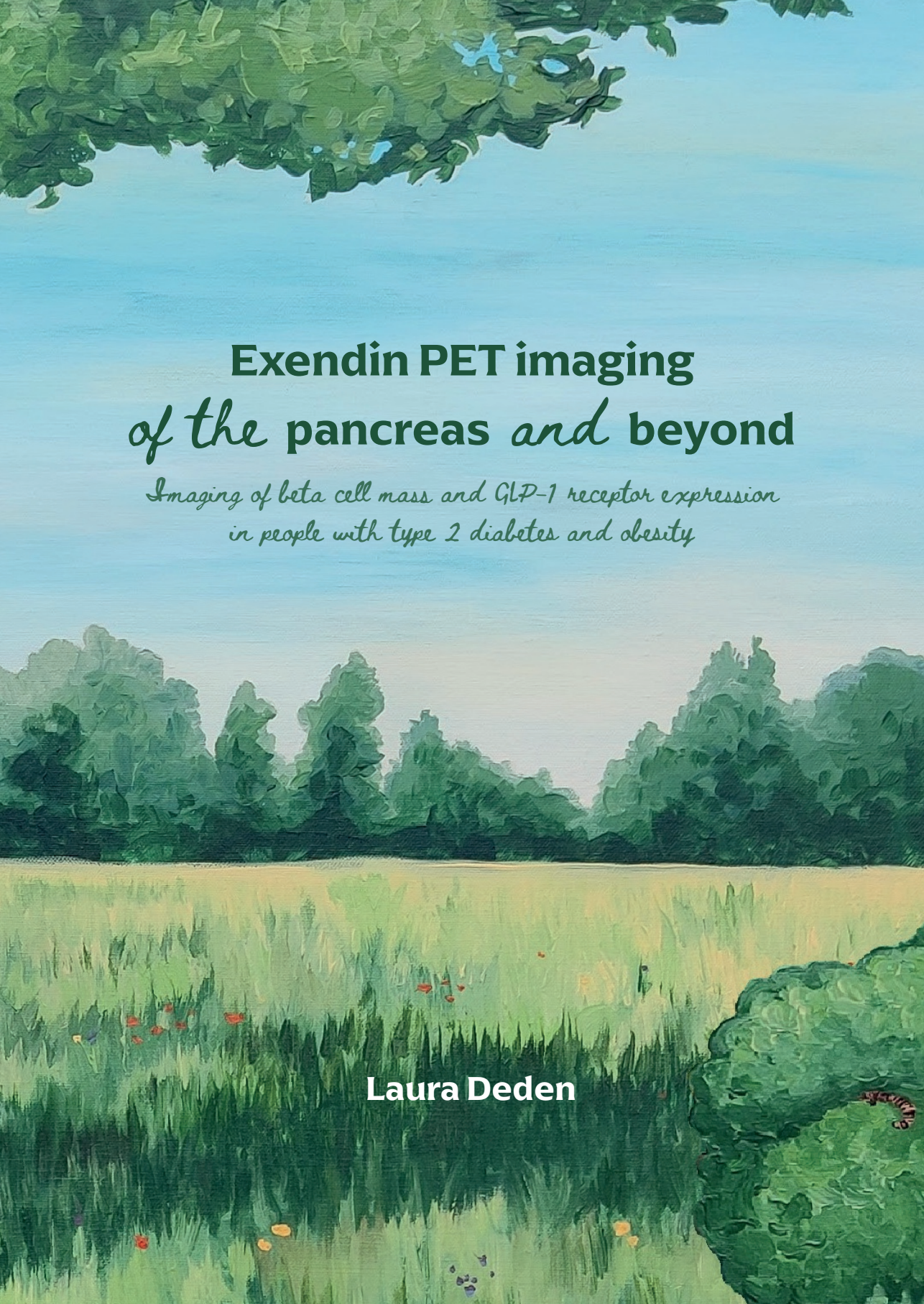


Exendin PET imaging *of the* pancreas *and* beyond

Imaging of beta cell mass and GLP-1 receptor expression in people with type 2 diabetes and obesity

Laura Deden

Exendin PET imaging of the pancreas and beyond

Imaging of beta cell mass and GLP-1 receptor expression
in people with type 2 diabetes and obesity

Laura Deden

COLOFON

The research presented in this thesis was carried out at the Radboud University Medical Center, Department of Medical Imaging, Nuclear Medicine and at Vitalys, part of Rijnstate.

The studies were financially supported by:
- Radboud University Medical Center
- Vitalys, part of Rijnstate

Printing of this thesis was financially supported by the Radboud University Nijmegen, Vitalys, Netherlands Association for the Study of Obesity (NASO) and Rijnstate Vriendenfonds.

ISBN: 978-94-6534-544-4
Cover design: Stephanie Maduro | SoliMondi.nl
Layout: Stephanie Maduro en ProefschriftMaken
Print: ProefschriftMaken | www.proefschriftmaken.nl

Copyright © Laura Deden, 2026
All rights are reserved. No part of this book may be reproduced, distributed, stored in a retrieval system, or transmitted in any form or by any means, without prior permission of the author of from the publisher holding the copyright of the published articles.

Exendin PET imaging of the pancreas and beyond

Imaging of beta cell mass and GLP-1 receptor expression
in people with type 2 diabetes and obesity

Proefschrift ter verkrijging van de graad van doctor
aan de Radboud Universiteit Nijmegen
op gezag van de rector magnificus prof. dr. J.M. Sanders,
volgens besluit van het college voor promoties
in het openbaar te verdedigen op

donderdag 22 oktober 2026
om 12.30 uur precies

door

Laura Naomi Deden
geboren op 27 januari 1989
te Hilversum

Promotoren

Prof. dr. M. Gotthardt
Prof. dr. E.J. Hazebroek (Wageningen University and Research)

Copromotor

Dr. M. Boss

Manuscriptcommissie

Prof. dr. M.T.E. Hopman
Prof. dr. R. Boellaard (Vrije Universiteit Amsterdam)
Dr. M.M. Smits

Paranimfen

Daphne Lobeek
Adrianne Hofboer

TABLE OF CONTENTS

Chapter 1	Thesis outline and general background	7
Chapter 2	Does Roux-en-Y gastric bypass surgery influence beta cell mass in people with Type 2 Diabetes? A clinical study using ^{68}Ga-exendin-4 PET/CT	21
Chapter 3	A 3D printed anatomical pancreas and kidney phantom for optimizing SPECT/CT reconstruction settings in beta cell imaging using ^{111}In-exendin	45
Chapter 4	Assessing scatter-based artefacts caused by high organ uptake in ^{68}Ga-exendin PET/CT using a 3D-printed phantom	65
Chapter 5	Quantification of organ-specific GLP-1 receptor expression in the pancreas and beyond by ^{68}Ga-exendin PET/CT imaging in humans with metabolic disease	85
Chapter 6	Brain Imaging of the GLP-1 Receptor in Obesity Using ^{68}Ga-NODAGA-exendin-4 PET	109
Chapter 7	General discussion and future perspectives	125
Appendices	English summary	141
	Nederlandse samenvatting	145
	Research data management	148
	Dankwoord	150
	PhD portfolio	154
	List of publications	156
	Curriculum Vitae	160



1

Introduction

THESIS OUTLINE

Glucagon-like peptide-1 (GLP-1) receptor imaging using radiolabeled Exendin-4 has been developed for non-invasive visualization of beta cells and assessment of beta cell mass *in vivo*. The first Exendin-based radiotracer that was used in humans was [^{111}In]In-Lys40(Ahx-DTPA)]exendin-4 (^{111}In-Ex4). Currently, PET radiotracers, such as [^{68}Ga]Ga-NODAGA-Exendin-4 (^{68}Ga-Ex4) are preferred for beta cell imaging. Until now, the value of GLP-1 receptor imaging has prominently been demonstrated in detecting insulinomas and studying beta cell mass in type 1 diabetes. This thesis covers the application of ^{68}Ga-Ex4 PET/CT for studying beta cell mass in type 2 diabetes (T2D) and for assessing extra-pancreatic GLP-1 receptor expression non-invasively in humans. In addition, certain challenges in image interpretation of this relative new radiotracer are addressed.

Chapter 1 is a general introduction on the central topics of this thesis, including T2D and obesity, the hormone GLP-1 and GLP-1 receptor agonists, and GLP-1 receptor imaging using radiolabeled Exendin-4.

Chapters 2 to 4 of this thesis cover beta cell imaging in T2D and obesity, including a clinical study and phantom studies. Besides decreased insulin sensitivity and a (relative) beta cell dysfunction as important underlying factors of T2D, T2D has been associated with a decline in beta cell mass. At the onset of T2D, beta cell mass is already decreased and it gradually declines further with disease progression. Interestingly, restoration of beta cell mass has been hypothesized in T2D remission after gastric bypass surgery. However, human data on beta cell mass in people with T2D is limited and, as a consequence, our understanding of the role of beta cell mass, beta cell mass loss, and beta cell restoration in T2D is incomplete.

In **chapter 2,** a pilot study on beta cell imaging in people with T2D and severe obesity who underwent gastric bypass surgery is presented. The high remission rates of T2D after gastric bypass surgery are incompletely understood and possibly, changes in beta cell mass play a role. Therefore, beta cell mass was determined by ^{68}Ga-Ex4 PET/CT before and one year after surgery in seven people with mild T2D (using only metformin before gastric bypass) and six people with more severe T2D (requiring insulin therapy before gastric bypass). In this study we demonstrated the potential of beta cell mass recovery and the ability to visualize changes in beta cell mass *in vivo* by Exendin-4 (Ex4) PET/CT. In line with the progressive decline in beta cell mass during T2D development, this study showed a lower beta cell mass in people requiring insulin therapy than those using only metformin prior to surgery. After surgery, beta cell mass remained unchanged in people only using metformin, while it increased in people requiring insulin therapy. This may reflect some recovery of lost beta cell mass. Changes in beta cell mass were not correlated with beta cell function, as measured by c-peptide response to arginine stimulation.

In clinical studies using radiolabeled Exendin-4, both with ^{111}In-Ex4 SPECT/CT and ^{68}Ga-Ex4 PET/CT, reliable quantification of the radiotracer uptake in the pancreas is challenged by very high uptake of the radiotracer in the kidneys. As a consequence, artefacts with increased or decreased activity concentration may appear around the kidneys. The appearance of these artefacts worsens with increasing abdominal size, i.e. in people with overweight and obesity. To understand the effect of these artefacts on pancreatic quantification, and to assess which reconstruction settings would be optimal to reduce these artifacts, a three-dimensionally (3D) printed phantom of the pancreas and kidneys was designed. Using this phantom, we were able to mimic human anatomy and tracer distribution by filling the organs with ^{111}In or ^{68}Ga solutions representing the tracer distribution in humans. In **chapter 3,** the design of this phantom and the artefacts as observed in ^{111}In-Ex4 SPECT/CT using different reconstruction settings are presented. In **chapter 4,** we used the pancreas-kidney phantom to assess the effect of the photopenic artefacts around the kidneys on the quantification of ^{68}Ga-Ex4 accumulation in ^{68}Ga-Ex4 PET/CT. In ^{68}Ga-Ex4 PET/CT, these artefacts were more prominent in people with increased body size. Therefore, body casings representing body sizes of people with normal weight, overweight and obesity were used. In these phantom studies it was demonstrated that phantoms can represent human imaging of radiolabeled Exendin-4 by SPECT/CT and PET/CT well. These phantom studies increased our understanding of quantification of radiolabeled Exendin-4 in the pancreas and the effect of artefacts surrounding the high uptake in the kidneys. Moreover, we were able to optimize acquisition, reconstruction and quantification methods, although the occurrence of artefacts could not be prevented completely. Especially in the obesity mimicking phantom severe artefacts remained unchanged even after optimization.

Chapter 5 and 6 address applications of ^{68}Ga-Ex4 PET/CT beyond the pancreas by assessing the extra-pancreatic accumulation of ^{68}Ga-Ex4 in humans. The whole-body accumulation pattern of this tracer has never been described in detail before. Understanding the normal accumulation pattern is important for correct assessment and interpretation of ^{68}Ga-Ex4 PET/CT images. In addition, assessing the extra-pancreatic uptake of the tracer is valuable for non-invasive assessment of GLP-1 receptor expression in humans. This is especially of interest since GLP-1 receptor agonists are being applied as anti-diabetic and anti-obesity medications and multiple other actions of these medications have been described. To date, data on GLP-1 receptor expression is scarce and has been limited to studies in animal models or human tissue samples due to the limited availability of tools to assess GLP-1 receptor expression in vivo. Findings in animals cannot directly be translated to humans due to interspecies differences. Moreover, human tissue samples cannot give insight into the dynamics of beta cell mass and GLP-1 receptor expression over time. In **Chapter 5,** we assessed the whole-body uptake distribution of ^{68}Ga-Ex4 and related these findings to known GLP-1 receptor expression patterns from the literature. **Chapter 6** specifically describes the accumulation of ^{68}Ga-Ex4 in the brain. The uptake

in the pituitary gland and the absence of uptake in other parts of the brain in 10 participants with T2D and severe obesity are described in this chapter. In these studies, it was shown that the accumulation of Ex4 corresponds with well-known locations of GLP-1 receptor expression, but also identifies organs in which GLP-1 receptor expression is less well understood. The findings in these chapters demonstrate the ability of ^{68}Ga-Ex4 PET/CT to visualize and quantify GLP-1 receptor expression *in vivo*.

Finally, **chapter 7** includes a summary of this thesis and the implications of these findings and future perspectives are discussed.

GENERAL BACKGROUND

Type 2 diabetes and obesity

Type 2 diabetes (T2D) and obesity are closely linked. The prevalence of both diseases is increasing worldwide with a growing burden on public health (1-5). T2D is characterized by persistent hyperglycemia (6, 7). Underlying mechanisms in T2D are decreased insulin sensitivity, increased insulin demand and a decreased beta cell function and mass (6, 8-10). Obesity is defined by body mass index (BMI) and divided into class 1 obesity with BMI 30-35 kg/m2, class 2 with BMI 35-40 kg/m2 and class 3, or severe obesity with BMI >40 kg/m2. It is a multifactorial disease, involving physical, behavioral, genetic, hormonal, and environmental factors as well as medication (11). Obesity is a major risk factor for the development of T2D, mainly because the accumulation of body fat and low-grade inflammation contribute to insulin resistance and beta cell dysfunction and loss (12-16).

The treatment of T2D and obesity involves similar strategies. The treatment of T2D is primarily aimed at maintaining adequate blood glucose levels and thereby prevent complications of hyperglycemia on the long-term. Traditional treatment of T2D consisted of pharmacological interventions to regulate glycemia. Over the years, improving lifestyle and reducing weight have become important elements in the treatment of T2D (17-20). Achieving and maintaining significant weight loss can even result in the remission of T2D, meaning the adequate regulation of blood glucose levels without the need for antidiabetics (17-19, 21-24). The primary treatment strategy to induce weight loss is a combined lifestyle intervention. When lifestyle interventions alone are not sufficient to reduce weight and improve health, pharmacotherapy or metabolic bariatric surgery can be advised (17, 20, 25, 26).

Pharmacotherapy options for weight loss have improved and therefore gained interest over the past 10 years. (38) Lately, the most prescribed weight loss stimulating medications were naltrexone/bupropion and glucagon-like peptide 1 (GLP-1) receptor agonists, e.g. liraglutide (26). GLP-1 receptor agonists were primarily developed as antidiabetics.

Due to their weight loss effect, GLP-1 receptor agonists have been used for weight loss therapy. Such anti-obesity medications can already achieve weight loss of more than 10% of the initial weight in 25-35% of people after one year of treatment (39-41). Currently, new generation GLP-1 receptor agonists (semaglutide, trade name Ozempic®) and combinations with other entero-pancreatic hormones such as glucose-dependent insulinotropic polypeptide (GIP) (tirzepatide, trade name Mounjaro®) achieve higher weight loss rates up to 10-20% on average (38, 42, 43). In future pharmacotherapy may even approach weight loss results as achieved with metabolic bariatric surgery.

To date, metabolic bariatric surgery is the most invasive, but also the most effective treatment for severe obesity, T2D and other obesity-related diseases (17, 19, 20, 22-26). The most frequently performed procedures are sleeve gastrectomy (SG) and Roux-en-Y gastric bypass surgery (RYGB) (27, 28). In SG, a significant part of the stomach is removed, resulting in a tube-shaped stomach. In RYGB, a small stomach pouch is created and the largest part of the stomach, the duodenum and part of the jejunum, are bypassed. Both procedures result in substantial and sustained weight loss of on average 30% of initial body weight (28-33). In addition, T2D remission rates are high, being 42-65% and 37-52%, 1 to 5 years after RYGB and SG, respectively (33-37). High T2D remission rates are even reached when insulin therapy is indicated. The underlying mechanisms include weight loss, improved insulin sensitivity and reduced insulin demand (44). In addition, beta cell recovery may also play a role in T2D remission after RYGB surgery (45). However, the underlying mechanisms of how beta cell mass contributes to T2D remission remain poorly understood and have not been studied in humans yet.

Glucagon-like peptide-1 (GLP-1) and GLP-1 receptor agonists

GLP-1 is an incretin hormone which has an important role in glucose- and weight homeostasis. It is secreted by the L-cells in the intestinal epithelium after ingestion of a meal and enhances glucose-stimulated insulin secretion by the beta cells. (46)

The first GLP-1 receptor agonist that has been discovered was Exendin-4, which was found in the saliva of the Gila monster (Heloderma Suspectum) (47). Currently, GLP-1 receptor agonists, like semaglutide and liraglutide, have an important role in the treatment of type 2 diabetes and obesity. These medications enhance postprandial insulin secretion and improve glucose regulation in T2D. In addition, they induce satiety and weight loss. Other actions of GLP-1 receptor agonists that have been observed include delaying gastric emptying, lowering blood pressure and positively affecting tissue regeneration and protection in, for example, the beta cells, and the nervous and cardiovascular system. (48-50) New GLP-1 receptor agonists continue to be developed, particularly to improve weight loss outcomes. In addition, indications for other diseases, like neurodegenerative and cardiac diseases are being investigated (46, 50-52).

The effects of GLP-1 and GLP-1 receptor agonists are mediated through the GLP-1 receptor. Consistent with the effect of GLP-1 on insulin secretion, the GLP-1 receptor is found at high densities on the pancreatic beta cells. Other cell types in the pancreas show little or no GLP-1 receptor expression in humans (46, 52-56). The GLP-1 receptor has been described in many other human tissues, including the cardiovascular tract, gastrointestinal system, brain, kidney, and on immune cells (46, 48, 49, 55, 57). However, a complete understanding of GLP-1 receptor mediated functions its tissue expression in human has not been reached yet.

The lack of knowledge on GLP-1 receptor functions in humans is a results of the scarce availability of tools to assess GLP-1 receptor expression and the lack of tools to assess GLP-1 receptor expression *in vivo*. As a result, the majority of data is from studies in animal models or from human tissues samples. Animal data cannot be translated directly to humans because several interspecies differences have been established; for example, the high GLP-1 receptor expression in the lungs in rodents versus the lack of GLP-1 receptor expression in lungs in humans (55). In addition, human tissue samples are not widely available for all organs and data from tissue samples cannot provide insight in the dynamics of GPL-1 receptor expression over time. The last is interesting, because it is known that GLP-1 receptor expression can vary over time, for example, upregulation of the receptor expression has been observed after cardiac ischemia and the level of receptor expression in the beta cells depends on glycemia as shown in rodents (58-61). However, to date the specifics on such dynamics in GLP-1 receptor expression and its relation with physiological processes in humans are largely unknown. To improve our understanding of GLP-1 receptor expression in human, real-time and *in vivo* visualization of the receptor expression is warranted.

Glucagon-like peptide-1 receptor imaging

Glucagon-like peptide-1 receptor imaging has been developed to address the unmet need for non-invasive visualization and quantification of beta cells in humans. Beta cells are located in the islets of Langerhans in the pancreas and produce and secrete insulin. The loss of beta cell mass, and the potential presence of residual beta cell mass in type 1 diabetes has been a topic of debate and research for years. Existing methods for determining beta cell mass have been inadequate for this purpose (62). In addition, the detection and localization of focal or locally increased beta cell density causing hyperinsulinemic hypoglycemia, e.g. in insulinoma, has been insufficient (63). Non-invasive imaging techniques could facilitate the study of beta cell mass and its dynamics and the detection of focal increases in beta cell density.

The challenges that had to be overcome to develop an adequate beta cell imaging technique have been the small volume of total beta cell mass (only 1-2% of pancreatic volume), the diffuse localization of beta cells throughout the pancreas and the need for

a highly specific target for beta cells (62, 64). To date, targeting the GLP-1 receptor with radiolabeled Exendin-4 is the most promising method for visualizing beta cells (62). Previous preclinical and clinical studies have shown that this radiotracer is highly specific for beta cells and that pancreatic uptake directly correlates with beta cell mass, while uptake of radiolabeled Exendin-4 by other pancreatic cell types is limited and does not interfere with beta cell imaging (54, 65-71).

The first clinically available radiotracer for GLP-1 receptor imaging was [^{111}In]In-Lys40(Ahx-DTPA)]exendin-4 (^{111}In-Ex4) (68). The uptake of this tracer can be imaged by single photon emission computed tomography/computed tomography (SPECT/CT). Currently, the radiotracer [^{68}Ga]Ga-NODAGA-Exendin-4 (^{68}Ga-Ex4) is used in combination with positron emission tomography (PET)/CT. The use of ^{68}Ga-Ex4 PET/CT is preferred to ^{111}In-Ex4 SPECT/CT because of its higher spatial resolution and more accurate quantification of radiotracer accumulation. Consequently, image quality and quantification are improved and lower radiation exposure is achieved (63, 70, 72).

Previous clinical studies using GLP-1 receptor imaging have demonstrated its value in detecting insulinomas and studying beta cell mass in type 1 diabetes (T1D). Nuclear imaging using radiolabeled Exendin-4 outperforms other types of imaging for the diagnosis and localization of insulinomas (73). In addition, beta cell imaging has led to several new insights into beta cell mass in T1D. As expected, the first clinical study in T1D showed a lower pancreatic uptake of ^{111}In-Ex4 in patients with T1D compared to non-diabetic controls (68). Data from this and subsequent studies supported the hypothesis of residual beta cells in a proportion of patients with T1D. A recent study suggested a clinical impact of this finding, as higher pancreatic accumulation of ^{68}Ga-Ex4 was observed in patients with T1D with better glucose regulation compared to those with worse glucose regulation (74). Finally, Jansen *et al.* demonstrated accumulation of radiolabeled Exendin-4 in the liver of patients who underwent a transplantation of islets of Langerhans in the liver for the treatment of T1D (75).

In the clinical studies reported in this thesis, GLP-1 receptor imaging has been used to study beta cell mass in human with T2D and obesity and to assess GLP-1 receptor expression beyond the pancreas.

REFERENCES

1. CBS. Meer obesitas en diabetes bij volwassenen met armoederisico 2022 [Available from: https://www.cbs.nl/nl-nl/nieuws/2022/40/meer-obesitas-en-diabetes-bij-volwassenen-met-armoederisico.
2. CBS. Obesitas afgelopen 40 jaar verdrievoudigd 2024 [Available from: https://www.cbs.nl/nl-nl/nieuws/2024/10/obesitas-afgelopen-40-jaar-verdrievoudigd.
3. WHO. Global report on diabetes. 2016.
4. WHO. Obesity and overweight 2025 [Available from: https://www.who.int/news-room/fact-sheets/detail/obesity-and-overweight.
5. WHO. Diabetes 2024 [Available from: https://www.who.int/news-room/fact-sheets/detail/diabetes.
6. American Diabetes Association Professional Practice C. 2. Diagnosis and Classification of Diabetes: Standards of Care in Diabetes-2025. Diabetes Care. 2025;48(1 Suppl 1):S27-S49.
7. Goyal R, Singhal M, Jialal I. Type 2 diabetes: StatPearls [Internet] Treasure Island (FL): StatPearls Publishing; 2023.
8. Chen C, Cohrs CM, Stertmann J, Bozsak R, Speier S. Human beta cell mass and function in diabetes: Recent advances in knowledge and technologies to understand disease pathogenesis. Mol Metab. 2017;6(9):943-57.
9. Kahn SE. The relative contributions of insulin resistance and beta-cell dysfunction to the pathophysiology of Type 2 diabetes. Diabetologia. 2003;46(1):3-19.
10. Weyer C, Bogardus C, Mott DM, Pratley RE. The natural history of insulin secretory dysfunction and insulin resistance in the pathogenesis of type 2 diabetes mellitus. J Clin Invest. 1999;104(6):787-94.
11. Oussaada SM, van Galen KA, Cooiman MI, Kleinendorst L, Hazebroek EJ, van Haelst MM, et al. The pathogenesis of obesity. Metabolism. 2019;92:26-36.
12. DeFronzo RA. Pathogenesis of type 2 diabetes mellitus. Med Clin North Am. 2004;88(4):787-835, ix.
13. Gregor MF, Hotamisligil GS. Inflammatory mechanisms in obesity. Annu Rev Immunol. 2011;29:415-45.
14. He W, Yuan T, Maedler K. Macrophage-associated pro-inflammatory state in human islets from obese individuals. Nutr Diabetes. 2019;9(1):36.
15. Solinas G, Karin M. JNK1 and IKKbeta: molecular links between obesity and metabolic dysfunction. FASEB J. 2010;24(8):2596-611.
16. Shoelson SE, Herrero L, Naaz A. Obesity, inflammation, and insulin resistance. Gastroenterology. 2007;132(6):2169-80.
17. American Diabetes Association Professional Practice C. 8. Obesity and Weight Management for the Prevention and Treatment of Type 2 Diabetes: Standards of Care in Diabetes-2025. Diabetes Care. 2025;48(1 Suppl 1):S167-S80.
18. Lean ME, Leslie WS, Barnes AC, Brosnahan N, Thom G, McCombie L, et al. Primary care-led weight management for remission of type 2 diabetes (DiRECT): an open-label, cluster-randomised trial. Lancet. 2018;391(10120):541-51.
19. Rothberg A, Lean M, Laferrere B. Remission of type 2 diabetes: always more questions, but enough answers for action. Diabetologia. 2024;67(4):602-10.
20. NHG. Diabetes mellitus type 2 2018 [updated 1-7-2025. Available from: https://richtlijnen.nhg.org/standaarden/diabetes-mellitus-type-2.

21. Ghanem OM, Abi Mosleh K, Kerbage A, Lu L, Hage K, Abu Dayyeh BK. Continued Diabetes Remission Despite Weight Recurrence: Gastric Bypass Long-Term Metabolic Benefit. J Am Coll Surg. 2024;238(5):862-71.
22. Lafarge JC, Aron-Wisnewsky J, Pattou F, Cucherat M, Blondet E, Lascols S, et al. French National Authority for Health assessment of metabolic surgery for type 2 diabetes remission-A meta-analysis in patients with class I to III obesity. Diabetes Metab. 2024;50(1):101495.
23. Sandoval DA, Patti ME. Glucose metabolism after bariatric surgery: implications for T2DM remission and hypoglycaemia. Nat Rev Endocrinol. 2023;19(3):164-76.
24. Yang Y, Miao C, Wang Y, He J. The long-term effect of bariatric/metabolic surgery versus pharmacologic therapy in type 2 diabetes mellitus patients: A systematic review and meta-analysis. Diabetes Metab Res Rev. 2024;40(5):e3830.
25. FMS. Chirurgische behandeling van obesitas 2020 [Available from: https://richtlijnendatabase.nl/richtlijn/chirurgische_behandeling_van_obesitas/indicatiestelling_bij_chirurgische_behandeling_van_obesitas.html.
26. FMS. Overgewicht en obesitas bij volwassenen en kinderen 2023 [Available from: https://richtlijnendatabase.nl/richtlijn/overgewicht_en_obesitas_bij_volwassenen_en_kinderen/volwassenen/gepersonaliseerde_zorg.html.
27. Brown W, Kow L, Anvari M, Ghaferi A, Morton J, Shikora S, et al. 8th Global registry report. 2023.
28. Nienhuijs SW, Bruinsma FFE. DATO Jaarverslag 2022. 2023.
29. Arterburn D, Wellman R, Emiliano A, Smith SR, Odegaard AO, Murali S, et al. Comparative Effectiveness and Safety of Bariatric Procedures for Weight Loss: A PCORnet Cohort Study. Ann Intern Med. 2018;169(11):741-50.
30. Homan J, Boerboom A, Aarts E, Dogan K, van Laarhoven C, Janssen I, et al. A Longer Biliopancreatic Limb in Roux-en-Y Gastric Bypass Improves Weight Loss in the First Years After Surgery: Results of a Randomized Controlled Trial. Obes Surg. 2018;28(12):3744-55.
31. Nijland LMG, Reiber BMM, Monpellier VM, Jacobs A, Hazebroek EJ, van Veen RN, et al. The association between patient attendance to a perioperative group-based lifestyle program and weight loss after bariatric surgery. Surg Obes Relat Dis. 2022;18(6):747-54.
32. Okkema S, Boerboom A, den Hengst W, Aarts E, Berends F, Hazebroek E. Five-year outcomes of a randomized controlled trial evaluating a non-adjustable ring in Roux-en-Y gastric bypass. Surg Endosc. 2025;39(4):2324-34.
33. Wolnerhanssen BK, Peterli R, Hurme S, Bueter M, Helmio M, Juuti A, et al. Laparoscopic Roux-en-Y gastric bypass versus laparoscopic sleeve gastrectomy: 5-year outcomes of merged data from two randomized clinical trials (SLEEVEPASS and SM-BOSS). Br J Surg. 2021;108(1):49-57.
34. Burger PM, Monpellier VM, Deden LN, Kooiman LBR, Liem RSL, Hazebroek EJ, et al. Standardized reporting of co-morbidity outcome after bariatric surgery: low compliance with the ASMBS outcome reporting standards despite ease of use. Surg Obes Relat Dis. 2020;16(11):1673-82.
35. Salminen P, Helmio M, Ovaska J, Juuti A, Leivonen M, Peromaa-Haavisto P, et al. Effect of Laparoscopic Sleeve Gastrectomy vs Laparoscopic Roux-en-Y Gastric Bypass on Weight Loss at 5 Years Among Patients With Morbid Obesity: The SLEEVEPASS RCT. JAMA. 2018;319(3):241-54.
36. Schauer PR, Kashyap SR, Wolski K, Brethauer SA, Kirwan JP, Pothier CE, et al. Bariatric surgery versus intensive medical therapy in obese patients with diabetes. N Engl J Med. 2012;366(17):1567-76.
37. Schauer PR, Bhatt DL, Kirwan JP, Wolski K, Aminian A, Brethauer SA, et al. Bariatric Surgery versus Intensive Medical Therapy for Diabetes - 5-Year Outcomes. N Engl J Med. 2017;376(7):641-51.

38. McGowan B, Ciudin A, Baker JL, Busetto L, Dicker D, Fruhbeck G, et al. Framework for the pharmacological treatment of obesity and its complications from the European Association for the Study of Obesity (EASO). Nat Med. 2025;31(10):3229-32.
39. Essop T, Tran K, Purdy AC, Daly SC. Comparative Effects of GLP-1 Agonists, Sleeve Gastrectomy and Roux-en-Y Gastric Bypass on Diabetes Mellitus Outcomes. Curr Diab Rep. 2024;24(12):273-89.
40. Iqbal J, Wu HX, Hu N, Zhou YH, Li L, Xiao F, et al. Effect of glucagon-like peptide-1 receptor agonists on body weight in adults with obesity without diabetes mellitus-a systematic review and meta-analysis of randomized control trials. Obes Rev. 2022;23(6):e13435.
41. Morissette A, Mulvihill EE. Obesity management for the treatment of type 2 diabetes: emerging evidence and therapeutic approaches. J Pharm Pharm Sci. 2024;27:13065.
42. Aronne LJ, Horn DB, le Roux CW, Ho W, Falcon BL, Gomez Valderas E, et al. Tirzepatide as Compared with Semaglutide for the Treatment of Obesity. N Engl J Med. 2025;393(1):26-36.
43. Rodriguez PJ, Goodwin Cartwright BM, Gratzl S, Brar R, Baker C, Gluckman TJ, et al. Semaglutide vs Tirzepatide for Weight Loss in Adults With Overweight or Obesity. JAMA Intern Med. 2024;184(9):1056-64.
44. Müller TD, Finan B, Bloom SR, D'Alessio D, Drucker DJ, Flatt PR, et al. Glucagon-like peptide 1 (GLP-1). Mol Metab. 2019;30:72-130.
45. Martinussen C. et al., Immediate enhancement of first-phase insulin secretion and unchanged glucose effectiveness in patients with type 2 diabetes after Roux-en-Y gastric bypass. Am J Physiol Endocrinol Metab. 2015;308(6):E535-44.
46. Guldstrand M, Ahrén B, Adamson U. Improved β-cell function after standardized weight reduction in severely obese subjects. Am J Physiol Endocrinol Metab. 2003;284:3 E557-E565
47. Eng J. Exendin peptides. Mt Sinai J Med. 1992;59(2):147-9.
48. Abu-Hamdah R, Rabiee A, Meneilly GS, Shannon RP, Andersen DK, Elahi D. Clinical review: The extrapancreatic effects of glucagon-like peptide-1 and related peptides. J Clin Endocrinol Metab. 2009;94(6):1843-52.
49. Drucker DJ. The Cardiovascular Biology of Glucagon-like Peptide-1. Cell Metab. 2016;24(1):15-30.
50. Holscher C. Protective properties of GLP-1 and associated peptide hormones in neurodegenerative disorders. Br J Pharmacol. 2022;179(4):695-714.
51. Brown E, Heerspink HJL, Cuthbertson DJ, Wilding JPH. SGLT2 inhibitors and GLP-1 receptor agonists: established and emerging indications. Lancet. 2021;398(10296):262-76.
52. Heppner KM, Perez-Tilve D. GLP-1 based therapeutics: simultaneously combating T2DM and obesity. Front Neurosci. 2015;9:92.
53. Arrojo EDR, Jacob S, Garcia-Prieto CF, Zheng X, Fukuda M, Nhu HTT, et al. Structural basis for delta cell paracrine regulation in pancreatic islets. Nat Commun. 2019;10(1):3700.
54. Da Silva Xavier G. The Cells of the Islets of Langerhans. J Clin Med. 2018;7(3).
55. Korner M, Stockli M, Waser B, Reubi JC. GLP-1 receptor expression in human tumors and human normal tissues: potential for in vivo targeting. J Nucl Med. 2007;48(5):736-43.
56. Segerstolpe A, Palasantza A, Eliasson P, Andersson EM, Andreasson AC, Sun X, et al. Single-Cell Transcriptome Profiling of Human Pancreatic Islets in Health and Type 2 Diabetes. Cell Metab. 2016;24(4):593-607.
57. Pyke C, Heller RS, Kirk RK, Ørskov C, Reedtz-Runge S, Kaastrup P, et al. GLP-1 receptor localization in monkey and human tissue: novel distribution revealed with extensively validated monoclonal antibody. Endocrinology. 2014;155(4):1280-90.

58. Buitinga M, Cohrs CM, Eter WA, Claessens-Joosten L, Frielink C, Bos D, et al. Noninvasive Monitoring of Glycemia-Induced Regulation of GLP-1R Expression in Murine and Human Islets of Langerhans. Diabetes. 2020;69(11):2246-52.
59. Gao H, Kiesewetter DO, Zhang X, Huang X, Guo N, Lang L, et al. PET of glucagonlike peptide receptor upregulation after myocardial ischemia or reperfusion injury. J Nucl Med. 2012;53(12):1960-8.
60. Ståhle M, Kytö V, Kiugel M, Liljenbäck H, Metsälä O, Käkelä M, et al. Glucagon-like peptide-1 receptor expression after myocardial infarction: Imaging study using (68)Ga-NODAGA-exendin-4 positron emission tomography. J Nucl Cardiol. 2020;27(6):2386-97.
61. Xu G, Kaneto H, Laybutt DR, Duvivier-Kali VF, Trivedi N, Suzuma K, et al. Downregulation of GLP-1 and GIP receptor expression by hyperglycemia: possible contribution to impaired incretin effects in diabetes. Diabetes. 2007;56(6):1551-8.
62. Gotthardt M, Eizirik DL, Cnop M, Brom M. Beta cell imaging - a key tool in optimized diabetes prevention and treatment. Trends Endocrinol Metab. 2014;25(8):375-7.
63. Jansen TJP, van Lith SAM, Boss M, Brom M, Joosten L, Behe M, et al. Exendin-4 analogs in insulinoma theranostics. J Labelled Comp Radiopharm. 2019;62(10):656-72.
64. Andralojc K, Srinivas M, Brom M, Joosten L, de Vries IJ, Eizirik DL, et al. Obstacles on the way to the clinical visualisation of beta cells: looking for the Aeneas of molecular imaging to navigate between Scylla and Charybdis. Diabetologia. 2012;55(5):1247-57.
65. Brom M, Andralojc K, Oyen WJ, Boerman OC, Gotthardt M. Development of radiotracers for the determination of the beta-cell mass in vivo. Curr Pharm Des. 2010;16(14):1561-7.
66. Brom M, Joosten L, Frielink C, Boerman O, Gotthardt M. (111)In-exendin uptake in the pancreas correlates with the beta-cell mass and not with the alpha-cell mass. Diabetes. 2015;64(4):1324-8.
67. Brom M, Joosten L, Frielink C, Peeters H, Bos D, van Zanten M, et al. Validation of (111)In-Exendin SPECT for the Determination of the beta-Cell Mass in BioBreeding Diabetes-Prone Rats. Diabetes. 2018;67(10):2012-8.
68. Brom M, Woliner-van der Weg W, Joosten L, Frielink C, Bouckenooghe T, Rijken P, et al. Non-invasive quantification of the beta cell mass by SPECT with ^{111}In-labelled exendin. Diabetologia. 2014;57(5):950-9.
69. Eriksson O, Laughlin M, Brom M, Nuutila P, Roden M, Hwa A, et al. In vivo imaging of beta cells with radiotracers: state of the art, prospects and recommendations for development and use. Diabetologia. 2016;59(7):1340-9.
70. Jansen TJP, Tokgoz S, Buitinga M, van Lith SAM, Joosten L, Frielink C, et al. Validation of radiolabelled exendin for beta cell imaging by ex vivo autoradiography and immunohistochemistry of human pancreas. EJNMMI Res. 2024;14(1):96.
71. Joosten L, Brom M, Peeters H, Bos D, Himpe E, Bouwens L, et al. Measuring the Pancreatic beta Cell Mass in Vivo with Exendin SPECT during Hyperglycemia and Severe Insulitis. Mol Pharm. 2019;16(9):4024-30.
72. Antwi K, Fani M, Heye T, Nicolas G, Rottenburger C, Kaul F, et al. Comparison of glucagon-like peptide-1 receptor (GLP-1R) PET/CT, SPECT/CT and 3T MRI for the localisation of occult insulinomas: evaluation of diagnostic accuracy in a prospective crossover imaging study. Eur J Nucl Med Mol Imaging. 2018;45(13):2318-27.
73. Boss M, Eriksson O, Mikkola K, Eek A, Brom M, Buitinga M, et al. Improved Localization of Insulinomas Using (68)Ga-NODAGA-Exendin-4 PET/CT. J Nucl Med. 2024;65(12):1959-64.
74. Jansen TJP, Brom M, Boss M, Buitinga M, Tack CJ, van Meijel LA, et al. Importance of beta cell mass for glycaemic control in people with type 1 diabetes. Diabetologia. 2023;66(2):367-75.

75. Jansen TJP, Buitinga M, Boss M, Nijhoff MF, Brom M, de Galan BE, et al. Monitoring beta-Cell Survival After Intrahepatic Islet Transplantation Using Dynamic Exendin PET Imaging: A Proof-of-Concept Study in Individuals With Type 1 Diabetes. Diabetes. 2023;72(7):898-907.



2

Does Roux-en-Y gastric bypass surgery influence beta cell mass in people with Type 2 Diabetes? A clinical study using ^{68}Ga-exendin-4 PET/CT

L.N. Deden[1,2], M. Boss[2], H. de Boer[3], E.Ow. Aarts[1], A.C. van Bon[3], I.M.C. Janssen[1], F.J. Berends[1], B.E. de Galan[4,5,6], E.J. Hazebroek[1,7], M. Gotthardt[2]

In preparation

ABSTRACT

Aim: High remission rates of type 2 diabetes (T2D) are observed after Roux-en-Y gastric bypass surgery (RYGB). Whether these effects are related to changes in beta cell mass remains unknown. In this study, we assessed beta cell mass using ^{68}Ga-exendin PET/CT in patients with T2D before and after RYGB surgery.

Materials and methods: Individuals with T2D undergoing RYGB surgery were included and divided into two groups: those using only metformin (METF) and those requiring insulin therapy (INS). Before and one year after RYGB, beta cell mass was assessed as total pancreatic activity (TPA) on ^{68}Ga-exendin PET/CT and beta cell function was determined by the c-peptide response to arginine stimulation divided by fasting blood glucose level (CPR_{ARGT}).

Results: Thirteen participants completed preoperative measurements (METF N=6, INS N=7). One METF participant was withdrawn from postoperative measurements. Participants lost 30±6.6% of total body weight. Complete remission of T2D occurred in all METF participants and in one INS participant. One INS participant achieved partial remission and two clinically improved glycemic control. Prior to RYGB, CPR_{ARGT} was lower in the INS than METF participants (0.68±0.30 vs 1.18±0.47 nmol.min.mmol-1, p=0.0383). Similarly, TPA was lower in the INS than in the METF participants (4.7±1.6 (N=5) vs. 6.9±1.5 (N=5) kBq/MBq, p=0.059). After RYGB, TPA increased in INS participants from 4.7±1.6 to 5.8±1.5 kBq/MBq (p=0.0013, N=5) and remained unchanged in the METF group (7.3±1.3 vs 7.3±1.7, p=0.9974, N=4). CPR_{ARGT} remained unchanged after RYGB, and was 0.61±0.29 nmol.min.mmol-1 in the INS group (p=0.439) and 1.23±0.51 to 0.81±0.29 nmol.min.mmol-1 in the METF group (p=0.203).

Conclusion: In people with T2D on insulin, pancreatic uptake of ^{68}Ga-exendin increased after RYGB surgery, reflecting recovery of beta cell mass. In people treated with metformin alone beta cell mass did not change. Beta cell function did not improve in individuals on insulin, neither in individuals using metformin only.

INTRODUCTION

Type 2 diabetes (T2D) is strongly associated with obesity, which is mediated first by insulin resistance and subsequently by (relative) insulin deficiency [1-3]. Obesity-induced decline of insulin sensitivity first stimulates pancreatic beta cells to increase insulin secretion to meet this raised demand. However, T2D ensues when insulin secretion can no longer compensate for this demand. Such (initially relative) beta cell dysfunction is usually accompanied by reduced beta cell mass and has been observed already early in the development of T2D [4-7]. As the disease progresses, insulin deficiency worsens and beta cell mass gradually declines further [7, 8].

Significant loss of at least 10-15% of initial total body weight can lead to remission of T2D [9-11]. Remission is defined as glucose levels, or HbA1c levels, in the non-diabetic range without the need for glucose-lowering medication for at least 3 months. [32] Overall, diet and lifestyle interventions have been shown to lead to T2D remission rates up to 61% after one year. However, this decreases to much lower rates in the long term, averaging 36% and 13% after two and five years, respectively [11, 12].

In people with severe obesity (>35kg/m2), bariatric surgery has been shown to improve glycemic control considerably up to the point of durable T2D remission. The most frequently performed procedures are Roux-en-Y gastric bypass surgery (RYGB) and sleeve gastrectomy (SG) [14, 15]. Both procedures result in significant and sustained weight loss and improved glycemic control, although RYGB is superior in terms of T2D remission with complete T2D remission rates of 73% and 51% one year and five years after surgery, respectively [16]. These remission rates are higher and more sustained as compared to lifestyle interventions [13]. It is known that RYGB surgery involves multiple endocrine and metabolic changes beyond significant weight loss, however the mechanism underlying is still incompletely understood [17-20].

Weight loss induced improvements in insulin sensitivity and reduced insulin requirements are the main factors in T2D remission. However, recovery of beta cell function and mass have been suggested to play a role in the T2D remission after RYGB as well. Several studies have shown improved insulin secretion rates in patients after RYGB [18, 19]. Animal studies have also suggested restoration of beta cell mass after RYGB [21-28]. To date, it is unclear if RYGB could lead to restoration of beta cell mass in humans.

Radiolabeled exendin-4 allows the non-invasive visualization and quantification of beta cells in humans by positron emission tomography (PET). Exendin-4 is a stable agonist of the glucagon-like peptide-1 receptor (GLP-1R), with excellent affinity and specificity for the GLP-1R, which is highly expressed on beta cells [29-31]. To improve our understanding of changes in beta cell mass and its role in the remission of T2D after RYGB, we

assessed beta cell mass in patients with T2D before and after undergoing RYGB surgery using ^{68}Ga-NODAGA-exendin-4 (^{68}Ga-exendin) PET/CT. In order to take the influence of residual beta cell function into account, we separately recruited people with diabetes using only metformin (METF) and those on insulin therapy (INS).

MATERIALS AND METHODS

Patient selection and outcome

Sixteen individuals diagnosed with T2D at least one year earlier, who were scheduled to undergo RYGB surgery, were included and divided into two groups. The METF group consisted of nine patients, whereas the INS group consisted of seven patients. Exclusion criteria were BMI above 50 kg/m2, waist circumference above 140 cm (to ensure that PET-CT could be performed), treatment with GLP-1 receptor agonists or dipeptidyl peptidase IV inhibitors (to prevent competition between the radiotracer and native GLP-1), estimated glomerular filtration rate (eGFR) <40 mL/min and pregnancy or the wish to become pregnant within 12 months.

The study was approved by the local ethics committee (METC Arnhem-Nijmegen, registered at clinical trials.gov: NCT03182231) and was conducted according to the guidelines of the Declaration of Helsinki. All participants were informed about the study and provided written informed consent before participation.

All assessments were performed before (0-10 weeks) and one year (12-15 months) after RYGB surgery.

Weight and diabetes remission

In all patients, weight, BMI and waist circumference were measured before and one year after RYGB. Weight change was calculated as percentage of total weight loss (%TWL). Status of T2D was assessed based on fasting blood glucose levels (FBG), HbA1c levels and use of glucose-lowering medication. After RYGB, T2D remission was classified as complete remission, partial remission or improvement following the guidelines of the ASMBS [32]. Complete remission was defined as achieving normoglycemia (HbA1c <42 mmol/mol and FBG <5.6 mmol/l) without the use of any glucose-lowering medication. Partial remission was defined as glycemia in the sub-diabetic range (HbA1c: 42-48 mmol/mol and FBG: 5.6-7.0 mmol/l) without the use of any glucose-lowering medication. Improvement in T2D was defined as a decrease in HbA1c of at least 5 mmol/mol, and at least halving of the dose of glucose-lowering drugs.

Beta cell function tests

Participants underwent a combined arginine stimulation (ARGT) and oral glucose tolerance (OGTT) test before and after RYGB surgery. These measurements were performed in the morning after an overnight fast for at least 12 hours (no food intake, not smoking, no oral glucose-lowering medication and no short actin insulin administration).

For the ARGT, 5 g arginine was administered intravenously within 45 seconds. C-peptide and glucose levels were measured 5 minutes prior to, and 2, 3, 4 and 5 minutes after arginine administration.

The OGTT was performed 30 minutes after arginine administration, when blood glucose and c-peptide levels had returned to baseline levels [33]. Participants received a standard dose of 75 g of glucose in 200 ml water orally. After RYGB, this dose was halved in 4 participants because they did not tolerate 75 g of glucose. C-peptide and glucose levels were measured shortly before, and 15, 30, 45, 60, 90, 120, 150 and 180 minutes after glucose intake.

Measures of beta cell function, glucose tolerance and insulin sensitivity

The early c-peptide response during arginine test (CPR_{ARGT}) was calculated as area under the curve of c-peptide blood levels ($AUC_{c\text{-}peptide}$, nmol*min/l) from baseline until 5 minutes and corrected for fasting blood glucose level (FG, mmol/l), since c-peptide response depends on the blood glucose level [34, 35]:

$$CPR_{ARGT} = \frac{AUC_{c-peptide}}{FG}$$

The c-peptide-glucose ratio during OGTT was calculated as c-peptide (nmol/ml) divided by blood glucose level (mmol/ml) at 15 and 30 minutes after glucose ingestion ($CPGR_{OGTT,15}$ and $CPGR_{OGTT,30}$, nmol/mmol).

$$CPGR_{OGTT,\ t} = \frac{c-peptide_t}{glucose_t}$$

In addition, the c-peptide index (nmol/mmol) at 30 minutes (CPI_{30}) was calculated as the increase in c-peptide level (nmol/ml) divided by the increase in blood glucose level (mmol/ml) from glucose intake (t=0) to 30 minutes after glucose intake:

$$CPI_{30} = \frac{c-peptide_{t=30}-c-peptide_{t=0}}{glucose_{t=30}-\ glucose_{t=0}}.$$

Since pre- and postoperative OGTT were incomplete in some participants, CPR_{ARGT} was used for further analyses. A comparison between CPR_{ARGT} and CPR_{OGTT} and CPI_{OGTT} in all participants with complete preoperative tests (N=13, including participants without postoperative follow-up) showed a strong correlation between arginine- and glucose-

stimulated c-peptide responses (Pearson R: 0.931-0.993, p<0.001, Figure 1), indicating that CPR_{ARGT} is a reliable measure for the beta cell function.

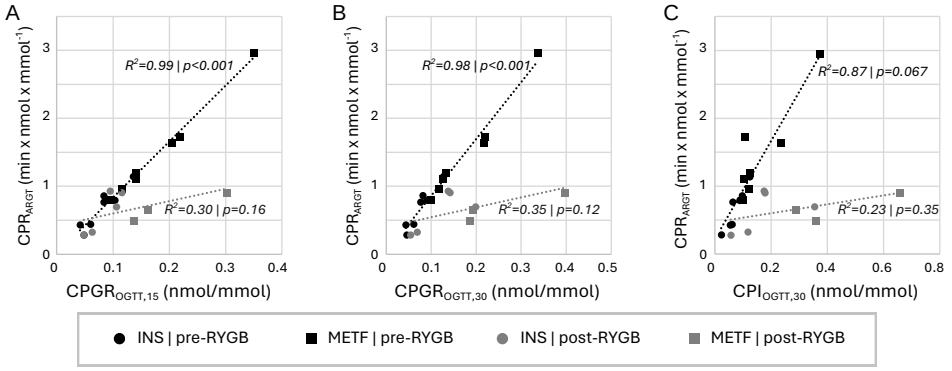


Figure 1. Scatterplots of individual values of c-peptide glucose ratio (CPGR) and c-peptide index (CPI) during OGTT ($CPGR_{OGTT,15}$, $CPGR_{OGTT,30}$ $CPI_{OGTT,30}$) and c-peptide response during arginine stimulation test (CPR_{ARGT}). Dotted lines represent regression before (black) and one year after Roux-en-Y gastric bypass surgery (RYGB). Preoperative values of $CPGR_{OGTT}$ were correlated almost perfectly.

^{68}Ga-exendin PET/CT

All patients underwent a ^{68}Ga-exendin PET/CT before and after RYGB.

Radiopharmaceutical preparation

Hydrochloric acid was purchased from Rotem Industries (Mishor Yamin: Israel), all other components were purchased as one disposable kit (reagent and hardware kit for synthesis of ^{68}Ga peptides using cationic purification, ABX, Germany). ^{68}Ga-NODAGA-exendin-4 was manufactured using a synthesizer module (GRP synthesizer, Scintomics, Germany) and gallium-68-chloride was obtained from a 68Ge/^{68}Ga generator (Galliapharm, Eckert and Ziegler, Germany). The generator was eluted with 10 ml of 0.1 M hydrochloric acid and gallium-68 was trapped on a polystyrene-H+ cartridge. The cartridge was eluted with 1.5 ml 5 M NaCl in 0.1 M hydrochloric acid into the reaction vial, containing 200 µl exendin-NODAGA (10 µg of peptide in water for injection, 475 µl 2.5 M 4-(2-hydroxyethyl)-1-piperazineethanesulfonic acid (HEPES) buffer and 50 µl ascorbic acid 100 mg/ml in water for injection. After 15 minutes incubation at 100°C, the vessel was cooled and 2 ml ethylenediaminetetraacetic acid (EDTA) 50 mM/ polysorbate 80 0.15% was added. ^{68}Ga-NODAGA-exendin-4 was purified on a HLB cartridge and sterilized by passing through a 0.2 µm filter (millex GV).

Administration of ^{68}Ga-exendin and PETCT acquisition

All participants received an intravenous injection with ^{68}Ga-exendin of 101±9.6 MBq (56-107 MBq), corresponding with a pharmaceutical dose of 4-7 µg of the peptide. In one participant, the radioactivity dose post-RYGB was decreased to 56 MBq due to logistic issues. All participants fasted for at least 4 hours before tracer administration, to avoid competition between the radiotracer and endogenous GLP-1. Fasting glucose levels were determined prior to administration and monitored up to one hour after administration. Intravenous infusion with 5% glucose at individual rates was started after injection of the radiotracer in participants with blood glucose levels below 3.5 mmol/ml or with a drop of blood glucose levels <4.0 mmol/ml shortly after radiotracer administration.

A PET/CT was acquired 61±4.3 minutes (55-70 min) after tracer injection, from the top of the head to the sacroiliac joint using a Siemens Biograph mCT-40 time-of-flight PET/CT scanner [ref Siemens]. Acquisition was performed for 7 minutes per bed-position in 5 bed-positions, A non-contrast enhanced, low-dose CT (40 mAs, 130 kV) was obtained for attenuation correction and anatomical reference. Ultrahigh definition reconstruction of the PET was performed using 3 iterations, 12 subsets and a post-reconstruction Gaussian filter of 3 mm in full width at half maximum. Other reconstruction settings included time of flight, model-based scatter correction, attenuation correction based on low-dose CT and correction for decay. The PET matrix was 200x200 and pixel size was 4.07 x 4.07 x 3.00 mm.

Image quality assessment

Image quality was assessed by an experienced nuclear medicine physician (MG), who was blinded to the allocations of participants. Image quality was judged as sufficient to good for most pre- and postoperative PET/CT scans. Distribution patterns in the pancreas and rest of the abdomen were similar at both timepoints for all participants. However, halo artefacts, i.e. photopenic areas surrounding the extreme activity concentration in the kidneys, occurred on several preoperative PET scans. The extent of this artefact and the degree in which the artefact affected quantification of pancreatic tracer accumulation was assessed using a five-point scale. The extent to which the artefact affected quantification of pancreatic uptake was scored as 0 when quantification was unaffected (no artefact or the pancreas was outside the artefact region) and up to 4 when uptake in (the affected part of) the pancreas was considered to be largely under- or overestimated due to the artefact. Images with scores 3 and 4 were excluded from analysis because of unreliable quantification of pancreatic uptake.

In three participants, the activity in the whole pancreas was affected considerably by the artefact (score 3-4) and preoperative pancreatic uptake measures were excluded from analyses. In three other participants, pancreatic activity was affected by a halo artefact in the caput (N=1) or cauda (N=2) only, and this part of the pancreas was excluded from

the analysis, both pre- and postoperatively. In the remaining participants, pancreatic activity was not or only minimally affected by a halo artefact (score 0-1) preoperatively. In postoperative PET/CT images, these artefacts did not play a significant role (due to the significant weight loss of the study participants).

Pancreatic uptake as measure for beta cell mass

Quantification of tracer uptake was performed using Inveon Research Workplace (version 4.1; Siemens Healthcare). Volumes of interest were manually drawn around the pancreas (VOI_{PANC}) based on the low-dose CT and corrected for misalignment on PET. These VOIs were dilated by 3 mm, to include spillover activity (VOI_{VOL}). Parts of this VOI containing activity originating from the kidneys or duodenum and parts largely affected by artefacts were excluded, resulting in VOI_{ACT}. For this purpose, a VOI was drawn around the kidneys based on CT and this VOI was dilated by 9 mm to include spillover. The duodenum was delineated based on CT and corrected for misalignment on PET. Radiotracer uptake in the excluded pancreas areas was assumed to be equal to the average uptake in the remaining pancreas, resulting in the mean activity concentration corrected for administered dose (A_{mean}):

$$A_{mean} = \left[kBq\ MBq^{-1}ml^{-1}\right] = \frac{mean\ activity\ concentration\ derived\ from\ VOI_{ACT}}{injected\ dose},$$

and total pancreatic activity corrected for administered dose (TPA):

$$TPA\ \left[kBq\ MBq^{-1}\right] = volume\ derived\ from\ VOI_{VOL}\ \bullet A_{mean}$$

For comparison with previous published studies, mean standard uptake value (SUV_{mean}), of pancreatic uptake was determined as:

$$SUV_{mean} = \frac{mean\ activity\ concentration\ derived\ from\ VOI_{ACT}\ [kBq/ml]}{\frac{injected\ dose\ [MBq]}{total\ body\ weight\ [g]}},$$

assuming that 1 g of tissue corresponds with 1 ml.

Analysis and statistics

Participant characteristics, measures of beta cell function and total pancreatic uptake were compared between the groups using an independent student's T-test. For comparisons at single timepoints, all participants with a ^{68}Ga-exendin PET/CT of sufficient quality and an ARGT at the specific timepoint were included. Comparison of pre- and postoperative measurements of beta cell function and beta cell mass was performed by paired sample t-tests. For this purpose, only participants with a complete study follow-up were included, i.e. ^{68}Ga-exendin PET/CT images of sufficient quality and ARGT at both timepoints. P-values below 0.05 were considered statistically significant. Correlation between measures of beta cell function and mass, and the changes in those measures

were analyzed using descriptive statistics by scatter graphs and linear regression analysis. Statistics were performed using SPSS (IBM Corp. IBM SPSS statistics for Windows version 22.0, Armonk, NY). Graphs were made using GNU Octave, version 5.2.0 [36].

RESULTS

In total, 16 participants were included, nine in the METF group and seven in the INS group. Twelve participants completed postoperative follow-up within 11-17 months after RYGB. One METF participant completed preoperative measurements, but was excluded from postoperative measurements due to treatment of an oncological disorder. Three METF participants were excluded because preoperative ^{68}Ga-exendin PET/CT failed due to technical reasons and repetition was not possible before undergoing the surgery. However, all of these participants completed preoperative ARGT and OGTT testing. Among the twelve participants with complete follow-up, preoperative OGTT failed in two and postoperative OGTT failed in another two participants. Participant enrolment is schematically shown in Figure 2.

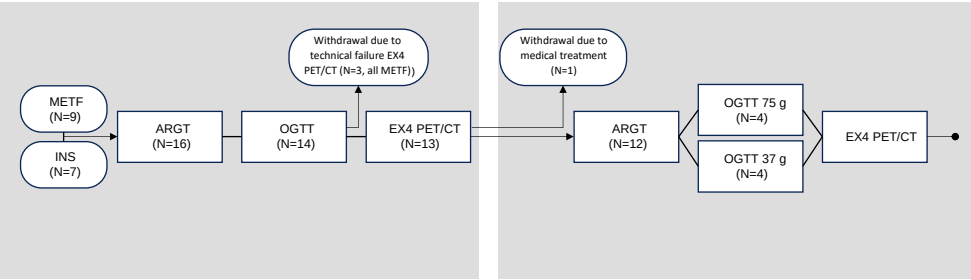


Figure 2. Flow diagram of participant enrolment, withdrawal and study tests.

Pancreatic uptake of ^{68}Ga-exendin was measured in ten participants before RYGB surgery (5 METF, 5 INS) and in twelve participants after RYGB surgery (5 METF, 7 INS). In nine participants, pancreatic uptake of ^{68}Ga-exendin could be measured before and after RYGB surgery (4 METF, 5 INS). Before RYGB surgery, pancreatic uptake measures were excluded from analyses in three participants, because the activity in the whole pancreas was affected considerably by the halo artefact (score 3-4).

Weight loss and T2D remission

All pre- and postoperative participant characteristics are summarized in table 1 and an overview of individual glycemic control parameters and glucose-lowering medication is given in supplemental table 1. At baseline, the INS and METF groups were comparable for age and body weight measures. Participants in the INS group had a longer diabetes duration and higher HbA1c than participants in the METF group. All INS participants used

long-acting insulin (51±5.6 IU/day), while six of these also used short acting insulin three times daily (48±45 IU/day), two used gliclazide (30 mg/day) and five used metformin (1.0-2.55 g/day). The METF participants all used solely metformin with a median dose of 1.0 g/day (range: 0.5-2.0 g/day).

One year after surgery, patients lost 34 ± 6 kg, corresponding to 30 ± 6.3% of total body weight loss (TBWL), neither of which differed statistically significantly between the INS and METF group. Within the METF group, all participants achieved complete remission of T2D. In the INS group, one participant had complete T2D remission, one had partial remission and two had clinically improved glycemic control, based on a drop in HbA1c and reduction of the use of glucose-lowering medication. Three participants had unchanged or worsened glycemic control, although use of glucose-lowering medication decreased.

Table 1. Characteristics prior to and one year after RYGB surgery.

	All pre-RYGB (N=13)	All post-RYGB (N=12)	METF pre-RYGB (N=6)	METF post-RYGB (N=5)	INS pre-RYGB (N=7)	INS post-RYGB (N=7)
Female (%)	10 (77%)	9 (75%)	6 (100%)	5 (100%)	4 (57%)	4 (57%)
Age (years)	51±8.5		49±11		53±6.2	
Weight (kg)	112±14	79±15	107±14	70±15	117±13	86±12
BMI (kg/m^2)	39±4.1	27±3.5	40±5.3	26±4.2	38±2.9	28±3.1
Total body weight loss (%)		30±6.6		35±5.9		27±4.9*
Waist (cm)	121±8.2	94±9.1	118±9.8	88±5.2	124 ±6.1	98±9.5
Duration T2D (years)	9.6±8.1		6±7.3		13±7.8	
Number of glucose lowering medication^	1 (1-4)	0 (1-2)	1 (1)	0	3 (1-4)	0 (0-1.5)
Insulin dose (IU/day)	n.a.	n.a.	n.a.	n.a.	99±50	10 (N=1)
Metformin dose (g/day)^	1.0 (0-2.55)	0 (0-1.5)	1.0 (0.5-2.0)	0	1.5 (0-2.55)	0 (0-1.5)
Fasting glucose (mmol/l)	9.1±2.5	6.7±3.1	8.1±1.51.5	4.5±0.36	9.9±2.9	8.3±3.2 *
HbA1c (mmol/mol)	63±12	44±15	56±8.5	33±5.4	69±11*	53±15*
Fasting c-peptide (nmol/l)	0.97±0.46	0.52±0.18	1.2±0.43	0.44±0.13	0.81±0.45	0.58±0.20

RYGB = Roux-en-Y gastric bypass surgery; METF = Participants only using metformin; INS = participants on insulin therapy; N = number of participants; BMI = body mass index; n.a. = not applicable. ^Data shown as median (minimum-maximum range); *statistically different from METF participants, p<0.05.

Beta cell mass

Individual measures of total pancreatic activity before and after RYGB surgery in the METF and INS participants are shown in Figure 3 and average measurements of mean tracer uptake concentrations and standard uptake values in table 3. At baseline, pancreatic ATot tended to be lower in the INS participants than in the METF participants (4.7±1.6 (N=5) vs. 6.9±1.5 (N=5) kBq/MBq, p=0.059). One year after RYGB, this difference between the INS

and METF group remained largely unchanged (5.7±1.2 (N=7) vs 7.3±1.5 (N=5) kBq/MBq, p=0.0723).

One year after RYGB, total pancreatic uptake in the INS group increased from 4.7±1.6 to 5.8±1.5 kBq/MBq (p=0.0013, N=5), while the uptake in the METF group did not change (7.3±1.3 vs 7.3±1.7, p=0.9974, N=4).

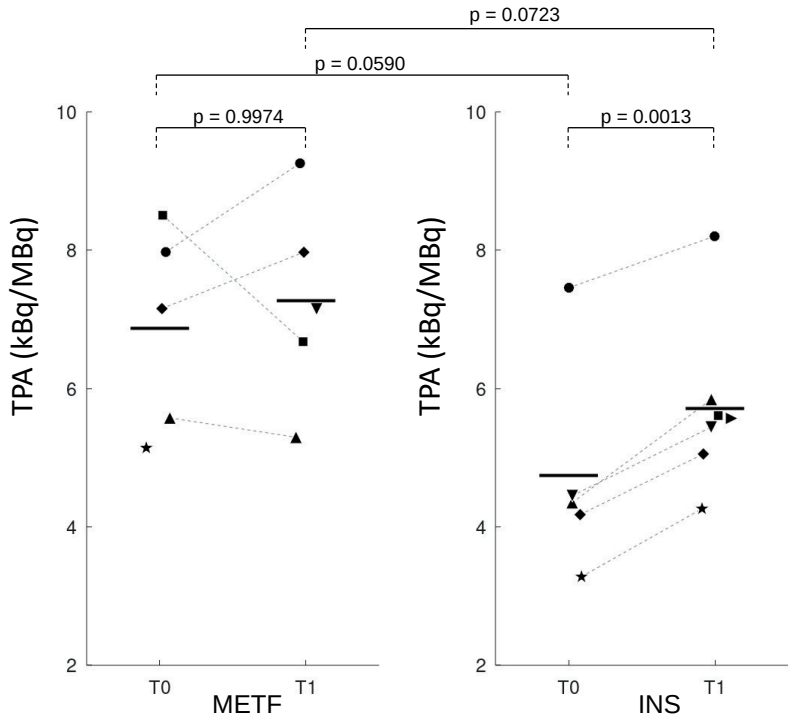


Figure 3. Individual measures of total pancreatic activity (TPA) in participants only using metformin (METF) and participants requiring insulin therapy (INS), before (T0) and one year after RYGB surgery (T1). The horizontal line represents the group average at both timepoints. The individual change in TPA is visualized by dashed lines. Total pancreatic activity remained similar after RYGB in the METF group. In the INS group, total pancreatic uptake increased in all individuals. Comparing METF and INS, the total pancreatic uptake was lower in the INS group than the METF group, before (T0) and after (T1) RYGB.

Table 2. Pancreatic uptake measured as mean activity (A_{mean}) and mean standard uptake value (SUV_{mean}) before and after Roux-en-Y gastric bypass surgery (RYGB).

	Baseline			One year after RYGB		
	N	A_{mean} (kBq/ml/MBq)	SUV_{mean}	N	A_{mean} (kBq/ml/MBq)	SUV_{mean}
METF	5	0.081 ± 0.012	4.3 ± 0.77	5	0.10 ± 0.0089	3.3 ± 0.65
INS	5	0.057 ± 0.0094	3.1 ± 0.62	7	0.078 ± 0.020	3.1 ± 0.59

Beta cell function

C-peptide response and glucose tolerance improved in all participants during OGTT, with the largest improvements in those with complete or partial remission of T2D. Individual glucose and c-peptide curves during ARGT and OGTT are shown in Figure 4 and beta cell capacity measures in table 3.

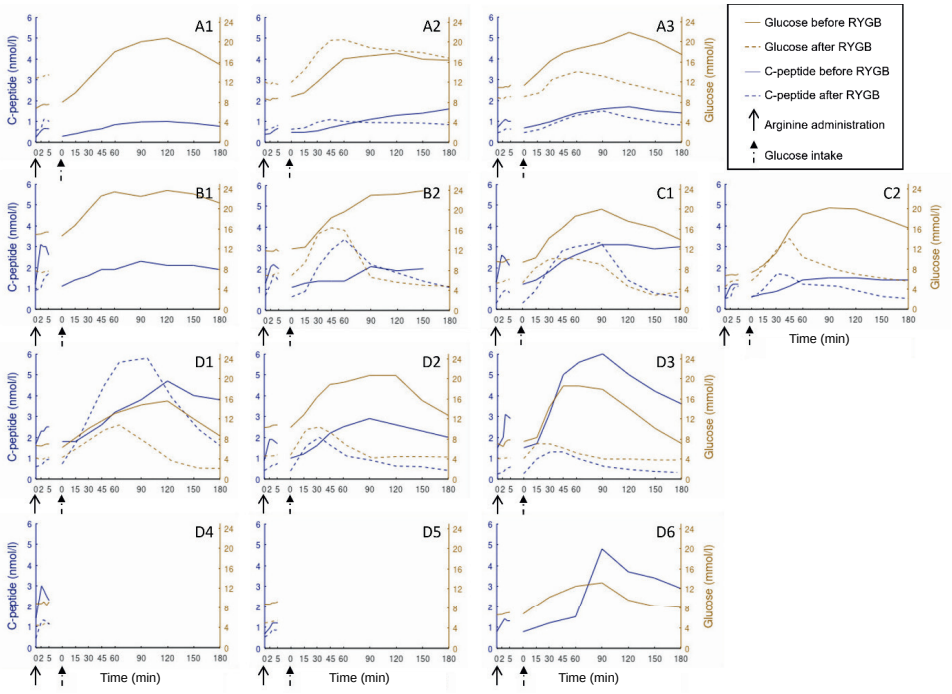


Figure 4. Individual blood glucose and c-peptide levels during arginine stimulation test (ARGT) and oral glucose tolerance test (OGTT). In A) INS participants with similar or worsened glycemic control one year after Roux-en-Y gastric bypass surgery (RYGB), in B) INS participants with clinically improved glycemic control one year after RYGB, in C) INS participants with partial or complete remission one year after RYGB and in D) METF participants; D1-5 with complete remission one year after RYGB, D6 was withdrawn after RYGB.

Table 3. Individual measures of beta cell capacity, beta cell mass and T2D remissions status

Participant	Group	Insulin dose T0	Insulin dose T1	Nr. oral GLM T0	Nr. oral GLM T1	T2D remission
■ A1	INS	68	0	0	0	None
◆ A2	INS	125	10	2	1	None
★ B1	INS	198	0	1	1	Imp
▲ B2	INS	110	0	1	1	Imp
▶ C1	INS	62	0	2	0	CR
● A3	INS	72	0	1	2	None
▼ C2	INS	60	0	0	0	PR
■ D1	METF	0	0	1	0	CR
◆ D2	METF	0	0	1	0	CR
▲ D3	METF	0	0	1	0	CR
▼ D4	METF	0	0	1	0	CR
● D5	METF	0	0	1	0	CR
★ D6	METF	0	W	1	W	W

T0 = baseline; T1 = one year after Roux-en-Y gastric bypass; GLM = glucose lowering medication; None = similar or worsened glucose regulation; Imp = clinically improved glucose regulation; PR = partial remission; CR = complete remission; W = withdrawal.

Prior to RYGB, CPR_{ARGT} was significantly lower in INS than in METF participants (0.68±0.30 vs. 1.18±0.47 nmol.min.mmol^{-1}, p=0.0383) (Figure 5). One year after RYGB, the average CPR_{ARGT} remained unchanged in both the INS group (0.61±0.29 nmol.min.mmol^{-1}, p=0.44) and the METF group (1.23±0.51 to 0.81±0.29 nmol.min.mmol^{-1}, p=0.20).

The CPR_{ARGT} was significantly lower in those without improved glycemic control (N=3, INS) compared to those with clinically significant improved glycemic control or T2D remission (N=9, INS and METF), both at baseline (0.39±0.087 vs. 1.08±0.42 nmol.min.mmol^{-1}, p=0.0198) and one year after RYGB (0.31±0.028 vs. 0.82±0.22 nmol.min.mmol^{-1}, p=0.0029).

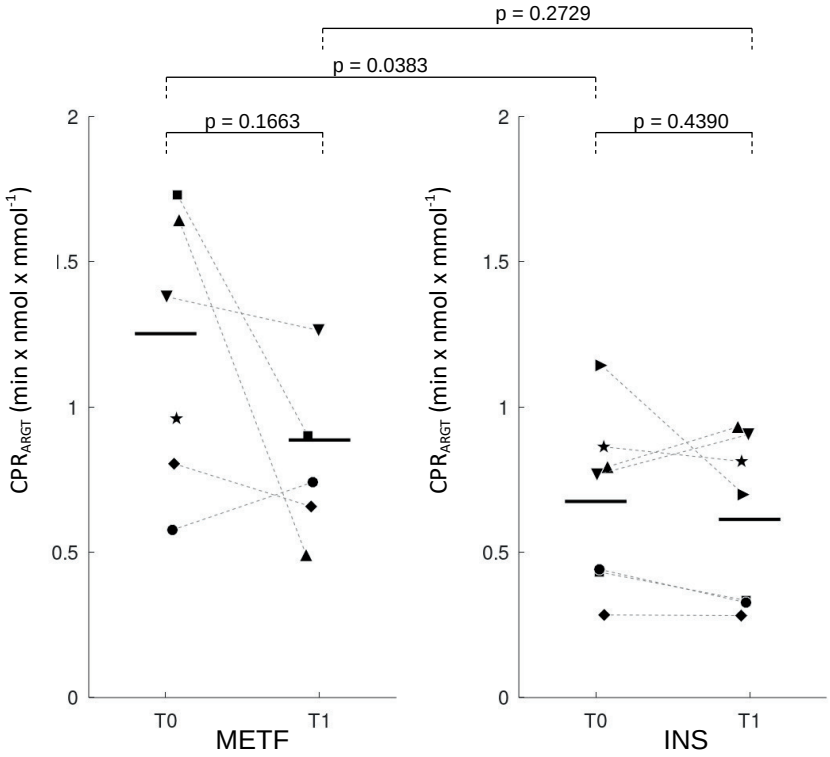


Figure 5. Individual measures of the c-peptide response during arginine test (CPR_{ARGT}) in participants only using metformin (METF) and participants requiring insulin therapy (INS), before (T0) and one year after RYGB surgery (T1). The horizontal line represents the group average at both timepoints. The individual change in CPR_{ARGT} is visualized by dashed lines. Before RYGB (T0), the average CPR_{ARGT}, is lower in the INS than METF group, this difference became smaller after RYGB (T1).

There was a positive correlation between the proportional change in total pancreatic uptake and the proportional change in CPR_{ARGT} (R= 0.79, p=0.0121; Figure 6A) and between the proportional change in total pancreatic uptake and the proportional change in total body weight (R=0.79; p=0.0106; Figure 6B). Similarly, the proportional change in CPR_{ARGT} correlated with the proportional change in total body weight (R=0.84, p=0.0051).

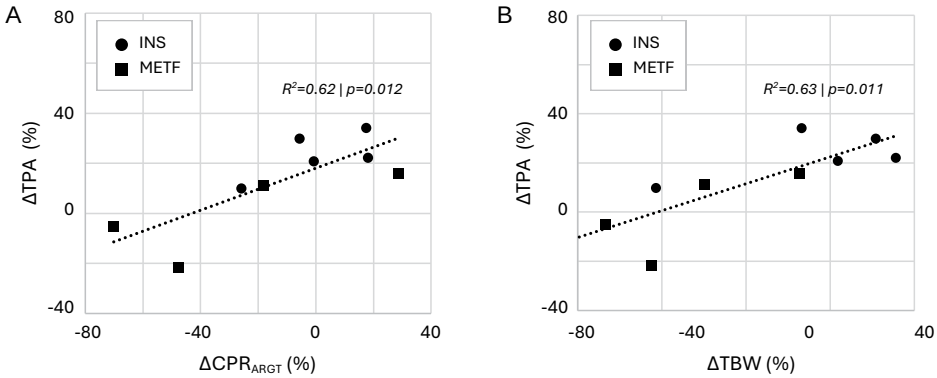


Figure 6. Scatter plots of the proportional change (%) of the total pancreatic uptake (ΔTPA) versus the proportional change in c-peptide response during arginine test (ΔCPR$_{ARGT}$) in A versus the proportional change in total body weight (ΔTBW) in B. Correlation between the parameters is visualized by the dotted line and R-squared (R^2) and p-values of regression analysis are shown. METF = participants only using metformin, INS = participants on insulin therapy.

No correlation between total pancreatic uptake and CPR$_{ARGT}$ was observed before (R=0.24, p=0.50) or after RYGB surgery (R=0.08, p=0.81) (Figure 7). Moreover, the rate of T2D remission was unrelated to total pancreatic uptake at baseline and to its proportional change. Finally, total pancreatic uptake did not correlate with blood glucose levels or HbA1c levels, neither at baseline, nor one year after RYGB or with the proportional change of these parameters (Figure 8).

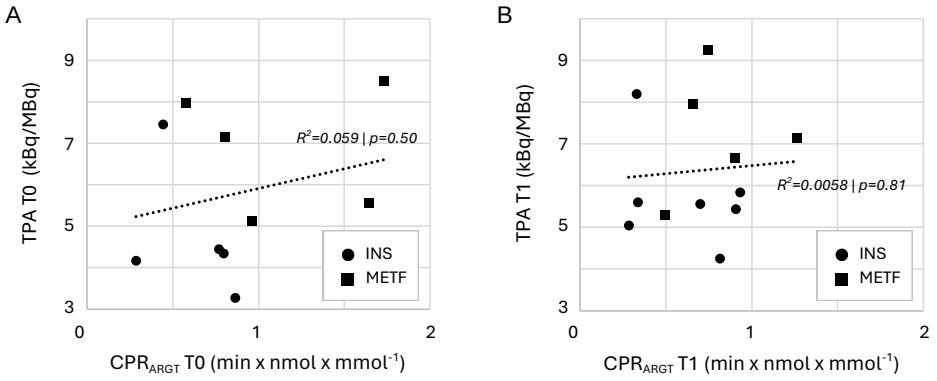


Figure 7. Scatter graphs of c-peptide response during arginine stimulation test (CPR$_{ARGT}$) versus total pancreatic uptake (TPA) at baseline (A) and one year after Roux-en-Y gastric bypass surgery (B). At neither of the timepoints there is any indication of a correlation between the measure of beta cell function and beta cell mass. Dotted lines represent linear regression analysis, including R-squared and p-values. METF = participants only using metformin, INS = participants requiring insulin therapy prior to surgery.

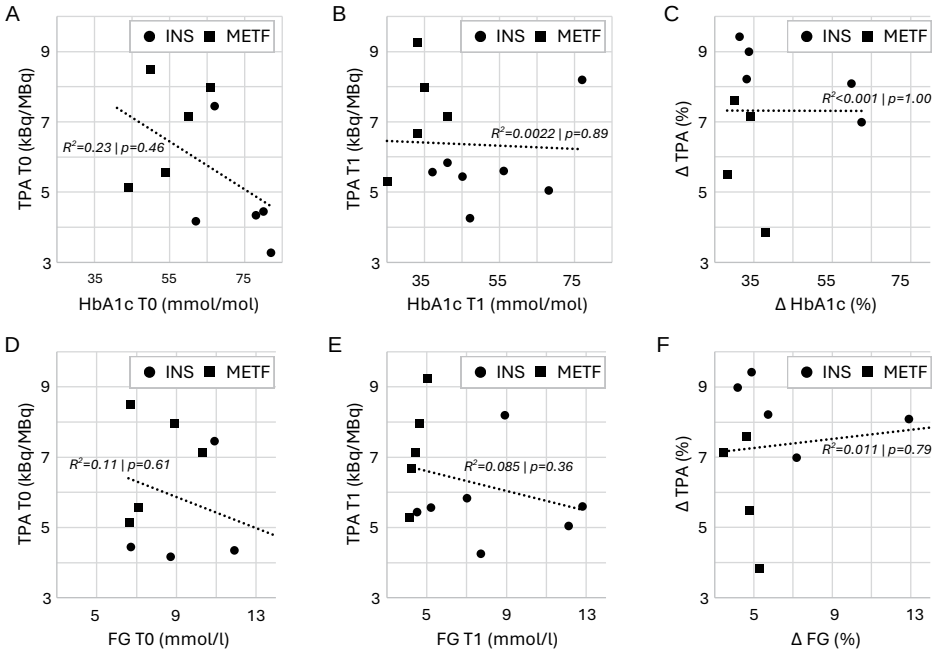


Figure 8. Scatter graphs showing the relation between total pancreatic ^{68}Ga-exendin uptake (TPA) and HbA1c levels (A-B) and fasting blood glucose levels (FG, D-E), before and after Roux-en-y gastric bypass surgery (RYGB). In C and F scatter graphs of the proportional changes in these parameters are shown. None of these graphs show an indication of correlation between the parameters. Dotted lines represent linear regression analysis, including R-squared and p-values. METF = participants only using metformin, INS = participants requiring insulin therapy prior to surgery.

DISCUSSION

In this clinical study, we investigated the effects of RYGB surgery on beta cell mass in patients with T2D by quantifying ^{68}Ga-exendin accumulation in the pancreas. The major findings of this study are: (1) prior to RYGB, both beta cell function and beta cell mass were lower in patients with insulin-treated T2D than in those treated with metformin alone; (2) one year after RYGB, beta cell mass, but not beta cell function, increased in all insulin-treated patients, while neither of these factors improved in metformin-treated participants; (3) the change in beta cell mass after RYGB correlated with the relative change in beta cell function. However , a direct correlation of beta cell mass with beta cell function at a single timepoint, before or one year after surgery, could not be demonstrated. Also, remission of T2D was unrelated to changes in either beta cell mass or function.

At baseline, pancreatic accumulation of ^{68}Ga-exendin and c-peptide response after arginine stimulation were higher in the METF group than the INS group. This observation is in line with participants in the INS group having further progressed T2D, with reduced

insulin secretion capacity and declined beta cell mass, as compared to the METF group, as reported previously [4-8,19]. In addition, the range of pancreatic SUV_{mean} values and individual variation at baseline were similar to values reported recently by Eriksson et al., who performed ^{68}Ga-exendin PET/CT and quantified pancreatic uptake in a cohort of T2D patients [37].

Remarkably, beta cell mass increased after RYGB surgery in the INS group, while no change was observed in the METF group. This increase in INS participants may reflect recovery of beta cell mass and is in line with findings of an increased beta cell mass in studies of animal RYGB models [21, 23, 25, 27, 28, 38, 39]. In humans, changes in BCM after RYGB surgery have never been studied directly. Nevertheless, the ability of the human beta cell mass to expand in response to increased insulin demand has been demonstrated in for example people with obesity and during pregnancy [40-42]. In the METF participants, substantial individual variability was observed, but on average BCM remained similar after RYGB surgery. This finding likely reflects an earlier stage in T2D development, in which beta cell mass has not yet declined significantly, or even increased, while beta cell function is no longer sufficient to meet the body's insulin demand.

Beta cell function (measured as c-peptide response after arginine stimulation) remained similar after RYGB in both groups. Similarly as for beta cell mass, the individual variation is larger in the METF group than in the INS group and a decrease in beta cell function was observed in two METF participants. This is consistent with previous findings that showed that insulin secretion in response to iv glucose-glucagon or arginine did declined in normal glucose tolerant participants, but did not change in T2D participants one year after RYGB surgery [43,50].

Beta cell mass and beta cell function did not correlate with each other in this study. In line with this, previous studies described a marked overlap in beta cell mass between individuals with and without diabetes, despite a clear difference in beta cell function between those individuals [5, 8]. In addition, loss of beta cell function has been shown to precede and exceed loss of beta cell mass [5, 8]. In vivo measurements of beta cell mass, such as with ^{68}Ga-exendin PET/CT described here, may help to improve our understanding of the relation between the loss of beta cell mass and beta cell function during the course of diabetes. Our finding that beta cell mass was higher in the METF group as compared to the INS group, points towards the importance of weight loss to prevent further deterioration of the disease early in the course of T2D. Moreover, BCM increased in the INS participants. Although this was not accompanied by an increase in first phase insulin secretion, it may possibly do play a role in improved glucose regulation as in T1D patients a larger beta cell mass was observed in patients with improved glucose regulation [51].

Some limitations of this study have to be considered. First, the assessment of beta cell mass by pancreatic ^{68}Ga-exendin uptake assumes stable GLP-1R expression. Yet expression of the GLP-1R is known to be downregulated during prolonged and severe hyperglycemia, which results in reduced uptake of exendin-4 based radiotracers [45-47]. Prior to surgery, blood glucose and HbA1c levels were higher in INS than in METF participants, so theoretically GLP-1R downregulation may have affected the pancreas uptake in INS participants. However, since the drop in HbA1c levels after RYGB surgery was smaller in the INS group than in the METF group, a difference in GLP-1R expression is unlikely to explain why the INS group showed a significant increase of total pancreas activity and the METF group did not. Therefore, glycaemia-related changes in GLP-1 receptor expression are not likely to have affected the pancreas uptake in this study.

Second, measurements of beta cell function were limited to the first phase insulin secretion and insulin sensitivity was not included. The OGTT failed or was incomplete in several participants, due to technical issues with cannulation or intolerance to the glucose load. Therefore, late-phase insulin secretion could not be analyzed. However, the c-peptide responses after arginine stimulation correlates very well with the acute c-peptide response after glucose stimulation and some even advocate that arginine stimulation may better than glucose stimulation estimate the early insulin secretion capacity of beta cells in T2D [48, 49]. Therefore, we do not consider this a relevant disadvantage of our study. However, we did not determine insulin sensitivity and its change after RYGB surgery, although improved insulin sensitivity as a major factor contributing to T2D remission after RYGB has been observed previously [17, 18, 34, 43, 44]. Future studies should aim to investigate the relationship between beta cell recovery and beta cell function and insulin secretion and insulin sensitivity.

Lastly, a technical limitation of our study is the halo artefact in the PET/CT scans performed at baseline, caused by severe obesity and the high kidney activity. Such artifacts may impair the reliability of the quantification of pancreatic ^{68}Ga-exendin uptake, forcing us to exclude three participants with severe halo artifacts. In another three participants, a minor part of the pancreas had to be excluded from analysis due to smaller halo artefacts. To overcome this potential limitation, we used identical pancreatic volumes of interest in pre- and postoperative scans, since ^{68}Ga-exendin accumulation was evenly distributed over the whole pancreas.

CONCLUSION

In conclusion, this is the first longitudinal study to assess changes in beta cell mass in people with obesity and type 2 diabetes before and after RYGB surgery by using ^{68}Ga-exendin PET/CT. Pancreatic ^{68}Ga-exendin accumulation was greater in METF than in INS participants. One year after RYGB, pancreatic ^{68}Ga-exendin uptake increased in INS, but not in METF participants. This points towards recovery of beta cell mass, that was lost over the course of T2D development. However, the increase in beta cell mass was not accompanied by an increase in first-phase insulin secretion. Nevertheless, these findings demonstrate the potential of beta cell recovery after RYGB surgery in humans.

REFERENCES

1. Daousi, C., et al., Prevalence of obesity in type 2 diabetes in secondary care: association with cardiovascular risk factors. Postgrad Med J, 2006. 82(966): p. 280-4.
2. Hu, Y., et al., Duration of obesity and overweight and risk of type 2 diabetes among US women. Obesity (Silver Spring), 2014. 22(10): p. 2267-73.
3. Weyer, C., et al., The natural history of insulin secretory dysfunction and insulin resistance in the pathogenesis of type 2 diabetes mellitus. J Clin Invest, 1999. 104(6): p. 787-94.
4. Butler, A.E., et al., Beta-cell deficit and increased beta-cell apoptosis in humans with type 2 diabetes. Diabetes, 2003. 52(1): p. 102-10.
5. Chen, C., et al., Human beta cell mass and function in diabetes: Recent advances in knowledge and technologies to understand disease pathogenesis. Mol Metab, 2017. 6(9): p. 943-957.
6. Esser, N., K.M. Utzschneider, and S.E. Kahn, Early beta cell dysfunction vs insulin hypersecretion as the primary event in the pathogenesis of dysglycaemia. Diabetologia, 2020. 63(10): p. 2007-2021.
7. Weir, G.C. and S. Bonner-Weir, Five stages of evolving beta-cell dysfunction during progression to diabetes. Diabetes, 2004. 53 Suppl 3: p. S16-21.
8. Rahier, J., et al., Pancreatic beta-cell mass in European subjects with type 2 diabetes. Diabetes Obes Metab, 2008. 10 Suppl 4: p. 32-42.
9. Holter, M.M., et al., Glucose Metabolism After Gastric Banding and Gastric Bypass in Individuals With Type 2 Diabetes: Weight Loss Effect. Diabetes Care, 2017. 40(1): p. 7-15.
10. Lean, M.E.J., et al., Durability of a primary care-led weight-management intervention for remission of type 2 diabetes: 2-year results of the DiRECT open-label, cluster-randomised trial. Lancet Diabetes Endocrinol, 2019. 7(5): p. 344-355.
11. Noronha, J.C., G. Thom, and M.E.J. Lean, Total Diet Replacement Within an Integrated Intensive Lifestyle Intervention for Remission of Type 2 Diabetes: Lessons From DiRECT. Front Endocrinol (Lausanne), 2022. 13: p. 888557.
12. UK, D. Weight loss can put type 2 diabetes into remission for at least 5 years, DiRECT study reveals. 2023 [cited 2023 14-12-2023]; Available from: https://www.diabetes.org.uk/about-us/news-and-views/weight-loss-can-put-type 2-diabetes-remission-least-five-years-reveal-latest-findings.
13. Pories, W.J., et al., Surgical treatment of obesity and its effect on diabetes: 10-y follow-up. Am J Clin Nutr, 1992. 55(2 Suppl): p. 582S-585S.
14. Angrisani, L., et al., Bariatric Surgery and Endoluminal Procedures: IFSO Worldwide Survey 2014. Obes Surg, 2017. 27(9): p. 2279-2289.
15. Poelemeijer, Y.Q.M., R.S.L. Liem, and S.W. Nienhuijs, A Dutch Nationwide Bariatric Quality Registry: DATO. Obes Surg, 2018. 28(6): p. 1602-1610.
16. Castellana, M., et al., Roux-en-Y Gastric Bypass vs Sleeve Gastrectomy for Remission of Type 2 Diabetes. J Clin Endocrinol Metab, 2021. 106(3): p. 922-933.
17. Batterham, R.L. and D.E. Cummings, Mechanisms of Diabetes Improvement Following Bariatric/Metabolic Surgery. Diabetes Care, 2016. 39(6): p. 893-901.
18. Bojsen-Moller, K.N., Mechanisms of improved glycaemic control after Roux-en-Y gastric bypass. Dan Med J, 2015. 62(4): p. B5057.
19. Chen, X., J. Zhang, and Z. Zhou, Targeting Islets: Metabolic Surgery Is More than a Bariatric Surgery. Obes Surg, 2019. 29(9): p. 3001-3009.
20. Taylor, R., A. Al-Mrabeh, and N. Sattar, Understanding the mechanisms of reversal of type 2 diabetes. Lancet Diabetes Endocrinol, 2019. 7(9): p. 726-736.

21. Camacho-Ramirez, A., et al., The influence of massive jejunectomy on endocrine pancreas of diabetic Goto-Kakizaki. Cir Cir, 2022. 90(5): p. 638-643.
22. Li, Z., et al., Roux-en-Y gastric bypass promotes expression of PDX-1 and regeneration of beta-cells in Goto-Kakizaki rats. World J Gastroenterol, 2010. 16(18): p. 2244-51.
23. Lindqvist, A., et al., Gastric bypass improves beta-cell function and increases beta-cell mass in a porcine model. Diabetes, 2014. 63(5): p. 1665-71.
24. Mendes, M.C., et al., Duodeno-jejunal bypass restores beta-cell hypersecretion and islet hypertrophy in western diet obese rats. Endocrine, 2018. 60(3): p. 407-414.
25. Mosinski, J.D., et al., Roux-en-Y gastric bypass restores islet function and morphology independent of body weight in ZDF rats. Am J Physiol Endocrinol Metab, 2021. 320(2): p. E392-E398.
26. Seifert, G., et al., Long-Term Diabetes Improvement After Duodenal Exclusion in Zucker Diabetic Fatty Rats Is Associated with Prevention of Strain-Specific Pancreatic Remodeling and Increased Beta Cell Proliferation. Obes Surg, 2022. 32(6): p. 1980-1989.
27. Zhang, S., et al., Increased beta-Cell Mass in Obese Rats after Gastric Bypass: A Potential Mechanism for Improving Glycemic Control. Med Sci Monit, 2017. 23: p. 2151-2158.
28. Zhou, X., et al., Pancreatic hyperplasia after gastric bypass surgery in a GK rat model of non-obese type 2 diabetes. J Endocrinol, 2016. 228(1): p. 13-23.
29. Brom, M., et al., Non-invasive quantification of the beta cell mass by SPECT with (1)(1)(1)In-labelled exendin. Diabetologia, 2014. 57(5): p. 950-9.
30. Gotthardt, M., et al., Beta cell imaging - a key tool in optimized diabetes prevention and treatment. Trends Endocrinol Metab, 2014. 25(8): p. 375-7.
31. Jansen, T.J.P., et al., Importance of beta cell mass for glycaemic control in people with type 1 diabetes. Diabetologia, 2023. 66(2): p. 367-375.
32. Brethauer, S.A., et al., Standardized outcomes reporting in metabolic and bariatric surgery. Obes Surg, 2015. 25(4): p. 587-606.
33. Fanni, G., et al., Response of multiple hormones to glucose and arginine challenge in T2DM after gastric bypass. Endocr Connect, 2022. 11(8).
34. Dirksen, C., et al., Exaggerated release and preserved insulinotropic action of glucagon-like peptide-1 underlie insulin hypersecretion in glucose-tolerant individuals after Roux-en-Y gastric bypass. Diabetologia, 2013. 56(12): p. 2679-87.
35. Larsson, H. and B. Ahren, Glucose-dependent arginine stimulation test for characterization of islet function: studies on reproducibility and priming effect of arginine. Diabetologia, 1998. 41(7): p. 772-7.
36. Eaton, J.W., et al. GNU Octave version 5.2.0 manual: a high-level interactive language for numerical computations. 2019; Available from: https://www.gnu.org/software/octave/doc/v5.2.0/
37. Eriksson, O., et al., Glucagonlike Peptide-1 Receptor Imaging in Individuals with Type 2 Diabetes. J Nucl Med, 2022. 63(5): p. 794-800.
38. Amouyal, C., et al., A surrogate of Roux-en-Y gastric bypass (the enterogastro anastomosis surgery) regulates multiple beta-cell pathways during resolution of diabetes in ob/ob mice. EBioMedicine, 2020. 58: p. 102895.
39. Miskelly, M.G., et al., GK-rats respond to gastric bypass surgery with improved glycemia despite unaffected insulin secretion and beta cell mass. Peptides, 2021. 136: p. 170445.
40. Linneman, A.K., et al., Pancreatic beta-cell proliferation in obesity. Advances in Nutrition, 2014. 5(3): p.0278-88
41. Inaishi J. et al., Beta-cell mass in obesity and type 2 diabetes, and its relation to pancreas fat: a mini-review. Nutrients, 2020. 12(12)

42. Usman T.O., Beta-cell compensation and gestational diabetes. Journal of biological chemistry, 2024. 299(12)
43. Bojsen-Moller, K.N., et al., Early enhancements of hepatic and later of peripheral insulin sensitivity combined with increased postprandial insulin secretion contribute to improved glycemic control after Roux-en-Y gastric bypass. Diabetes, 2014. 63(5): p. 1725-37.
44. Gavin, T.P., et al., Insulin sensitivity is related to glycemic control in type 2 diabetes and diabetes remission after Roux-en Y gastric bypass. Surgery, 2014. 155(6): p. 1036-43.
45. Buitinga, M., et al., Noninvasive Monitoring of Glycemia-Induced Regulation of GLP-1R Expression in Murine and Human Islets of Langerhans. Diabetes, 2020. 69(11): p. 2246-2252.
46. Lehtonen, J., et al., Beta cell specific probing with fluorescent exendin-4 is progressively reduced in type 2 diabetic mouse models. Islets, 2015. 7(6): p. e1137415.
47. Xu, G., et al., Downregulation of GLP-1 and GIP receptor expression by hyperglycemia: possible contribution to impaired incretin effects in diabetes. Diabetes, 2007. 56(6): p. 1551-8.
48. Robertson, R.P., AIRarg and AIRgluc as predictors of insulin secretory reserve. Transp Proc, 2004. 36(4): p. 1040-1.
49. Sjöstrand, M., et al., Assessment of beta-cell function in young patients with type 2 diabetes: arginine-stimulated insulin secretion may reflect beta-cell reserve. J of Internal Medicine, 2013. 275(1): p.39-48.
50 . Guldstrand, M., Ahrén, B., Adamson, U., Improved beta cell function after standardized weight reduction in severely obese subject. Am. J. Phys. – Endo. And Metab. 2003. 284:3, E557-E565
51. Jansen, T., Brom, M., Boss, M. et al., Importance of beta cell mass for glycaemic control in people with type 1 diabetes. Diabetologia, 2023. 66(2):367-375.



3

A 3D printed anatomical pancreas and kidney phantom for optimizing SPECT/CT reconstruction settings in beta cell imaging using ^{111}In-exendin

Wietske Woliner-van der Weg[1], Laura N. Deden[2], Antoi P. W. Meeuwis[1], Maaike Koenrades[3,4], Laura H. C. Peeters[5], Henny Kuipers[3], Geert Jan Laanstra[3], Martin Gotthardt[1], Cornelis H. Slump[3], Eric P. Visser[1]

EJNMMI Phys. 2016 Dec 7;3:29. doi: 10.1186/s40658-016-0165-0

ABSTRACT

Background: Quantitative single photon emission computed tomography (SPECT) is challenging, especially for pancreatic beta cell imaging with ^{111}In-exendin due to high uptake in the kidneys versus much lower uptake in the nearby pancreas. Therefore, we designed a three-dimensionally (3D) printed phantom representing the pancreas and kidneys to mimic the human situation in beta cell imaging. The phantom was used to assess the effect of different reconstruction settings on the quantification of the pancreas uptake for two different, commercially available software packages.

Methods: 3D-printed, hollow pancreas and kidney compartments were inserted into the National Electrical Manufacturers Association (NEMA) NU2 image quality phantom casing. These organs and the background compartment were filled with activities simulating relatively high and low pancreatic ^{111}In-exendin uptake for, respectively, healthy humans and type 1 diabetes patients. Images were reconstructed using Siemens Flash 3D and Hermes Hybrid Recon, with varying numbers of iterations and subsets and corrections. Images were visually assessed on homogeneity and artefacts, and quantitatively by the pancreas-to-kidney activity concentration ratio.

Results: Phantom images were similar to clinical images and showed comparable artefacts. All corrections were required to clearly visualize the pancreas. Increased numbers of subsets and iterations improved the quantitative performance but decreased homogeneity both in the pancreas and the background. Based on the phantom analyses, the Hybrid Recon reconstruction with 6 iterations and 16 subsets was found to be most suitable for clinical use.

Conclusions: This work strongly contributed to quantification of pancreatic ^{111}In-exendin uptake. It showed how clinical images of ^{111}In-exendin can be interpreted and enabled selection of the most appropriate protocol for clinical use.

INTRODUCTION

The development of a non-invasive, imaging-based method for quantification of the beta cell mass could greatly enhance our understanding of the complex pathophysiology underlying the development of diabetes. Therefore, we have studied the use of pancreatic uptake of ^{111}In-exendin as an imaging biomarker for the beta cell mass preclinically, and recently also in type 1 diabetes (T1D) patients and healthy humans (1). Pancreatic uptake of ^{111}In-exendin is low compared to the uptake in the nearby kidneys and strongly varies amongst healthy humans, in which at least a factor seven of difference in pancreatic uptake was observed (2). This is in line with the expected variation in beta cell mass. The average uptake in T1D patients is even two and a half times lower than in healthy volunteers (2). In order to use this tracer as a biomarker for beta cell mass, reliable quantification of the uptake is required.

To improve quantification of pancreatic ^{111}In-exendin uptake in this clinical study, a phantom mimicking the human situation was required. Quantitative single photon emission computed tomography (SPECT) is challenging in general (3–5), mostly due to the relatively low detection efficiency as compared to positron emission tomography (PET), and the more complicated attenuation correction. With the use of ordered subset expectation maximization (OSEM) reconstruction and adequate correction methods, quantification of SPECT images is currently viable and attractive (4), and it enables quantification of gamma-emitting radionuclides, like ^{111}In. Imaging and quantification of the pancreatic beta cells with ^{111}In-exendin is even more challenging, due to the high uptake in the nearby kidneys versus the low uptake in the pancreas (1).

The initial reconstructions in this clinical study (1) were made with the SPECT/CT software that we generally use in the clinic, Syngo Flash 3D (Siemens Medical, Erlangen, Germany). This reconstruction algorithm led to a low count rim surrounding the kidneys that should most likely be considered as an artefact. Thereafter, we used another available reconstruction package: Hybrid Recon oncology (Hermes Medical Solutions, Stockholm, Sweden). This reconstruction algorithm also led to image features that should most probably be considered as artefacts; a low count rim surrounding the kidneys was also present, similar to Flash 3D, but less pronounced, and a hotspot in the spinal area was observed. These features are shown in Table 1.

Table 1. Initial findings with reconstruction settings of clinical scans

	Flash3D	Hybrid Recon
Version	Siemens Syngo MI.SPECT applications E.soft 2009a, 8.1.15.7 service pack 2	HERMES P5 Gold 4.6A Hybrid Recon 1.1.2
Reconstruction algorithm	OSEM3D	OSEM3D, MAP_{MRP}, $MAP_{smoothing}$
#iterations - #subsets	6-16	4-16
Attenuation correction	CT-based	CT-based
Scatter correction	Triple energy window, SPECT based	CT, Monte Carlo-based
Both photopeaks of ^{111}In reconstructed	Yes	Yes
Collimator correction	Mathematically calculated 3D cone beam modelling	Mathematically calculated 3D cone beam modelling
Post reconstruction filtering	Gaussian FWHM = 0.84 cm	Gaussian FWHM = 0.84 cm
Most obvious artefacts in the initial human images	Large low-intensity rim around kidneys	Small low-intensity rim around kidneys, somewhat increased intensity in the vertebrae region

As already mentioned, adequate correction methods are a key for quantitative use of SPECT images. Commercial SPECT (CT) reconstruction algorithms have been developed for general purpose imaging, and not specifically to quantify low uptake in a specific organ (pancreas), with high activity in nearby organs (kidneys). The origin of artefacts, their influence on quantification, and sometimes even the presence of artefacts cannot reliably be investigated in human, because the true distribution of the radiotracer is unknown. Also, details about the working of commercially available reconstruction software are not always available to the user; partially, the software is a black box. Therefore, the use of phantoms is of major importance for recognizing and understanding the origin of reconstruction artefacts, and in our case, also to enable reliable quantification in beta cell imaging. Normally, phantoms in nuclear medicine imaging consist of simple geometrical shapes such as spheres, cylinders and rods. However, these are less suitable to mimic the ^{111}In-exendin distribution in the pancreas and kidneys in humans. Therefore, in this study, an anatomical phantom was developed and used.

In the last few years, 3D printing has become an established method for fast and affordable production of advanced and customized phantoms for medical imaging (6–10). We employed this technique to create an anatomical phantom containing a pancreas, two kidneys and a background region for optimizing the SPECT/CT reconstructions to allow quantification of the pancreatic uptake of ^{111}In-exendin in the clinical study (1).

The objective of this work was to mimic human ^{111}In-exendin imaging with this custom-made anatomical phantom to clarify how the human images should be interpreted (e.g.

whether artefacts play a role). This is important in visualization and quantification of the low pancreatic uptake, since this is challenged by relatively high kidney activity. Using the phantom, we assessed different reconstruction settings for two different commercially available software packages and selected the most suitable reconstruction protocol for visualization and quantification of pancreatic ^{111}In-Exendin uptake.

MATERIALS AND METHODS

We designed and printed 3D anatomical inserts representing the pancreas and kidneys that can be placed within the casing of the National Electrical Manufacturers Association (NEMA) NU2 image quality body phantom (11) after removing the standard spheres and cylinder inserts.

This anatomical phantom was filled with known activity concentrations to simulate SPECT imaging of T1D patients (low pancreatic uptake) and healthy humans (higher pancreatic uptake).

All SPECT/CT images were acquired using an integrated SPECT/CT scanner (Symbia T16, Siemens Healthcare, Molecular Imaging, Hoffman Estates, IL, USA) equipped with parallel-hole medium-energy collimators. Software of the before mentioned two vendors (Flash 3D, Hybrid Recon) and different reconstruction settings were tested to find the optimal algorithm and settings. After evaluation of the phantom results, the optimal reconstruction protocol was applied to human data of the clinical study. Details about the phantom development, the experiments and image analysis are described below.

Phantom development

The pancreas and kidney organ models and their relative positions were based on an MRI dataset of a male patient of 87 kg. Forty sequential T2 weighted HASTE images were acquired with a Siemens Magnetom TrioTim 3.0 Tesla MRI scanner as part of another clinical study. The volumes and distances between the organs measured in the MRI images were compared to those in CT images of humans imaged with ^{111}In-exendin, to make sure the anatomy was representative for our study population.

Images were processed in Mimics v.14.0 (Materialise HQ, Leuven, Belgium). Solid 3D models of the kidneys and the pancreas were created from segmentations that were performed on the axial images. The models were smoothed with a first-order Laplacian (70 iterations, smooth factor 0.9) and exported as 3D triangular surface meshes (STL-files). Using the open source software Meshlab (v.1.3.2, http://meshlab.sourceforge.net/), the surfaces were further processed to create a realistic anatomical model; abnormal bulges and sharp edges were removed or smoothed and holes were filled. The solid bodies were

transformed to hollow organ models with a wall thickness of 4 mm with Meshlab and SolidWorks (v. 2012, Dassault Systèmes SolidWorks Corp., Waltham, MA, USA), and flanges were added for fixation of the organs. Then, the organ models were 3D-printed with an Objet Eden250™ printer (Stratasys, Eden Prairie, MN, USA) based on ultra-thin layer PolyJet™ technology. Printer specifications include a layer thickness of 16 µm, tray size of 260×260×200 mm and accuracy of 100 µm. The material used for printing was the transparent standard plastic VeroClear RGD810, which is comparable with PMMA, which has a polymerized density of 1.18–1.19 g/cm3 and Zeff=6.56 (12). This is in the same range as soft tissue with an Zeff=6.35 (12). The non-soluble support material was taken out by hand.

To enable filling with radioactive solution, holes were drilled in the organs, in which nylon screws sealed with rubber O-rings were placed. The printed organs were placed within the NEMA casing and fixated with screw threads in the original screw holes in the lid of the NEMA casing (Fig. 1).

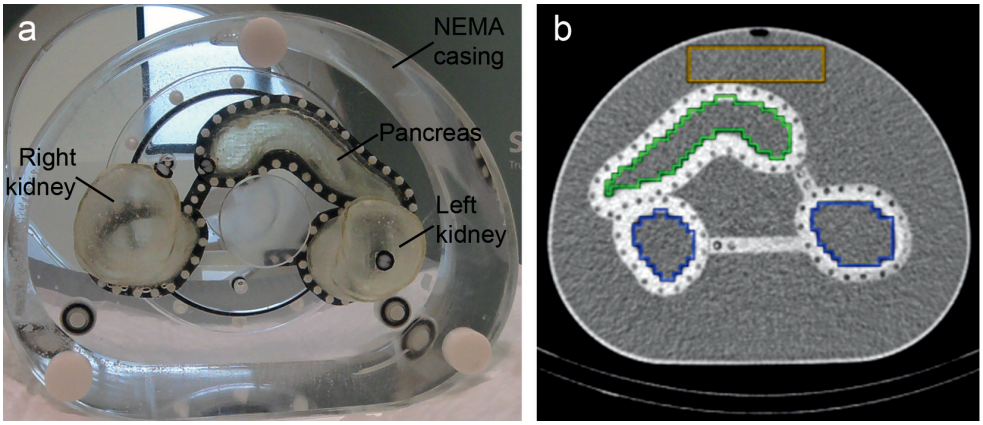


Figure 1. a) A photograph of the 3D-printed pancreas and kidney compartments in the NEMA-NU2 image quality phantom casing. B) A CT cross-section of the phantom showing the regions of interest in the kidneys, pancreas and background

The volumes of the pancreas and kidney inserts were measured by weighing the organs empty and filled with water. The volume of the background in the NEMA casing was measured by filling it with water with a graduated cylinder.

Reconstruction software

Reconstruction software Flash 3D and Hybrid Recon were used. In both software packages, a 3D ordered subset expectation maximization (OSEM3D) algorithm was available. In Hybrid Recon also, a maximum a posteriori (MAP) algorithm with a smoothing prior (MAPsmoothing) and with a median root prior (MAPMRP) was available. With the smooth-

ing prior, it is hypothesized that the pancreas activity is more homogeneously distributed in the images. The MAPMRP preserves edges and hotspots more than the smoothing prior but also assumes a locally monotonic image (13). Scatter, CT map-based attenuation and collimator correction were applied as available in the reconstruction software. Reconstruction settings are given in the experiment descriptions ('Phantom experiment 1' and 'Phantom experiment 2'), and more details about the reconstruction software and methods are given in Table 1.

Phantom experiment 1—high pancreas activity (simulating healthy individuals)

This first experiment aimed to investigate the different reconstruction software and settings in a simulation of ^{111}In-exendin imaging in non-diabetic, healthy human (relatively high pancreas uptake compared to T1D patients). Activity concentrations for the pancreas, kidneys and background in the phantom were based on an estimation of the uptake of ^{111}In-exendin in Flash 3D reconstructions of the first three healthy humans from the clinical study (1). As a measure for the uptake, the number of reconstructed counts in the pancreas, kidneys and background of these humans was retrieved by delineating the pancreas and kidneys and a background volume using the Inveon Research Workplace (IRW) software (Siemens Inc, Munich, Germany). The corresponding amount of ^{111}In activity to be inserted into the phantom compartments was calculated by multiplying these intensities with a calibration factor determined from SPECT imaging of a cylindrical phantom with the same acquisition and reconstruction settings as the human SPECT scans. The pancreas-to-kidney activity concentration ratio was 1:57, the pancreas-to-background ratio 1:0.005. Table 2 provides the volumes of the compartments and the amount of ^{111}In activity within the compartments. To avoid sticking of ^{111}In to the phantom wall, 0.05% Tween was added to the solution.

Table 2. Phantom and filling characteristics

		Pancreas	Left kidney	Right kidney	Background	Pancreas-to-kidney ratio
	Volume (mL)	82	206	222	$9.26 * 10^{3}$	
Experiment 1	Activity concentration ^{111}In at start time of the scan (MBq/mL)	$3.94*10^{-3}$	0.226	0.226	$2.11*10^{-5}$	1:57
	Total activity ^{111}In at scan time (MBq)	0.32	46.6	50.2	0.20	
Experiment 2	Activity concentration ^{111}In at scan time (MBq/mL)	$1.93*10^{-3}$	0.209	0.209	$2.10*10^{-5}$	1:108
	Total activity ^{111}In at scan time (MBq)	0.16	43.1	46.5	0.19	

The acquisition protocol for the phantom imaging was the same as used for humans imaged with ^{111}In-exendin at our department (1). To avoid possible incorrect handling of different detector-to-object distances and disturbing quantitative use of the images, the phantom was scanned with a fixed radius of rotation (25 cm), a fixed bed height (13 cm) and 128 views in step-and-shoot mode (64 views per camera head) with an acquisition time of 40 s per view. Symmetric 15% energy windows over the 171 and the 245 keV photopeaks were used, with additional 7% lower and upper scatter windows, resulting in a total of six energy windows per scan.

To determine the optimal number of iterations and subsets in the reconstruction protocols, different settings were applied, in OSEM3D, based on the available combinations; 6/16 (6 iterations and 16 subsets), 12/16, 12/32, 18/16, 18/32, 24/32, 30/32 and 32/32 for Hybrid Recon were chosen and 3/16, 6/16, 6/62, 12/16, 12/32, 18/16, 18/32, 24/16, 24/32, 30/16 and 30/32 for Flash 3D. Preliminary tests showed that quantification improved with increasing the numbers of iterations and subsets. We therefore used higher numbers compared to what is commonly applied in clinical use (knowing this would increase inhomogeneity).

The analysis of the results was performed as will be described in the subsection 'phantom image analysis'.

Phantom experiment 2 - low pancreas activity (simulating T1D patients)

The second experiment was performed for further verification of the findings of the first experiment, with experimental settings that simulate the T1D patients we imaged with ^{111}In-exendin. In T1D patients, the pancreas uptake is even lower than in healthy human. Visualization of the lower uptake is even more demanding regarding the reconstruction protocol. Therefore, for further investigation of reconstruction details, we chose to use this T1D simulation instead of the simulation of a healthy situation in experiment 1.

Phantom filling was based on measurements in T1D patients of the clinical study (1). The pancreas-to-kidney activity concentration ratio was 1:108, the pancreas-to-background ratio 1:0.01. Activity concentrations in each compartment are shown in Table 2. Acquisition was performed with the same settings as in experiment 1. In the first experiment, reconstructions performed with Hybrid Recon led to more representative activity ratios (see results, 'Activity concentration ratios in the phantom images'). Therefore, Hybrid Recon was used for reconstruction of the data in this second experiment, and more reconstruction settings were examined. Not only OSEM3D but also $MAP_{smoothing}$ and MAP_{MRP} reconstructions were made. The $MAP_{smoothing}$, MAP_{MRP} and OSEM3D images were reconstructed with three sets of iterations and subsets: 6/16, 12/16 and 18/32.

After analysing these different reconstruction methods, we also paid attention to the effect of several correction settings (scatter correction (SC), attenuation correction (AC) and collimator correction (CC)) on the pancreas visualization and quantification. Reconstructions using OSEM3D were performed with all corrections, with CC and AC, with only CC, and without corrections. Other correction combinations were not available in the software.

Phantom image analysis

All phantom images were visually assessed, and intensities of the different compartments were determined, to decide which reconstruction software and settings lead to the best images for quantification of the ^{111}In-exendin uptake in the pancreas.

Visual assessment focussed on homogeneity within the pancreas and kidneys, on artefacts, and on the position of the pancreas in the CT images compared to the position in the SPECT images.

For quantitative analysis, pancreas and kidneys were manually delineated as volumes of interest (VOI) on CT using the IRW software. In the background, a box-shaped VOI was defined anterior of the pancreas compartment (Fig. 1b). As a measure for the uptake, the average number of reconstructed counts per voxel was retrieved for all VOIs. In order to keep it concise, in this manuscript we call the number of reconstructed counts per voxel, 'intensity'.

Recovery of activity was calculated as the measured intensity (counts/ml) divided by the real activity concentration (Bq/ml). Also, pancreas-to-background and pancreas-to-kidney intensity ratios were calculated and compared to the real activity concentration ratios.

Verification of phantom-based optimization on human images

As a final test, the optimized reconstruction protocol determined from the phantom experiments will be applied to data of the clinical study (1). These images were acquired with the same acquisition settings as both phantom experiments and were acquired 24 hours after injection, within the same imaging session as the low-dose CT. SPECT imaging took about 45 min.

RESULTS

SPECT imaging of the 3D-printed phantom (Fig. 1) led to images that were similar to human images in terms of visualization of the pancreas and kidneys and artefacts (Fig. 2).

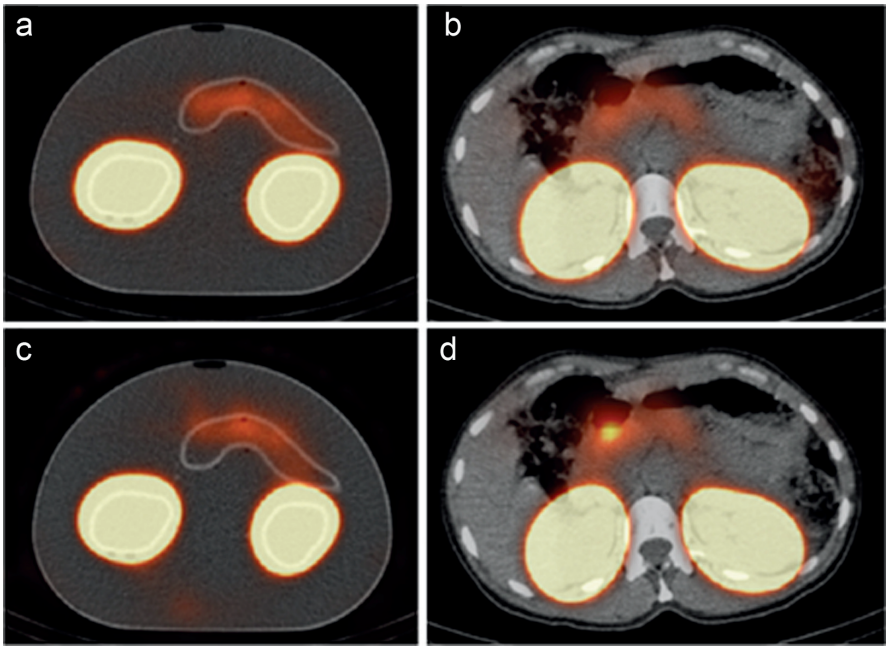


Figure 2. Reconstructed SPECT/CT images of the phantom from experiment 1 (**a**, **c**) and a healthy human (**b**, **d**). **a**, **b** Images made with Hybrid Recon OSEM3D and **c, d** Flash 3D OSEM3D images. All reconstructions were performed with 6 iterations and 16 subsets and used attenuation, scatter, and collimator correction

Homogeneity and intensity within the 3D-printed organs

Increasing the number of iterations or subsets led to noisier images, which resulted in more spots in the pancreas (Fig. 3 for Hybrid Recon, Flash 3D gives similar results). In humans, these spots in the pancreas could easily be misinterpreted as inhomogeneous uptake of ^{111}In-exendin, which could be related with the patient having an insulinoma.

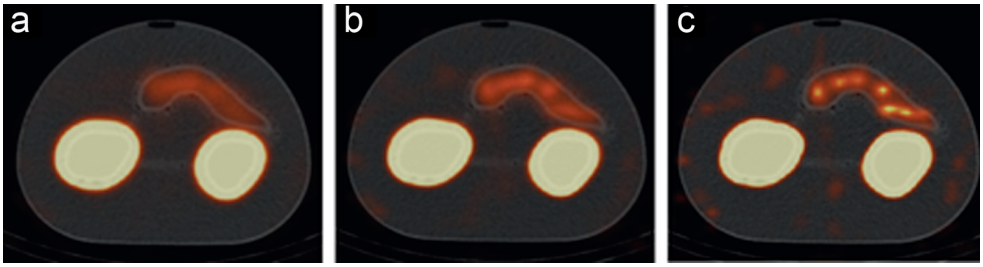


Figure 3. The effect of increasing the number of iterations: image **a** was made with 6 iterations and 16 subsets, **b** with 12 iterations and 32 subsets and **c** with 32 iterations and 32 subsets. All images were reconstructed with Hybrid Recon OSEM3D with attenuation, collimator and scatter correction. Window and level settings are the same in all images and were chosen so that the pancreas was visible

In Flash 3D reconstructions, the intensity in the tail and the edge of the head of the pancreas (close to the kidney) was lower compared to that in the other parts of the pancreas. Also, it seems that the pancreas position on SPECT is more towards anterior compared to CT (Fig. 2c). In Hybrid Recon, the position of the pancreas is similar in SPECT and CT, and the intensity was more homogeneous across the entire pancreas. For a high number of iterations (18 iterations, 32 subsets) in Hybrid Recon, the intensity distribution in the pancreas was more homogeneous with the MAP reconstructions compared with the OSEM3D reconstruction.

In both Flash 3D and Hybrid Recon, the intensity in the kidneys is high and not homogeneously distributed (see 'Artefacts in the phantom images' and Fig. 4a). However, the intensity was similar for the different reconstruction settings within Flash 3D as well as within Hybrid Recon.

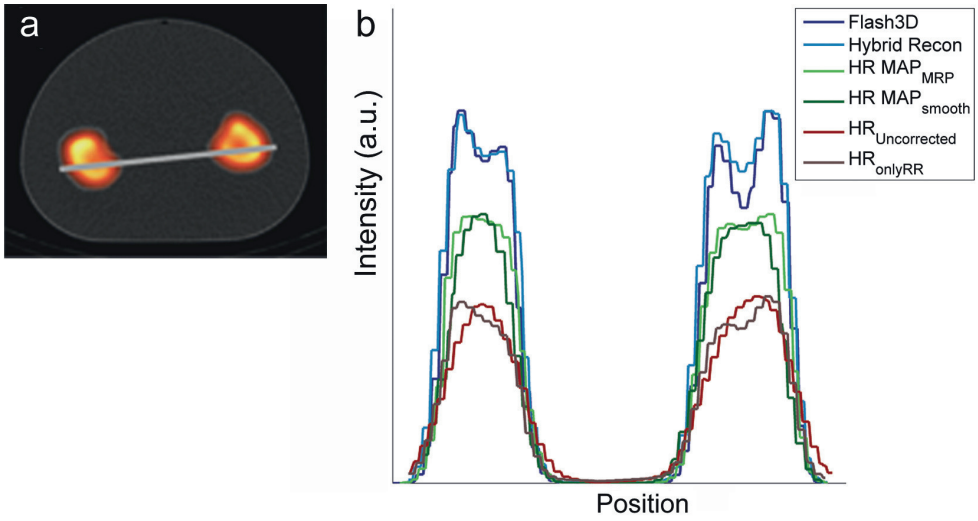


Figure 4. a) The Hybrid Recon OSEM3D reconstruction of the phantom with attenuation, collimator and scatter correction, 6 iterations and 16 subsets. The window/level was scaled such that variations in intensity in the kidneys were visible. **b)** Line profiles through the kidneys (line positioned as in **a** for a Hybrid Recon and Flash 3D reconstruction with 6 iterations and 16 subsets, attenuation scatter and collimator correction

The effect of the corrections was tested with Hybrid Recon OSEM3D and MAPMRP with 6 iterations and 16 subsets in the second experiment. As default, we used all the corrections. Only to investigate the effect of corrections on the images, we limited the use of corrections and made several reconstructions. As expected, AC results in a large increase in the number of counts in the whole phantom. Notably, applying the SC on top of the AC and CC influences the low intensity areas (pancreas and background) more than the high intensity areas (kidneys). In the kidneys, the measured activity concentration

decreased by 15%, while a decrease of 71% and 88% was seen in the pancreas and the background, respectively. The reconstructed images with the available correction combinations (CC + AC + SC, none, CC and CC + AC) are shown in Fig. 5. All three corrections were required to be able to identify the pancreas in the second experiment, simulating the low pancreas activity.

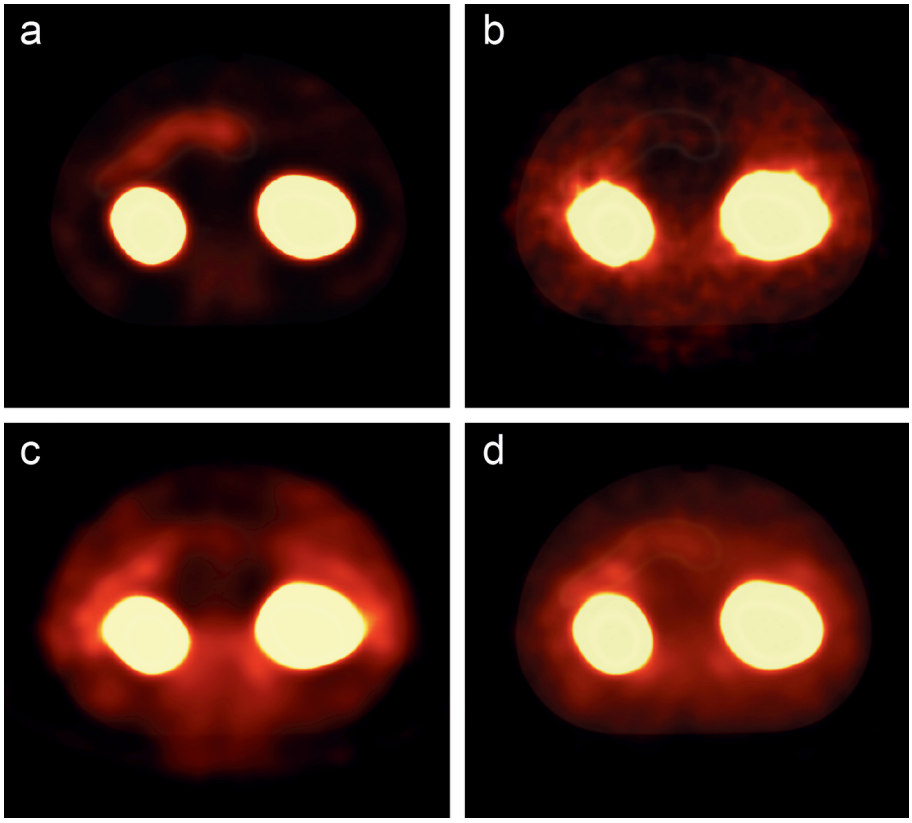


Figure 5. Images from the second experiment, all reconstructed using HybridRecon OSEM3D with 6 iterations and 16 subsets and different corrections. In **a**, collimator, attenuation and scatter correction was applied; in **b**, no corrections were applied; in **c**, only collimator correction was applied; and in **d**, collimator and attenuation correction was applied. Activity in the pancreas was only observed well if all corrections were applied

Artefacts in the phantom images

In all Flash 3D and Hybrid Recon reconstructions with CC, there seems to be a high intensity rim inside the kidneys, as if there was a cortex in the phantom with a higher activity (Fig. 4a); these images also show a low-intensity shell around the kidneys (Fig. 6). This ring artefact with under- and overshoot appears like the Gibbs phenomenon. In the Flash 3D images, the low-intensity rim is more pronounced than in the Hybrid Recon reconstruc-

tions. In the OSEM3D reconstructions without CC and in the MAP reconstruction, this artefact did not appear (Fig. 6b).

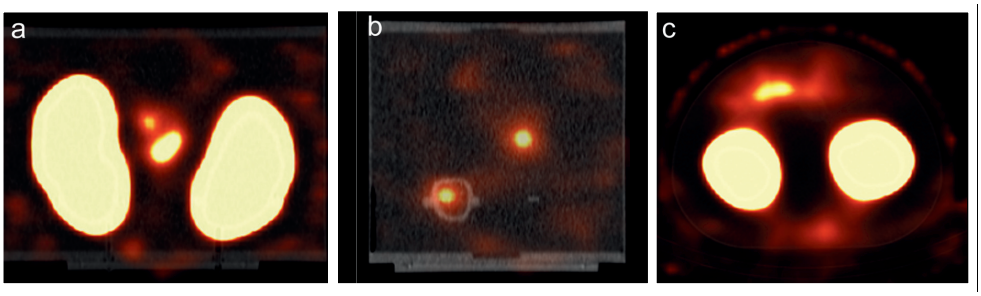


Figure 6. Phantom images from the first experiment reconstructed with Hybrid Recon (**a** coronal view, **b** sagittal view) and Flash 3D (**c** axial view) using 12 iterations and 16 subsets. Scaling was adjusted such the low background intensity is visible. The image reconstructed with Hybrid Recon shows hotspots in the centre between the kidneys (**a**, **b**) with similar intensity as the pancreas between the kidneys, as shown in **b**. In the Flash 3D reconstructed image, a higher intensity region is observed at the back of the phantom. Furthermore, in both images in the background, a low count rim around the kidneys can be observed

Both Hybrid Recon and Flash 3D showed an area in the background in which the intensity is higher than the average background intensity. For Hybrid Recon, this area is located between the kidneys; in Flash 3D, this area is less intense and located more at the back, centrally posterior to the kidneys (Fig. 6). With MAPsmoothing, this artefact was least pronounced.

Activity concentration ratios and recovery in the phantom images

Figure 7a, b shows the pancreas-to-kidney intensity ratio for reconstructions with Hybrid Recon and Flash 3D with different numbers of iterations and subsets of the experiments 1 and 2. For both reconstruction programmes, the pancreas-to-kidney ratio increases with an increasing number of iteration times the number of subsets. In experiment 1, the ratio of the Hybrid Recon reconstruction is closer to the real ratio than the Flash 3D ratio.

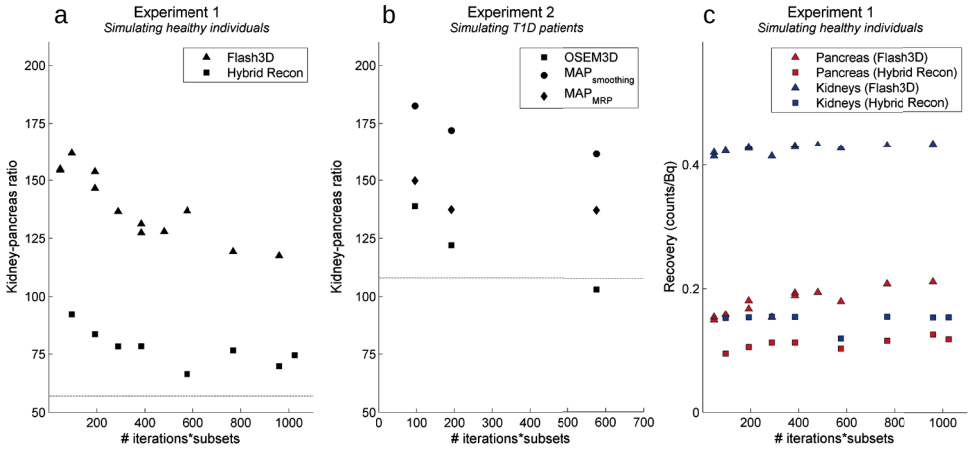


Figure 7. Measured kidney-to-pancreas intensity ratios (as 1/pancreas-to-kidney ratio) in experiment 1 and 2. **a** Measured kidney-to-pancreas intensity ratio for Flash 3D and Hybrid Recon OSEM3D reconstructions in the first experiment. **b** Measured kidney-to-pancreas ratio for Hybrid Recon OSEM3D, MAP-MRP and MAP-smooth reconstructions in the second experiment. Both figures show the measured intensity ratios. The actual activity concentration ratio, based on the real activity concentrations in the 3D-printed organs, is depicted by the *striped lines*. **c** Recovery on the *y*-axis calculated as reconstructed counts/inserted activity (counts/ml)/(Bq/ml). *OSEM* ordered subset expected maximum, *MAP* maximum a posteriori, *MRP* median root prior.

In experiment 2, the OSEM3D reconstruction leads to more realistic ratios than the MAP reconstructions. For 12 iterations with 16 subsets, the pancreas-to-kidney ratio is 1:122 with OSEM3D, 1:137 for MAPMRP and 1:172 for MAPsmoothing, while the real ratio was 1:108.

The average pancreas-to-background ratios from respectively the Flash 3D and the Hybrid Recon OSEM3D reconstructions were 1:0.21 and 1:0.037. The actual ratio was 1:0.005. Within Hybrid Recon, the OSEM3D reconstructions (compared to the MAP reconstructions) lead to ratios that were closest to the actual ratio although large variation can occur due to the low background activity concentration.

Increasing the number of iterations and subsets resulted in increased intensities, demonstrated by the uncorrected recoveries of activities in Fig. 7c. Relatively, this increase was larger in the pancreas than in the kidneys and larger in Flash 3D compared to Hybrid Recon. As an example, comparing 6/16 and 30/32, the relative increase is approximately 35% in the pancreas (Flash 3D 42%, Hybrid Recon 25%) and around 3% in the kidneys (Flash 3D 3.2%, Hybrid Recon 1.4%). In addition, recovery of activity was larger in the kidneys than in the pancreas; this difference was smaller in Hybrid Recon than in Flash 3D (Fig. 7c), corresponding with the more realistic ratios with Hybrid Recon.

Verification of results on human images

After comparing the results of the different reconstruction protocols, Hybrid Recon with the OSEM3D reconstruction with 6 iterations, 16 subsets, SC, AC and CC was selected for reconstruction of the human data of our clinical trial (1) (Fig. 2b). Small differences can be observed between this Hybrid Recon reconstruction and the initial Flash 3D reconstruction (Fig. 2d). In Hybrid Recon, the intensity within the background and the pancreas is more homogeneous compared in Flash 3D, and a difference in shape of the pancreas is observed. The human SPECT images are similar to the phantom images reconstructed with the optimal Hybrid Recon settings (Fig. 3a) and initial Flash 3D settings (Fig. 3c).

DISCUSSION

We have developed a phantom that mimics the human situation for ^{111}In-exendin imaging, by 3D-printing pancreas and kidney compartments for insertion into the NEMA NU2 image quality phantom casing. The phantom was used for optimization of SPECT reconstruction. Available non-anatomical phantoms mimic the human ^{111}In-exendin images of the pancreas and kidneys less accurately. Our 3D-printed phantom led to images that, including artefacts, appeared similar to human ^{111}In-exendin images.

The inserted activity in each compartment of the phantom was homogeneously distributed, and therefore, in the reconstructed images, the measured intensity should also be homogeneous. Lower numbers of iterations and subsets gave a more homogeneous intensity, especially in the pancreas. As a result of the incorporated smoothing or median root priors, the images from MAP reconstructions were smoother and more homogeneous within the compartments than the OSEM3D images. Nevertheless, in human, these MAP reconstructions could only be used with a lot of caution because in some human, the true pancreatic spatial distribution of activity need not be homogeneous due to a higher glucagon-like peptide-1 (GLP-1) receptor expression in certain areas of the pancreas, e.g. in the case of an insulinoma. The use of a prior with too much smoothing could reduce the visibility of such regions.

The same applies to filtering. In order to 'keep the activity in the organ' and preserve actual hotspots, we used limited filtering (a Gaussian kernel with FWHM of 0.84 cm for Flash 3D and 0.96 cm for Hybrid Recon, corresponding to about twice the voxel size, therewith fulfilling the Nyquist criterion). A larger filter could have been used to obtain smoother images; however, the herewith increased possibility of homogeneous visualization of actually inhomogeneous uptake would have negatively affected the assessment of optimal algorithm performance.

Increasing the number of iterations and subsets improves the recovery of activity in the pancreas (Fig. 7c) and the pancreas-to-kidney ratio (Fig. 7a). It is generally recognized that in iterative reconstructions, more spatial details are visualized when increasing the number of iterations (14). However, when using too many iterations also, the image noise increases (15). This leads to increased inhomogeneity in the pancreas, which, again, would not correspond to the actual activity distribution.

A limitation of the phantom is its static nature: In the phantom, the activity is distributed homogeneously within the compartments, and in contrast to patients, there is no movement of organs during the acquisition. In patients, breathing and potentially inhomogeneous distribution of beta cells can induce hotspots within the pancreas.

The Hybrid Recon OSEM3D reconstruction with a relatively low number of iterations and subsets was chosen for the human reconstructions. Extrapolation on Fig. 7a, c indicates that a lower number of iterations and subsets would worsen the pancreas-to-kidney ratio and the recovery of activity in the pancreas.

Scatter correction reduces the intensity in the pancreas more strongly than in the kidney. Possibly, an overcorrection in the pancreas area could explain why the actual pancreas-to-kidney ratio could not be reached with the used protocols. Visually, on the SPECT image, the Gibbs artefact, which was introduced by the collimator correction, seems to be more pronounced in Flash 3D (Fig. 6). However, quantitatively, the difference between Flash 3D and Hybrid Recon was less pronounced (see line profile in Fig. 4b); both have a very low number of counts in the surrounding of the kidneys (lower than the background activity).

It appears that the position of the pancreas is more anterior in the Flash 3D reconstructions (Fig. 2c). This might also be caused by the Gibbs artefact that 'absorbs' a part of the counts in the pancreas. Therefore, it seems that the pancreas is visualized more anteriorly compared to the images reconstructed with Hybrid Recon.

All corrections, SC, CC and AC, were required to distinguish the pancreas in the second experiment; thus, all corrections are necessary in beta cell imaging with ^{111}In-exendin.

So, finally, we selected the reconstruction method that resulted in an optimal visualization of the pancreas and optimal quantitative performance (i.e. pancreas-to-kidney ratio). Hybrid Recon with an OSEM3D reconstruction with 6 iterations, 16 subsets, SC, CC and AC was herewith selected and used for the clinical study. With a different imaging purpose, the optimal settings may be different.

CONCLUSION

3D-printing of a phantom that mimics the human pancreas and kidneys was showed to be useful for optimization of ^{111}In-exendin imaging. Phantom experiments enabled optimization of the reconstruction protocol in clinical studies. This work contributed to clarify the relationship between SPECT ^{111}In-exendin images and the actual situation in humans. So, the use of this custom-made phantom provided essential information for beta cell quantification.

REFERENCES

1. Brom M, Woliner-van der Weg W, Joosten L, Frielink C, Bouckenooghe T, Rijken P, et al. Non-invasive quantification of the beta cell mass by SPECT with 111In-labelled exendin. Diabetologia. 2014;57:950–9. doi: 10.1007/s00125-014-3166-3.
2. Woliner-van der Weg W, Brom M, Behe M, Tack CJJ, Boerman OC, Janssen MJR, et al. SPECT imaging of In-111-exendin in patientswith type 1 diabetes and healthy controls. Eur J Nucl Med Mol Imaging. 2014;41:S311–S.
3. Ritt P, Vija H, Hornegger J, Kuwert T. Absolute quantification in SPECT. Eur J Nucl Med Mol Imaging. 2011;38:S69–77. doi: 10.1007/s00259-011-1770-8.
4. Bailey DL, Willowson KP. An evidence-based review of quantitative SPECT imaging and potential clinical applications. J Nucl Med. 2013;54:83–9. doi: 10.2967/jnumed.112.111476.
5. Bailey DL, Willowson KP. Quantitative SPECT/CT: SPECT joins PET as a quantitative imaging modality. Eur J Nucl Med Mol Imaging. 2014;41:S17–25. doi: 10.1007/s00259-013-2542-4.
6. Gear JI, Long C, Rushforth D, Chittenden SJ, Cummings C, Flux GD. Development of patient-specific molecular imaging phantoms using a 3D printer. Med Phys. 2014;41:082502. doi: 10.1118/1.4887854.
7. Driscoll B, Keller H, Coolens C. Development of a dynamic flow imaging phantom for dynamic contrast-enhanced CT. Med Phys. 2011;38:4866–80. doi: 10.1118/1.3615058.
8. Beekman FJ, Vastenhouw B, van der Wilt G, Vervloet M, Visscher R, Booij J, et al. 3-D Rat brain phantom for high-resolution molecular imaging. P Ieee. 2009;97:1997–2005. doi: 10.1109/JPROC.2009.2028363.
9. Bieniosek MF, Lee BJ, Levin CS. Technical note: characterization of custom 3D printed multimodality imaging phantoms. Med Phys. 2015;42:5913–8. doi: 10.1118/1.4930803.
10. Mayer R, Liacouras P, Thomas A, Kang M, Lin L, Simone CB., 2nd 3D printer generated thorax phantom with mobile tumor for radiation dosimetry. Rev Sci Instrum. 2015;86:074301. doi: 10.1063/1.4923294.
11. Association NEM . Performance measurements of positron emission tomographs. Rosslyn: Association NEM; 2007. NEMA Standards Publication NU 2-2007.
12. Bos AJ, Draaisma FS, Okx WJ. Inleiding tot de stralingshygiëne. Den Haag: Sdu Uitgevers bv; 2007.
13. Kangasmaa T, Sohlberg A, Kuikka JT. Reduction of collimator correction artefacts with bayesian reconstruction in spect. Int J Mol Imaging. 2011;2011:630813. doi: 10.1155/2011/630813.
14. Cherry SR, Sorensen JA, Phelps ME. Physics in nuclear medicine. Philadelphia: Saunders, Elsever inc.; 2012.
15. Boellaard R, Krak NC, Hoekstra OS, Lammertsma AA. Effects of noise, image resolution, and ROI definition on the accuracy of standard uptake values: a simulation study. J Nucl Med. 2004;45:1519–27.



4

Assessing scatter-based artefacts caused by high organ uptake in ^{68}Ga-exendin PET/CT using a 3D-printed phantom

L.N. Deden[1,2], A.P.W. Meeuwis[1], M. Buitinga[1,3,4], M. Boss[1], I. Rausch[5], T. Beyer[5], E.P. Visser[1], M. Gotthardt[1], D. Lobeek[1]

Submitted

ABSTRACT

Introduction: PET quantification of the pancreatic accumulation of [^{68}Ga]Ga-exendin-4 (^{68}Ga-exendin-4) is challenged by spill-over or photopenic artefacts, as observed especially in patients with obesity. Using a 3D printed pancreas-kidney phantom in body casings mimicking individuals with normal weight (NW), overweight (OW) and severe obesity (OB) we investigated the effect of scatter-related artefacts on the quantification of pancreatic uptake in ^{68}Ga-exendin-4 PET/CT. In addition, the effect of adjustments in acquisition time (AT) and reconstruction methods was explored.

Methods: The phantom was filled with ^{68}Ga-activity concentrations corresponding with human ^{68}Ga-exendin-4 PET/CT. Images were reconstructed for AT of 5, 7, 10 and 20 minutes from list-mode data. The effect of prompt gamma correction (PGC) and absolute versus relative scatter scaling on reconstructed PET images was explored. Activity concentration (AC) was measured in spherical volumes in the the kidneys and pancreas. Recovery coefficients (RC) were calculated as $AC_{measured}/AC_{known}$ * 100%.

Results: The phantoms mimicked human ^{68}Ga-exendin-4 PET/CT very well. In the NW and OW phantoms no artefacts occurred, but a large photopenic artefact occurred in the OB phantom. Visually, PGC prevented minor spill-over artefacts in the OW phantom, but did not affect the photopenic artefact in the OB phantom. Absolute instead of relative scatter scaling did not reduce or resolve artefact occurrence neither. Increasing AT did not affect PET/CT reconstructions visually. However, it improved pancreas RC in the OB phantom, although RC remain low (max 52%±23%). In the NW and OW phantom pancreas RC was 77±4.5% and 80±4.1%. The pancreas body was largely unaffected by the photopenic artefact, reflected by similar RC values in all phantoms (80 ± 16%, 77 ± 14%, 73 ± 27%, for NW, OW and OB respectively, AT=10 minutes).

Conclusion: In the presence of a large photopenic artefact in the OB phantom, the RC of the whole pancreas was unreliable. The effect was only limited on the pancreas body. Most optimal settings included acquisition times of at least 7 minutes per bed position and applying prompt gamma correction for PET reconstruction. However, these settings did not reduce or prevent the appearance of a photopenic artefact in the OB phantom.

INTRODUCTION

A promising technique to improve our understanding of changes in beta cell mass and its role in type 1 and type 2 diabetes is [^{68}Ga]Ga-exendin-4 positron emission tomography/computed tomography (^{68}Ga-exendin-4 PET/CT) (1-3). Until now, beta cell mass has mainly been studied using immunohistochemical analysis of resected or postmortem pancreatic tissue. As a result, beta cell mass is determined only in small tissue samples and is our understanding of changes in global beta cell mass in the whole pancreas limited. By using ^{68}Ga-exendin-4 PET/CT beta cell mass can be visualizes and quantified. The radiotracer [^{68}Ga]Ga-exendin-4 (^{68}Ga-exendin-4) binds to the GLP-1 receptor, which is highly expressed on beta cells of the human pancreas. This radiotracer is internalized into the beta cell. The amount of uptake has been correlated with beta cell mass. Quantification of the pancreatic uptake of ^{68}Ga-exendin-4 allows us to measure beta cell mass which linearly correlates to activity concentrations in the pancreas (1-4).

Reliable quantification of the pancreatic accumulation of ^{68}Ga-exendin-4 is however challenged by image artefacts, as have been recognized in human studies (e.g. Clinicaltrial.gov numbers NCT03189953, NCT02542059, NCT03182231, NCT03182192). Especially photopenic artefacts, also called halo or washout artefacts, have been observed in individuals with overweight or obesity (see Figure 1). These artefacts can be induced by incorrect scatter correction during PET reconstruction. Important factors contributing to the appearance of these artefacts are likely the large tissue-to-background ratio due to the high retention of the radiotracer in the kidney and large body sizes in individuals with obesity. When the number of scatter events is being overestimated and the scatter estimate becomes larger than the measured counts, a photopenic artefact appeared in the reconstructed PET image (5).



Figure 1. Maximum intensity projections of ^{68}Ga-exendin-4 PET of participants of a human study (NCT03182231), with normal weight (NW), overweight (OW) and obesity (OB).

Commonly used scatter correction methods are based on the single scatter simulation algorithm, which estimates the shape of the scatter contribution (6, 7). This scatter estimate is scaled to the PET data. For scaling, two methods can be applied: relative or absolute scatter scaling. Relative scatter scaling is the standard in clinical setting. The scatter estimate is scaled by fitting the data to the tail of the PET data. This tail is the data outside the contours of the individual which are assumed to only consist of scatter events. Another method for scaling the scatter estimate is absolute scaling. This method does not use the PET emission data for scaling the scatter estimate (5). Using absolute scaling in scatter reconstruction may reduce the appearance of photopenic artefacts, as observed in clinical ^{68}Ga-PSMA PET/MR (5).

Methods to improve PET/CT in larger individuals in general include longer acquisition times, applying point spread function (PSF) and time of flight (TOF) (8, 9). Longer acquisition times may also reduce the occurrence of photopenic artefacts (10). In addition, prompt gamma correction and adaptions in scatter correction methods may also reduce the appearance of photopenic artefacts in PET/MRI using ^{68}Ga-labeled radiotracers. However, these improvements did not resolve scatter-related artefacts completely or were not available and tested for ^{68}Ga PET/CT (5, 10-12).

The effect of photopenic artefacts on the quantification of pancreatic uptake of ^{68}Ga-exendin-4 and the effect of increasing acquisition time, prompt gamma correction and absolute scatter scaling on the appearance of photopenic artefacts in ^{68}Ga-exendin-4 PET/CT has never been investigated before. Therefore, aim of this study was to investigate if pancreatic accumulation of ^{68}Ga-exendin-4 can be measured reliably on ^{68}Ga-exendin-4 PET/CT, especially in the presence of photopenic artefacts in individuals with larger body sizes. In addition, the effect on reconstructed PET images and pancreatic activity quantification of extended acquisition times, prompt gamma correction and absolute versus relative scatter scaling were explored. Regular available PET phantoms cannot mimic ^{68}Ga-exendin-4 tracer distribution, pancreas and kidney anatomy and larger body sizes and are not useful. Therefore, we used a specifically developed 3D-printed phantom of the pancreas and kidneys inserted in enlarged body casings simulating individual with overweight and obesity

MATERIALS AND METHODS

Phantom design

Previously, a 3D-printed insert of the pancreas and kidneys was developed by Woliner et al., based on a MRI dataset of a male with normal weight (13). The 3D-printed organs were placed in the National Electrical Manufacturers Association (NEMA) NU2 image quality body phantom to mimic the distribution of ^{68}Ga-exendin-4 in a normal weight individual (13, 14). To simulate increasing body sizes in overweight and obesity, two enlarged body casings that were similarly shaped as the NEMA NU2 phantom were designed (Figure 2) (15). The standard NEMA casing mimics a normal weight (NW) individual with a waist size of 85 cm and normal BMI (18-25 kg/m^2). Waist size and BMI of the custom-made cases were based on measurements of patients who underwent gastric bypass surgery. The custom-made body cases mimic individuals with overweight (OV), with corresponding waist of 100 cm and BMI of 28-32 kg/m^2, and individuals with severe obesity (OB), with corresponding waist size of 130 cm and BMI of 40-45 kg/m^2.

Phantom experiments

A PET/CT study of all phantoms was performed. The kidneys, pancreas and background were filled with a homogeneous solution of Gallium-68. Aimed activity concentrations were 2.2, 35.0 and 0.041 kBq/ml in the pancreas, kidneys and background compartment respectively. These activity concentrations were based on concentrations as determined from ^{68}Ga-exendin-4 PET/CT scans of participants in ongoing studies (NCT02542059, NCT03182192). These PET/CT scans were performed one hour after injection of 100 MBq ^{68}Ga-exendin-4. (own work, unpublished). All ^{68}Ga-solutions and empty syringes were measured in a clinical radionuclide dose calibrator to obtain the actual injected activity. The actual activity concentrations in all compartments are summarized in table 1.

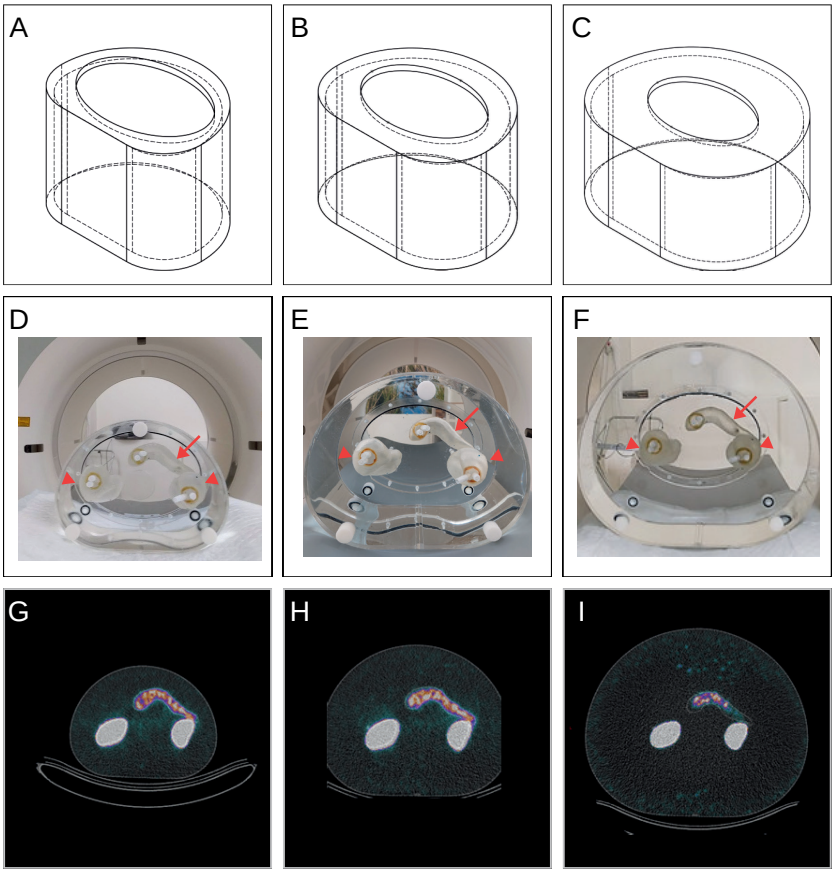


Figure 2. Overview of all three phantoms. From left to right: the normal weight phantom, overweight phantom and obesity phantom. From top to bottom: schematic design of the body cases, pictures of the phantom including 3D printed pancreas-kidney insert and axial slice of the fused PET/CT of the phantoms filled with ^{68}Ga. Arrow heads indicate the kidneys and the arrow the pancreas.

Table 1. Activity concentrations of ^{68}Ga in all compartments in the phantoms at the start of PET/CT acquisition

	Normal weight	Overweight	Obese
Pancreas (kBq/ml)	1.88	2.22	2.08
Kidneys (kBq/ml)	30.2	35.6	33.1
Background (kBq/ml)	0.042	0.052	0.046

PET/CT acquisition and reconstruction

An overview of all image reconstructions with the different settings for acquisition time (AT), time frames selected from the list-mode data and the applied corrections for scatter, attenuation and prompt gamma's is shown in table 2.

Image acquisition was performed using the Siemens Biograph 40mCT PET/CT system (software version VG60A) (Siemens Healthcare, Erlangen, Germany). All PET data were acquired in list mode for 20 to 30 minutes in a single bed position. All PET acquisitions were followed by a low dose CT which was acquired following clinical protocol and used for attenuation correction (automatically modulated X-ray tube voltage and current using Care kV and Care Dose4D on [100-140 kV, 50 mAs reference]; rotation time = 0.5 s; pitch = 1.0; 512×512 voxels; 0.98 pixel spacing). All CT images were reconstructed with a B31f convolution kernel and slice thickness of 2 mm.

From the list-mode PET data, image reconstructions from the first 5, 7, 10 and 20 minutes of the acquisition were derived. Images were reconstructed using ordered subset expectation maximization (OSEM) using 3 iterations and 21 subsets, including point spread function (PSF) and time-of-flight (TOF), and with a 3 mm full width at half maximum post-reconstruction Gaussian filter. Image voxel size was 2.0 x 2.03 x 2.03 mm. Correction for attenuation, scatter (single scatter simulation with relative scatter scaling [model-based]), prompt gamma, decay, randoms and dead time were applied. For visual assessment, image reconstructions without scatter correction (SC) and without SC and attenuation correction (AC) were performed for acquisition of 5 minutes (first 5 minutes from-list mode data).

In addition, image reconstructions with SC using relative scatter scaling (SC_{rel}) and absolute scatter scaling (SC_{abs}), both without prompt gamma correction (PGC) were performed using vendor provided external reconstruction software. For these reconstruction the longest available acquisition time was derived from the list-mode data (i.e. 20, 35 or 30 minutes for the NW, OW and OB, respectively).

Table 2. Reconstruction parameters of all reconstructed PET images. Correction for decay, randoms and dead time was applied in all image reconstructions.

	AT (time frame from list-mode data) [min]	Corrections	Reconstruction software
Relative SC PET reconstructions	5 (0-5)	AC, SC_{rel}, PGC	PET/CT machine
	7 (0-7)	AC, SC_{rel}, PGC	
	10 (0-10)	AC, SC_{rel}, PGC	
	20 (0-20)	AC, SC_{rel}, PGC	
Uncorrected PET reconstructions	5 (0-5)	PGC	PET/CT machine
	7 (0-7)	PGC	
Only AC PET reconstructions	5 (0-5)	AC, PGC	PET/CT machine
	7 (0-7)	AC, PGC	
Absolute SC PET reconstrcutions	20 to 35 (all available list-mode data)	AC, SC_{abs}	Vendor provided external reconstruction software
	20 to 35 (all available list-mode data)	AC, SC_{rel}	

AT = acquisition time, AC = attenuation correction, SC_{rel} = scatter correction with relative scatter scaling, SC_{abs} = scatter correction with absolute scatter scaling, PGC = prompt gamma correction

Visual assessment

The presence of spill-over or photopenic artefacts was assessed visually by LD and MG. The extent of the scatter artefacts and the degree in which the artefact affected quantification of the pancreas was visually assessed as no artefact (no artefact observed or a small artefact which will probably not affect quantification of activity in the pancreas), a minor artefact (relative small artefact which probably affects quantification in (a part of) the pancreas to some degree), or a large artefact (a large artefact which results in large underestimation of activity concentration in (almost the whole) the pancreas).

Quantitative assessment

For quantitative analyses volumes of interests (VOI) were delineated using Inveon Research Workplace software version 4.1 (Siemens Healthcare, Erlangen, Germany), as shown in Figure 3. In the kidneys, three spherical VOIs of 5.9-6.4 ml were placed in the center of the upper, middle and lower third of the volume. In the pancreas, three ellipsoid VOIs as large as possible, were placed centrally in the pancreas head, body and tail (2.1, 2.0 and 0.63 ml, respectively).

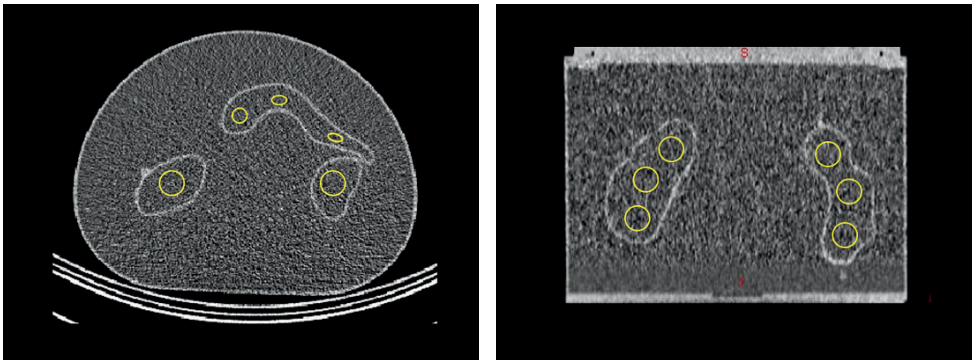


Figure 3. Overview of the spherical VOI placement in the pancreas and kidneys in the NW phantom. In the OW and OB phantom, VOIs were placed identical as in the NW phantom. In the pancreas VOI were placed centrally in the pancreas head, body and tail. In the kidneys the VOI were placed centrally in the top, middle and bottom section.

For pancreas and kidneys, the mean activity concentration and standard deviation were measured from the three VOIs. Activity concentration Recovery Coefficients (RC) were calculated as measured mean activity concentration divided by the true activity concentration multiplied by 100% (mean RC ± SD):

$$\frac{AC_{mean}}{AC_{known}} \bullet 100\,\%$$

Image quality was assessed by the coefficient of variation (CoV) of the activity concentration in the pancreas and kidneys and the size of the photopenic artefact. The CoV was calculated as the standard deviation / mean. The size of the artefact was approximated by the number of voxels with value zero within the phantom volume. All quantitative measures were compared between the normal weight phantom, the overweight and obesity phantom.

RESULTS

Visual assessment

The three different phantom casings resulted in PET/CT images of the kidneys and pancreas that were similar as compared to human ^{68}Ga-exendin-4 PET/CT, as shown in Figure 4A versus 4B).

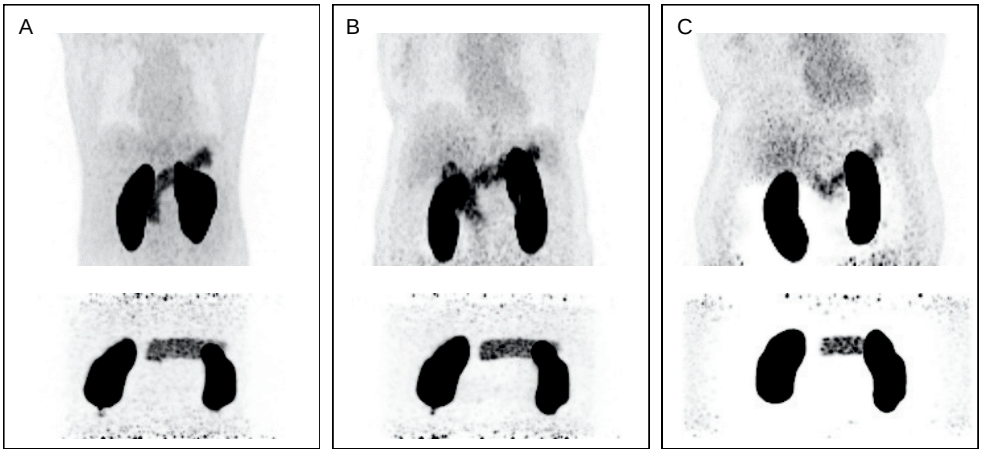


Figure 4. On top, maximum intensity projections of ^{68}Ga-exendin-4 PET of participants of a human study (NCT03182231), with normal weight (NW), overweight (OW) and obesity (OB). In comparison, the maximum intensity projections of the PET of the NW, OW and OB phantom are shown at the bottom. Arrow heads indicate the kidneys and the arrow the pancreas.

Photopenic artefacts appeared similar in the OB phantom as in individuals with obesity, mainly affecting pancreatic head or tail (Figure 1 and 4). The artefacts are induced with applying scatter correction, as seen when comparing uncorrected PET reconstructions (Figure 5F), PET reconstructions with only AC (Figure 5E) and PET reconstruction with AC and SC (Figure 5A-B).

The number of scatter events increased with increasing body size. In the OB phantom and the pancreas can hardly be distinguished from scattering surrounding the kidneys in the scatter-uncorrected PET/CT (Figure 5E). In line, the scatter fraction applied for the scatter correction was over in the OB phantom and around 40% in the NW and OW phantom.

Image reconstructions with SCrel and PGC (Figure 5A-B) showed no artefacts on visual assessment in the NW and OW phantoms and a large photopenic artefact in the OB phantom. Increasing the acquisition time did not affect the artefact in the OB phantom on visual assessment (Figure 5A versus B).

Image reconstruction with SC_{rel} without PGC (Figure 5C), resulted in similar PET images for the NW phantom (no artefacts) and the OB phantom (large photopenic artefact) as the primary image reconstructions performed on the PET/CT machine (SC_{rel} and PGC, Figure 5A-B). In the OW phantom, a minor spill-over artefact was observed (Figure 5C).

The effect of absolute versus relative scatter scaling, without PGC is shown in Figure 5E versus 5F. When SC_{abs} was applied, a large photopenic artefact appeared in all three

phantoms (Figure 5F), while this artefact was absent in the NW and OW phantom when applying SC_{rel} (Figure 5E).

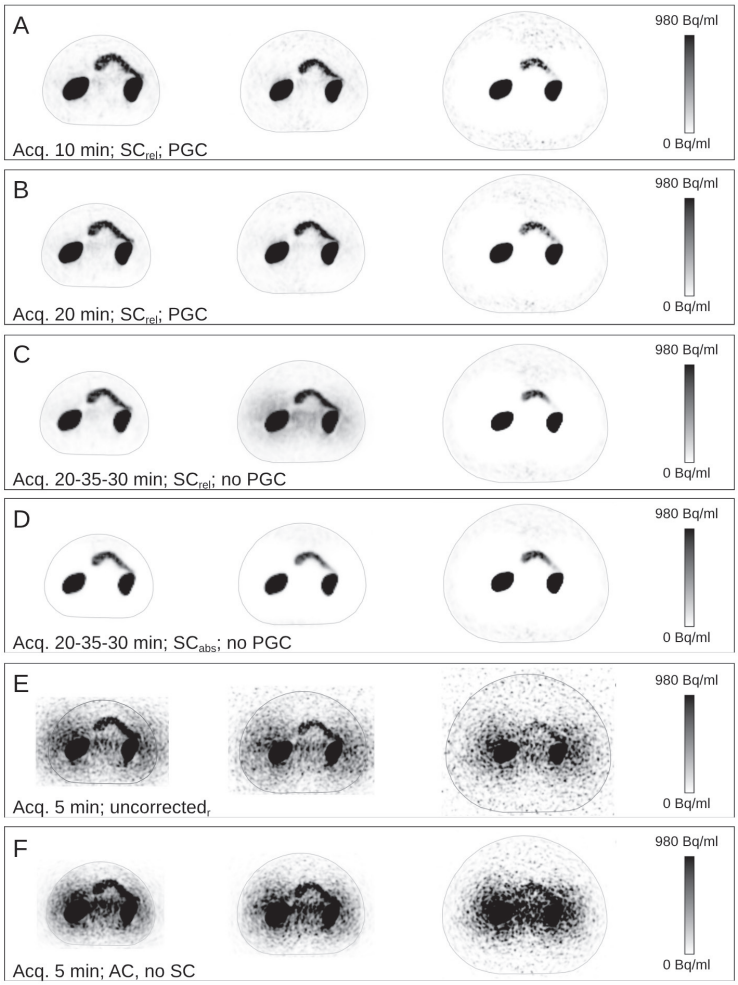


Figure 5. Axial slice of the PET of the normal weight (NW), overweight (OV) and obesity (OB) phantom in experiment 1 (A) and experiment 2 (B-G), showing an increase in spill-over (A) or photopenic artefacts (B,C) with increasing body size. Increasing acquisition time from 10 to 20 minutes, resulted in some improvements in image quality, i.e. a more homogenic activity distribution and reduced artefact size, but did not significantly improved the photopenic artefact in the OB phantom (B,C). The uncorrected and only AC corrected PET, demonstrated that artefacts are related to scatter correction (B-E). In PET reconstructed without prompt gamma correction (PGC), overspill artefacts appeared in the NW and OW phantoms (A,F). PGC did not improve PET of the OB phantom. Absolute scatter scaling (SS) did not largely improve the PET reconstructions when compared to relative scatter scaling (F,G).

Abbreviations: NW = normal weight, OW = overweight, OB = obesity, acq. = acquisition time, AC = attenuation correction, SC = scatter correction, SS = scatter scaling.

Quantitative assessment

The RC in the pancreas was similar in the NW and OW phantom (77 ± 4.5 and 80 ± 4.1%, respectively ;with AT = 10 min). Increasing the acquisition time did not improve RC of the pancreas in the NW and OW phantom (Figure 6). However, the number of voxels with value zero decreased and CoV improved with increasing acquisition time. Both plateaued from an acquisition time of 7 minutes (Figure 7).

In the OB phantom, the RC in the pancreas was decreased (33 ± 29%, AT=10 min) as compared to the NW phantom, as is in line with the observed large photopenic artefact. Increasing the acquisition time improved RC (Figure 6, decreased the size of the photopenic artefact (i.e. the number of voxels with value 0, Figure 7A) and increased the CoV (Figure 7B). Nevertheless, at acquisition time of 20 minutes all measurements remained worse as compared to the NW and OW phantom (the RC was only 52 ± 23% and almost 50% of the voxels had value 0) and a plateau was not reached for any of the measurements.

Lastly, to investigate the effect the location of the pancreas with respect to the kidneys, we compared RC of the pancreas head, body and tail, data is shown in Figure 6B-D. Only in the OB phantom, the RC differed between the pancreas regions. The RC in the pancreas tail and body was lower than in the NW and OW phantoms, but the RC in the pancreas body was similar as in the NW and OW phantom (80 ± 16%, 77 ± 14%, 73 ± 27%, for NW, OW and OB respectively, with AT 10 minutes).

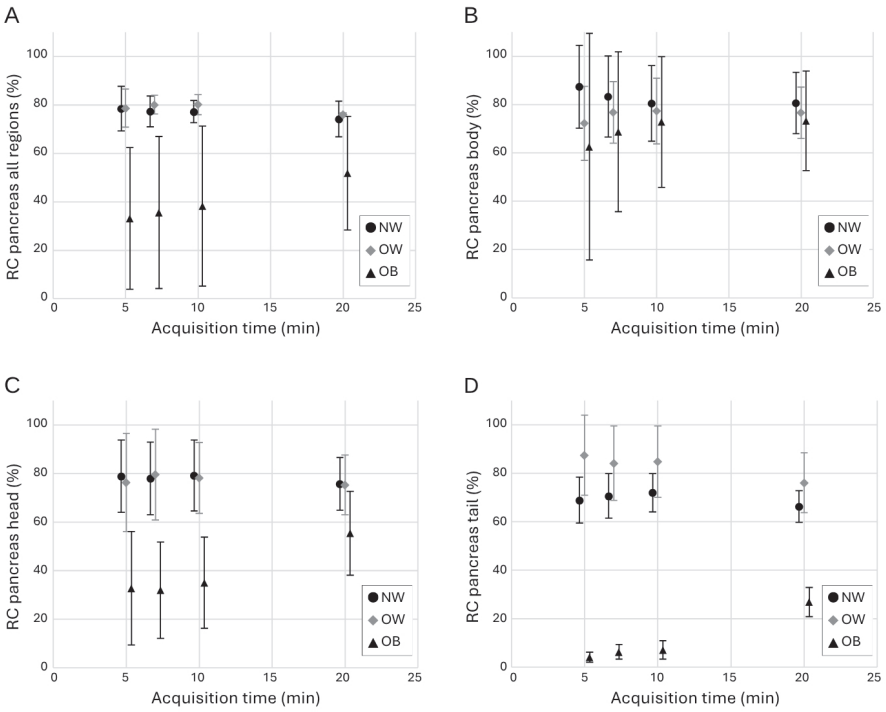


Figure 6. Mean activity concentration recovery coefficient (RC) in all pancreas VOI (A) and in the pancreas body (B), head (C) and tail (D), for increasing acquisition time in the normal weight (NW), overweight (OW) and obesity (OB) phantom. In A, the error bar shows standard deviation of the three VOIs, in C-D the error bars show the standard deviation of voxels within the VOI. Standard reconstructed PET of experiment 2, including PGC.

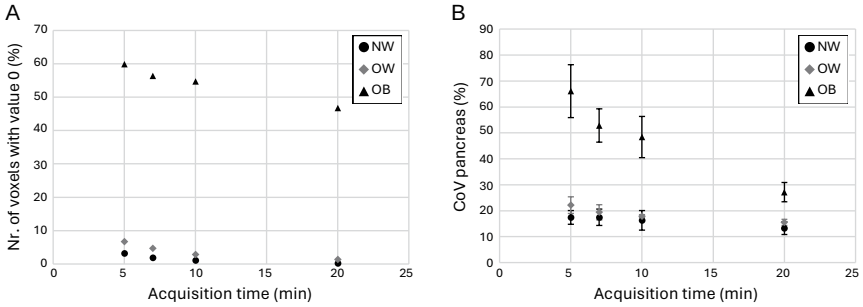


Figure 7. This figure shows the effect of acquisition time on the size of the photopenic artefacts (as percentage of the number of voxels with value 0 with respect to the total number of voxels) and the coefficient of variation in the volumes of interest in the pancreas (as percentage standard deviation / mean). Increasing acquisition time reduced the size of the photopenic artefact in the OB phantom, shown in A. The coefficient of variation in the pancreas decreased with increasing acquisition time, shown in B. In the NW and OW phantom a plateau can be observed from 7 minutes. The largest decrease in CoV is observed in the OB phantom, but a plateau is not reached.

In the kidneys, the RC was reduced in the OW and OB phantom in comparison to the NW phantom, and the lowest RC was measured in the OW phantom (91 ± 1.4, 76 ± 4.5 and 81 ± 0.7% in the NW, OW and OB phantom, respectively; with AT = 10 min). The RC in the kidneys did not change with increasing acquisition time (Figure 8).

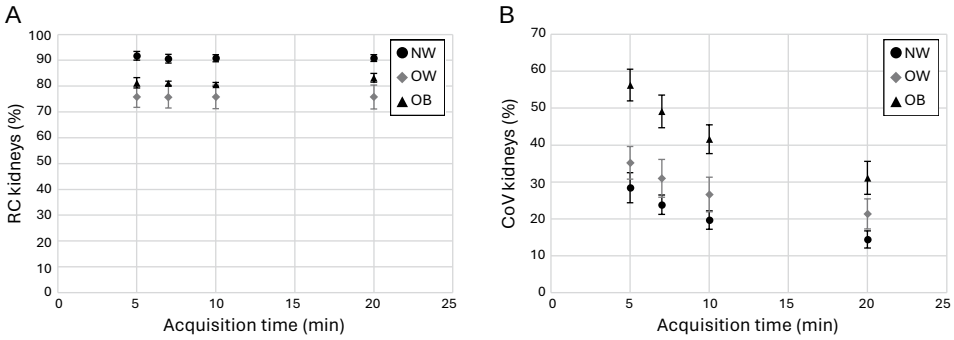


Figure 8. The recovery coefficient in the kidneys is similar for all three phantoms and did not change with increasing acquisition time (A). Little decrease in the coefficient of variation was observed with increasing acquisition time in all three phantoms similarly (B).

DISCUSSION

This phantom study showed the negative effect of increased body size on the appearance of photopenic artefacts and consequently on the quantification of the activity concentration in the pancreas in ^{68}Ga-exendin-4 PET/CT. The 3D-printed pancreas-kidney phantom placed in enlarged body casings resulted in similar PET/CT images as human ^{68}Ga-exendin-4 PET/CT, including the appearance of photopenic artefacts in the obesity phantom (Figure 1). As expected, recovery of activity from the whole pancreas was reduced in the presence of the photopenic artefact in the obesity phantom (Figure 5). Therefore, if photopenic artefacts appear in ^{68}Ga-exendin-4 PET/CT, one should be aware of unreliable quantification of pancreatic activity, representing a challenge for determination of beta cell mass in obese individuals.

The used 3D printed pancreas-kidney phantom and larger body casings were essential in this phantom study, because larger body sizes and the radiotracer specific activity distribution of ^{68}Ga-exendin-4 with very high uptake in the kidneys, both contribute the occurrence of the photopenic artefact surrounding the kidneys. Regular phantoms, such as the NEMA NU2, mimic normal weight individuals and operate with fixed sized spherical inserts that should be placed in predetermined places. These phantoms will therefore not be able to properly simulate specific anatomy and thus cannot simulate radiotracer specific activity distribution. Previously, the normal weight phantom as used in this study was shown to effectively mimic ^{111}In-exendin SPECT/CT (5). Moreover, Heusser et

al. showed that an anatomic pelvis phantom was able to mimic ^{68}Ga-PSMA-11 PET/MRI and scatter related artefacts (5). Larger body sizes were previously mimicked by enlarging the NEMA NU2 phantom by using water bags or a larger phantom (9, 16). The 3D printed phantom in three different sized body casings in our study successfully mimicked ^{68}Ga-exendin PET/CT in different sized individuals.

As expected, applying scatter correction induced the photopenic artefact surrounding the kidneys in ^{68}Ga-exendin-4 PET/CT (as shown in Figure 4A-B,E vs. 4F). The commonly used scatter correction methods using tail-fitted single scatter simulation, which have been optimized for FDG-PET/CT and in individuals with normal weight. However, in the presence of large uptake-to-background ratios with many local scatter events (as in the kidneys) and reduced tail data (as in larger body sizes together with the lack of ^{68}Ga-exendin-4 accumulation in adipose tissue and skin), the scatter estimate can be determined incorrectly. This may cause unreliable scatter estimates (5, 17, 18).

The appearance of photopenic artefacts in the obesity phantom was not reduced or resolved by increasing acquisition time, Although increasing the acquisition time did not affect the image reconstruction visually (Figure 4A vs. 4B), it slightly decreased the size of the photopenic artefact in the OB phantom (Figure 5A) and increased the RC in the pancreas (Figure 5) and improved CoV (Figure 5B) in all phantoms. In future, image quality and quantification of ^{68}Ga-exendin-4 PET/CT might be improved by weight adjusted acquisition times in individuals with overweight of obesity.

Neither could applying PGC or applying absolute scatter scaling instead of relative scatter scaling reduce or resolve the photopenic artefacts in the obesity phantom. The benefit of PGC and absolute scatter scaling in other studies was limited. The use of PGC may reduce the occurrence of photopenic artefacts partly, but is not sufficient to prevent photopenic artefacts (5, 10, 19). In the study of Heusscher et al., the maximization of the scatter fraction to 40% resulted in the largest reduction of photopenic artefacts and the difference between absolute an relative scatter scaling was only small (5). Overall, it seems that neither PGC nor SC_{abs} is able to sufficiently reduce or prevent photopenic artefacts and thereby improve the the quantification of tracer accumulation in the pancreas in ^{68}Ga-exendin-4 PET/CT.

Future studies are warranted to optimize scatter-correction methods in reconstruction protocols for ^{68}Ga-exendin-4 PET/CT (and for the use of other non-FDG PET tracers with high uptake in specific non-targeted organs). These reconstruction protocols should be widely available on available clinical PET/CT systems. This is important, because in addition to diagnostic precision, the quantification of activity becomes increasingly relevant for prediction and response monitoring of (radionuclide) therapy in cancer (20-22).

Few methods to improve scatter correction and to reduce or resolve the appearance of photopenic artefacts have been examined. As mentioned before, reducing the maximum scatter fraction to 40% reduced the photopenic artefact and improved quantification of activity in ^{68}Ga-PSMA PET/MRI in normal weight individuals and in a normal weight anatomic pelvis phantom (5). Moreover, Lindeman et al. showed that un-renormalized absolute scatter correction in human ^{68}Ga-PSMA PET/MRI reduced the presence of photopenic artefacts and improved the quantified activity concentrations (17). Wangerin et al. optimized the algorithm of scatter estimation for PET/MRI geometry and non-FDG tracers by accounting for targeted radiotracer uptake, smaller scatter tails and prompt gamma emission. This resulted in significantly smaller or complete resolved photopenic artefacts in human ^{68}Ga-RM2 and ^{68}Ga-PSMA-11 PET/MRI (11). Lastly, a maximum-likelihood algorithm instead of conventional scatter scaling methods improved scatter correction and reduced photopenic artefacts in [^{68}Ga]Ga-RGD PET/MRI of normal weight individuals (18, 23). The majority of these studies were performed in ^{68}Ga PET/MRI and normal weight individuals, but similar strategies are likely to be effective in ^{68}Ga-exendin-4 PET/CT as well. To test such algorithms, it is essential that these options become more widely available and if effective be available on clinical PET/CT systems.

Another strategy to resolve or reduce photopenic artefacts in ^{68}Ga-exendin-4 PET/CT might be to reduce the accumulation of the radiotracer in the kidneys, since the appearance of the artefacts is positively related with the organ-to-background ratio (5). As an example, in ^{68}Ga-PSMA PET/CT the administration of diuretics reduces the accumulation of highly concentrated radiotracer in the bladder and thereby improves visual and quantitative assessment of the prostate (24). However, reducing renal accumulation of ^{68}Ga-exendin-4 is more challenging, because kidney accumulation is caused by reabsorption and retention in the proximal tubules via the scavenger receptors cubilin and megalin and cannot be reduced by diuretics (25). Previous studies have shown that gelofusine reduces renal accumulation of ^{111}In-labeled exendin, and thereby improves quantification of pancreatic uptake of ^{111}In-exendin-4 on SPECT/CT (26). To what extent such reduction is needed to prevent photopenic artefacts has not yet been examined. To study that, the phantoms as used in this study will be useful.

A major limitation of the current study might be the truncation of a small part of the phantom case on both sides of the phantom on the CT of the overweight phantom (see Figure 2C). As a consequence, attenuation may be underestimated during AC leading to a loss of recovery of up to 20% (27). In our study, the RC in the pancreas seemed unaffected by the truncation, but truncation may explain the reduced recovery of activity in the kidneys in the overweight phantom (supplementary Figure 1). In addition, in cases there is activity in the region outside the PET/CT field of view, truncation may lead to incorrect scatter correction and photopenic artefacts (28). In our study, the truncated part of the phantom was small and the activity concentration was very low. Therefore, truncation

artefacts due to inadequate scatter correction are unlikely and visual assessment did not show scatter-related artefacts. In clinical PET/CT routine, truncation of CT is common practice, especially in individuals with obesity. To prevent truncation of the arms, it is important to perform PET/CT with the hands up. However, truncation of the abdomen occurs as well in large body sizes. To compensate for truncation or activity outside the PET/CT field of view, correction methods can be applied (27, 28).

CONCLUSION

The pancreas-and-kidney phantom in different sized body casings mimicked ^{68}Ga-exendin-4 PET/CT in individuals with normal weight, overweight and obesity very well. Quantification of pancreatic activity concentration is negatively affected and thus not reliable when photopenic artefacts appear in large body sizes. To perform the most reliable measurements of pancreatic ^{68}Ga-exendin-4 uptake, we suggest that quantification is performed in the whole pancreas when no scatter-related artefacts are visible. In case of photopenic artefacts that partly overlap with the pancreas, only those regions that are not within the artefact region, e.g. only the pancreas body should be selected for quantification (requiring that pancreatic tracer uptake is heterogeneously distributed over the whole pancreas). When the whole or majority of the pancreas is within a photopenic artefact, reliable quantification of pancreatic uptake is not possible. Most optimal PET/CT was obtained when prompt gamma correction was applied and acquisition time was at least 7 minutes, in ^{68}Ga-exendin-4 PET/CT one hour after injection of 100 MBq radiotracer and using the available reconstruction software on the PET/CT machine as used here. However these acquisition and reconstruction settings did not resolve the appearance of photopenic artefacts in patients with obesity, as illustrated with our OB phantom.

REFERENCES

1. Brom M, Woliner-van der Weg W, Joosten L, Frielink C, Bouckenooghe T, Rijken P, et al. Non-invasive quantification of the beta cell mass by SPECT with (1)(1)(1)In-labelled exendin. Diabetologia. 2014;57(5):950-9.
2. Jansen TJP, Tokgoz S, Buitinga M, van Lith SAM, Joosten L, Frielink C, et al. Validation of radiolabelled exendin for beta cell imaging by ex vivo autoradiography and immunohistochemistry of human pancreas. EJNMMI Res. 2024;14(1):96.
3. Jansen TJP, Brom M, Boss M, Buitinga M, Tack CJ, van Meijel LA, et al. Importance of beta cell mass for glycaemic control in people with type 1 diabetes. Diabetologia. 2023;66(2):367-75.
4. Brom M, Joosten L, Frielink C, Peeters H, Bos D, van Zanten M, et al. Validation of (111)In-Exendin SPECT for the Determination of the beta-Cell Mass in BioBreeding Diabetes-Prone Rats. Diabetes. 2018;67(10):2012-8.
5. Heusser T, Mann P, Rank CM, Schafer M, Dimitrakopoulou-Strauss A, Schlemmer HP, et al. Investigation of the halo-artifact in 68Ga-PSMA-11-PET/MRI. PLoS One. 2017;12(8):e0183329.
6. Watson CC. New, faster, image-based scatter correction for 3D PET. IEEE Transactions on Nuclear Science. 2000;47(4):1587-94.
7. Watson CC, Newport D, Casey ME, deKemp RA, Beanlands RS, Schmand M. Evaluation of simulation-based scatter correction for 3-D PET cardiac imaging. IEEE Transactions on Nuclear Science. 1997;44(1):90-7.
8. Akamatsu G, Mitsumoto K, Ishikawa K, Taniguchi T, Ohya N, Baba S, et al. Benefits of point-spread function and time of flight for PET/CT image quality in relation to the body mass index and injected dose. Clin Nucl Med. 2013;38(6):407-12.
9. Taniguchi T, Akamatsu G, Kasahara Y, Mitsumoto K, Baba S, Tsutsui Y, et al. Improvement in PET/CT image quality in overweight patients with PSF and TOF. Ann Nucl Med. 2015;29(1):71-7.
10. Noto B, Buther F, Auf der Springe K, Avramovic N, Heindel W, Schafers M, et al. Impact of PET acquisition durations on image quality and lesion detectability in whole-body (68)Ga-PSMA PET-MRI. EJNMMI Res. 2017;7(1):12.
11. Wangerin KA, Baratto L, Khalighi MM, Hope TA, Gulaka PK, Deller TW, et al. Clinical Evaluation of (68)Ga-PSMA-II and (68)Ga-RM2 PET Images Reconstructed With an Improved Scatter Correction Algorithm. AJR Am J Roentgenol. 2018;211(3):655-60.
12. Conti M, Eriksson L. Physics of pure and non-pure positron emitters for PET: a review and a discussion. EJNMMI Phys. 2016;3(1):8.
13. Woliner-van der Weg W, Deden LN, Meeuwis AP, Koenrades M, Peeters LH, Kuipers H, et al. A 3D-printed anatomical pancreas and kidney phantom for optimizing SPECT/CT reconstruction settings in beta cell imaging using (111)In-exendin. EJNMMI Phys. 2016;3(1):29.
14. (NEMA) NEMA. NEMA Standards Publication NU 2-2007: Performance Measurements of Positron Emission Tomographs. 2007.
15. Peters SMB, van der Werf NR, Segbers M, van Velden FHP, Wierts R, Blokland K, et al. Towards standardization of absolute SPECT/CT quantification: a multi-center and multi-vendor phantom study. EJNMMI Phys. 2019;6(1):29.
16. Santoro M, Della Gala G, Paolani G, Zagni F, Civollani S, Strolin S, et al. A novel figure of merit to investigate (68)Ga PET/CT image quality based on patient weight and lesion size using Q.Clear reconstruction algorithm: A phantom study. Phys Med. 2023;106:102523.
17. Lindemann ME, Guberina N, Wetter A, Fendler WP, Jakoby B, Quick HH. Improving (68)Ga-PSMA PET/MRI of the Prostate with Unrenormalized Absolute Scatter Correction. J Nucl Med. 2019;60(11):1642-8.

18. Bal H, Kiser JW, Conti M, Bowen SL. Comparison of maximum likelihood and conventional PET scatter scaling methods for (18) F-FDG and (68) Ga-DOTATATE PET/CT. Med Phys. 2021;48(8):4218-28.
19. Hong I, Rothfuss H, Fürst S, Michel C, Nekolla SG, Bendriem B, et al. Prompt gamma correction for Ga-68 PSMA PET studies. IEEE Nuclear Science Symposium and Medical Imaging Conference. 2015.
20. Wahl RL, Jacene H, Kasamon Y, Lodge MA. From RECIST to PERCIST: Evolving Considerations for PET response criteria in solid tumors. J Nucl Med. 2009;50 Suppl 1(Suppl 1):122S-50S.
21. Heinzel A, Boghos D, Mottaghy FM, Gaertner F, Essler M, von Mallek D, et al. (68)Ga-PSMA PET/CT for monitoring response to (177)Lu-PSMA-617 radioligand therapy in patients with metastatic castration-resistant prostate cancer. Eur J Nucl Med Mol Imaging. 2019;46(5):1054-62.
22. Hartrampf PE, Huttmann T, Seitz AK, Kubler H, Serfling SE, Schlotelburg W, et al. SUV(mean) on baseline [(18)F]PSMA-1007 PET and clinical parameters are associated with survival in prostate cancer patients scheduled for [(177)Lu]Lu-PSMA I&T. Eur J Nucl Med Mol Imaging. 2023;50(11):3465-74.
23. Overbeck N, Ahangari S, Conti M, Panin V, Azam A, Kurbegovic S, et al. Improved Positron Emission Tomography Quantification: Evaluation of a Maximum-Likelihood Scatter Scaling Algorithm. Diagnostics (Basel). 2024;14(11).
24. Rauscher I, Maurer T, Fendler WP, Sommer WH, Schwaiger M, Eiber M. (68)Ga-PSMA ligand PET/CT in patients with prostate cancer: How we review and report. Cancer Imaging. 2016;16(1):14.
25. Gotthardt M, van Eerd-Vismale J, Oyen WJ, de Jong M, Zhang H, Rolleman E, et al. Indication for different mechanisms of kidney uptake of radiolabeled peptides. J Nucl Med. 2007;48(4):596-601.
26. Buitinga M, Jansen T, van der Kroon I, Woliner-van der Weg W, Boss M, et al. Succinylated gelatin improves the theranostic potential of radiolabeled Exendin-4 in insulinoma patients. J Nuc Med. 2019;60(6):812-6.
27. Beyer T, Bockisch A, Kuhl H, Martinez MJ. Whole-body 18F-FDG PET/CT in the presence of truncation artifacts. J Nucl Med. 2006;47(1):91-9.
28. Magota K, Numata N, Shinyama D, Katahata J, Munakata Y, Maniawski PJ, et al. Halo artifacts of indwelling urinary catheter by inaccurate scatter correction in (18)F-FDG PET/CT imaging: incidence, mechanism, and solutions. EJNMMI Phys. 2020;7(1):66.



5

Quantification of organ-specific GLP-1 receptor expression in the pancreas and beyond by ^{68}Ga-exendin PET/CT imaging in humans with metabolic disease

Laura N. Deden[1,2], Marti Boss[1], Edo O. Aarts[2], Hans de Boer[3], Cees J. Tack[4], Mijke Buitinga[1,5,6], Ignace M.C. Janssen[2], Eric J. Hazebroek[2,7], Bastiaan E. de Galan[4,8,9], Martin Gotthardt[1]

Submitted

ABSTRACT

Knowledge about the actions of glucagon-like peptide 1 (GLP-1) and its receptor agonists in humans is increasing. However, understanding of GLP-1 receptor (GLP-1R) expression and its relation with GLP-1 signaling remains incomplete. Therefore, we assessed GLP-1R expression in humans through measurement of ^{68}Ga-NODAGA-exendin-4 (^{68}Ga-exendin) accumulation, visually and quantitatively, by positron emission tomography/computed tomography (PET/CT) in 62 participants included from ongoing studies. Clear radiotracer uptake was observed in the pancreas and duodenum in all participants. In addition, uptake was observed in salivary glands and the pituitary the majority of participants, in the myocardium of four participants and uptake in glandular breast tissue and uterus and ovary of half of the female participants. No accumulation higher than blood pool was observed in liver, adipose tissue and muscles. Our data confirm accumulation of ^{68}Ga-exendin in organs with well-known GLP-1R expression, such as pancreas and duodenum. Moreover, accumulation was observed in organs in which the physiological role of GLP-1R expression remains unclear, such as pituitary gland, salivary glands, glandular breast tissue and myocardium. These findings suggest that ^{68}Ga-exendin PET/CT is a promising tool to increase knowledge about physiological GLP-1R signaling and to elucidate patho-physiological mechanisms underlying (variable) treatment responses of GLP-1R agonists in humans.

INTRODUCTION

Glucagon-like peptide-1 (GLP-1) is an incretin hormone which is secreted in response to food intake from the intestinal L-cells, located with increasing density from duodenum to colon (1). An important action of GLP-1 is stimulation of glucose-dependent insulin release from pancreatic beta cells and suppression of glucagon secretion. For this reason, GLP-1 receptor agonists (GLP-1RAs) have been developed, which are currently widely used to regulate blood glucose in the treatment of type 2 diabetes mellitus (2). Moreover, GLP-1RAs have a broad range of non-glucose regulatory effects, such as delaying gastric emptying, inducing satiety centrally and exerting beneficial effects on body weight (1, 3). In addition, GLP-1RAs have a lowering effect on blood pressure and are hypothesized to play a role in tissue regeneration and protection, for example in beta cells, the central nervous system and the heart (3-5).

Despite the fact that the underlying mechanisms of these actions are not completely understood, the combined actions have resulted in the adoption of GLP-1RAs as pharmacotherapy for the treatment of obesity and benefits for the treatment of neurodegenerative diseases have been described (1, 2, 5, 6).

Actions of GLP-1 and GLP-1RAs are mediated via the GLP-1 receptor (GLP-1R). Therefore, understanding GLP-1R expression in humans will increase our understanding of the actions of GLP-1RAs. The GLP-1R is expressed in high density on beta cells in the pancreas (7). In line with the wide range of extra-pancreatic effects, expression of the GLP-1R has also been demonstrated in for example the cardiovascular system, intestinal tract, brain, lungs, kidneys and immune cells (1, 3, 4, 7, 8). However, GLP-1R expression has mainly been studied in animal models, and because of several interspecies differences, these results cannot be translated to humans directly (1, 7, 9). Moreover, detection of the GLP-1R in humans has been limited to tissue samples and often relies on mRNA assessments which may not represent actual receptor expression. Therefore, the specificity of these detection methods has been questioned and such single tissue samples also cannot represent known variations in GLP-1R expression over time (8). A specific method to assess GLP-1R expression *in vivo* across tissues of interest is highly warranted to will fill this gap.

In this study, ^{68}Ga-NODAGA-exendin-4 (^{68}Ga-exendin) positron emission tomography/computed tomography (PET/CT) has been applied to assess human GLP-1R expression *in vivo*. Exendin-4 is a stable GLP-1R agonist and radiolabeled exendin-4 binds to the GLP-1R with high specificity (10-13). Internalization of the tracer receptor complex and metabolic trapping leads to a high sensitivity (by increasing specific uptake in GLP-1R positive tissues while the tracer is washed out blood and tissues not expressing the GLP-1R), allowing for specific detection of even very low levels of GLP-1R expression (10).

The accumulation of ^{68}Ga-exendin has been assessed in multiple organs from head-thoracic-abdominal PET/CT images of participants of ongoing clinical trials. These data present organ-specific GLP-1R expression patterns *in vivo*, which was compared with locations and actions of GLP-1R expression in human as described in literature.

MATERIALS AND METHODS

Participants

The uptake pattern of ^{68}Ga-exendin was reviewed in patients that underwent thoracic-abdominal or head-thoracic-abdominal ^{68}Ga-exendin PET/CT between December 2015 and December 2019 in our center. No selection was done based on patient characteristics or underlying disease. All individuals included in this analysis participated in other clinical trials (Clinicaltrial.gov numbers NCT03189953, NCT02542059, NCT03182231, NCT03182192, NCT03923114, NCT03785275), and had (a history of) adult hyperinsulinemic hypoglycemia (AHH), type 1 or type 2 diabetes mellitus, obesity and a history of gastric bypass surgery (RYGB). All these studies were reviewed and approved by the medical ethical and local research committee.

Radiopharmaceutical preparation and administration

Hydrochloric acid was purchased from Rotem Industries (Mishor Yamin: Israel). All other components were purchased as one disposable kit (reagent and hardware kit for synthesis of ^{68}Ga peptides using cationic purification, ABX, Germany). ^{68}Ga-exendin was manufactured using a synthesizer module (GRP synthesizer, Scintomics, Germany). Gallium-68-chloride was obtained from a ^{68}Ge/^{68}Ga generator (Galliapharm, Eckert and Ziegler, Germany). The generator was eluted with 10 ml of 0.1 M hydrochloric acid and gallium-68 was trapped on a polystyrene-H+ cartridge. The cartridge was eluted with 1.5 ml 5 M NaCl in 0.1 M hydrochloric acid into the reaction vial, containing 200 µl exendin-NODAGA (10 µg of peptide in water for injection), 475 µl 2.5 M 4-(2-hydroxyethyl)-1-piperazineethanesulfonic acid (HEPES) buffer and 50 µl ascorbic acid 100 mg/ml in water for injection. After 15 minutes incubation at 100°C, the vessel was cooled and 2 ml ethylenediaminetetraacetic acid (EDTA) 50 mM/ polysorbate 80 0.15% was added. ^{68}Ga-exendin was purified on a HLB cartridge and sterilized by passing through a 0.2 µm filter (millex GV).

All patients received [^{68}Ga]Ga-NODAGA-exendin- (^{68}Ga-exendin) intravenously, with an activity of 75-100 MBq, corresponding with a pharmacological dose of 4-7 µg of peptide. Before administration, all participants fasted for four hours, to prevent competition between the radiotracer and endogenous GLP-1. After administration of ^{68}Ga-exendin, glucose levels (point-of-care test of venous blood sample) and blood pressure were monitored up to one hour after administration, and thereafter if indicated. Patients

with hyperinsulinemic hypoglycemia are at risk of hypoglycemia, therefore continuous glucose infusion was started in these participants as well as in those with post-bariatric hypoglycemia and low glucose levels (<4.0 mmol/l) prior to injection. In addition, participants with diabetes received glucose infusion if they had hypoglycemia prior to injection (<3.5 mmol/l) or low glucose levels (<4.0 mmol/l) shortly after injection.

PET/CT acquisition

One hour after injection (62±7.1 minutes), PET/CT was performed on a Siemens Biograph mCT-40 time-of-flight PET/CT scanner (Siemens Healthcare, Erlangen, Germany). In all participants, the abdominal region was visualized as part of the standard imaging protocol, using two or three bed positions with 5 to 10 minutes per bed position. Thorax, pelvic and head and neck region were (partially) imaged, depending on study protocol in 57, 8 and 41 participants, respectively. Low dose CT (40 mAs, 130 kV) was obtained without contrast and applied for attenuation correction and anatomical localization. The PET was reconstructed using ultrahigh definition, time of flight, scatter and attenuation correction and post-reconstruction Gaussian filter of 3 mm FWHM settings.

Visual assessment

All PET/CT images were visually assessed in axial, sagittal and coronal directions. Based on literature and a first overall view of PET/CT of all participants by three readers, organs with possible GLP-1R specific ^{68}Ga-exendin accumulation and background tissues were defined. The organs of interest are: pancreas, proximal duodenum, female reproductive system, heart, small intestine, lungs, salivary glands, lacrimal glands, nasal tissue, pituitary and brain. Furthermore, uptake in the kidneys caused by excretion and tubular reabsorption was assessed (14). Accumulation patterns (for defining tissues for quantitative assessment) were assessed in all participants and defined as no uptake, moderate uptake or clear uptake. Moderate uptake is described as just visible above background or adjacent soft tissue and clear uptake as clearly seen above background or adjacent soft tissue. In addition, in liver, spleen and blood pool the activity levels were assessed. These activity levels were assumed to be GLP-1R unspecific and background.

Uptake quantification

Quantification of tracer uptake was performed using Inveon Research Workplace (version 4.1; Siemens Healthcare, Erlangen, Germany). Volumes of interests (VOIs) were drawn in pancreas, proximal duodenum, kidneys, parotid glands and pituitary gland (organs with visually clearly identifiable tracer uptake) and in thoracic aorta, liver and spleen for background measures. All VOIs were drawn to include all (possible) uptake from the organs, except for kidneys, spleen and liver. In the kidneys, VOIs were drawn based on anatomical location on CT and in spleen and liver ellipsoid VOIs were placed equally distributed through the organs, two VOIs of 2-10 ml and three VOIs of 25-50 ml, respectively. Within each VOI, a VOI with threshold of 70% of the maximum value was determined ($VOI_{70\%}$).

Quantification measures that were calculated from these $VOI_{70\%}$ were: mean activity concentration corrected for injected dose ($ACID_{70\%}$ [Bq/MBq·ml]), maximum standard uptake value (SUV_{max}) and mean SUV ($SUV_{70\%}$). For ACID, the activity concentration (Bq/ml) was divided by injected dose (MBq), corrected for decay. This measure was performed because body weight is expected to have a minor effect on tissue uptake of a peptide-based tracers. SUV values were calculated as: *activity concentration (kBq/g) / [injected dose (MBq) / body weight (g)],* corrected for decay and assumed that 1 g tissue corresponds with 1 ml.

Uptake over time

In fourteen participants (ten female, four male), PET/CT was available one (T1) and two (T2) hours after ^{68}Ga-exendin administration. Change in uptake between both time points were compared between organs (pancreas, breast tissue, liver and spleen) and blood pool, to further differentiate between specific and blood pool uptake. Specific uptake mechanisms will cause increased tracer accumulation over time, while in blood pool there is wash out. Mean activity in blood pool, liver and spleen were determined from VOIs as previously described. In the pancreas and breast, an ellipsoid VOI was placed centrally in the pancreas head and glandular breast tissue, respectively. All VOIs were placed at corresponding anatomical positions at both time points. Uptake values were decay corrected to the scan start time. To be able to compare pancreas with blood pool, uptake values were normalized to 1 in both organs.

Statistics

Regression coefficients of activity at T1 (AT1) versus T2 (AT2) were calculated using linear regression. Regression coefficients of organs were compared to blood pool (measured in descending thoracic aorta and left ventricle), using general linear model analysis with terms AT1, AT2, type of tissue and interaction. P-values smaller than 0.05 were considered statistically significant. Descriptive means are expressed ± standard deviation. All statistics were performed using SPSS (SPSS statistics version 22, IBM, United States).

RESULTS

In this analysis, 62 participants were included. Baseline characteristics of the participants are shown in table 1. The average injected activity of ^{68}Ga-exendin was 98±11 MBq. Administration of ^{68}Ga-exendin was well-tolerated in nearly all participants. Reported side effects within one hour after administration were nausea and vomiting (N=1, 1.6%), dizziness (N=2, 3.2%) and, rapid decrease in blood glucose level for which continuous glucose infusion was started (N=1, 1.6%). Hypotension did not occur in any of 51 participants in which blood pressure was checked after radiotracer administration. Blood glucose levels were checked prior and up to one hour after radiotracer administration in 51 participants. Sixteen participants who were susceptible to develop hypoglycemia after radiotracer

administration, received continuous glucose infusion preventively. This included 12/13 of the participants with AHH, 3/10 participants with post-bariatric hypoglycemia and one participant with T2D who had hypoglycemia before radiotracer administration. Of these 16 participants, two participants with AHH developed hypoglycemia (<3.0 mmol/l) after radiotracer administration. On average, maximum decrease in blood glucose levels was 0.8 ± 1.3 mmol/l in these 16 participants. In the remaining 35 patients, one participant received continuous glucose infusion because of a rapid decrease in blood glucose level. Of the remaining 34 participants, 31 had a mild decrease in blood glucose levels with a maximum of 1.5 ± 1.3 mmol/l in the first hour after ^{68}Ga-exendin administration. A detailed description of these side-effects is given in table 2.

Table 1. Characteristics of all participants, as included from several studies and grouped per study topic.

	All	AHH	T1D	T2D and obesity
N	62	13	10	39
Female	74%	62%	60%	82%
Age (years)	47 ± 12	46 ± 16	42 ± 16	48 ± 8.9
Weight (kg)	87 ± 20	74 ± 13	76 ± 13	94 ± 20
HH	37%	100%	n.a.	26%
T2D	32%	n.a.	n.a.	51%
Post-RYGB	39%	n.a.	n.a.	62%

Data are shown as absolute number, percentage (%) or mean ± standard deviation. AHH: adult hyperinsulinemic hypoglycemia, T1D: type 1 diabetes mellitus, T2D: type 2 diabetes mellitus, RYGB: Roux-en-Y gastric bypass, HH: hyperinsulinemic hypoglycemia, n.a.: not applicable.

Table 2. Side effects that occurred within one hour after ^{68}Ga-exendin injection.

Side effect	N	Description of side effect
Nausea or vomiting	2	Two participants with type 1 diabetes; one participant received anti-emetic drug once, in the other participant nausea disappeared within 30 minutes.
Dizziness	1	In a participant with type 1 diabetes, complaints disappeard within 30 minutes without intervention.
Hypoglycemia (blood glucose level < 3 mmol/l)	2	In two (out of 13) participants with AHH; continuous glucose infusion was started.
Continuous glucose infusion to prevent hypoglycemia	17	In adult hyperinsulinemic hypoglycemia (12/13), post-bariatric hypoglycemia (3/10) and type 2 diabetes (2/15). In patients at risk for hypoglycemia (N=16), continuous glucose infusion was started to prevent hypoglycemia. In one participant with type 2 diabetes, continuous glucose infusion was started because of a quick decrease in blood glucose levels to <4 mmol/l in the first 15 minutes after administration. On average, maximum decrease in blood glucose levels was 0.8 ± 1.3 mmol/l in those 17 participants.
Hypotension	0	Occurred in none of the participants.

Visual assessment

Clear ^{68}Ga-exendin uptake was observed in all participants in the kidneys, pancreas and proximal duodenum (Figure 1). The uptake in the kidneys was mainly observed in the renal cortex and to a lesser extend in ureters and bladder. In the pancreas, activity was equally distributed, except for focally increased uptake in insulinomas. Activity accumulation in the duodenum was seen in the proximal part adjacent to the gastric antrum.

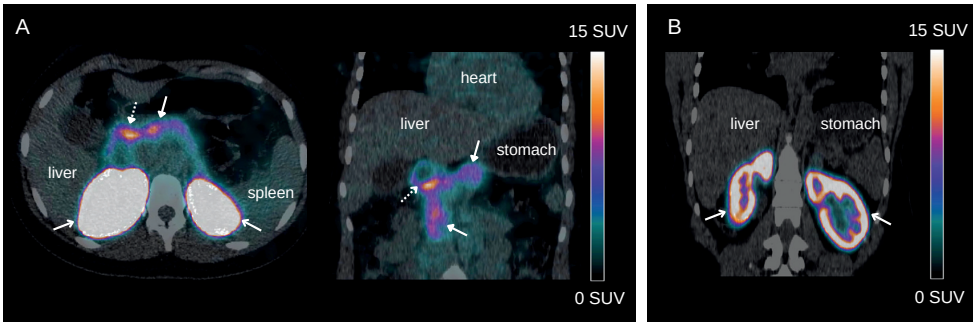


Figure 1. Known accumulation of ^{68}Ga-exendin-4 in the pancreas, duodenum and renal cortex. In all participants GLP-1 receptor specific accumulation of Ga^{68}-Exendin was observed in the pancreas (solid arrow) and proximal duodenum (dotted arrow), in 1A. In the kidneys (open arrows) very high, non-receptor specific uptake occurs, as shown in 1A. Specifically, the radiotracer accumulates in the renal cortex, as shown in 1B by increasing the maximum scaling value. SUV = standardized uptake value.

Uptake was often observed in the salivary glands (95%), the pituitary gland (78%), nasal mucosa (83%), lacrimal glands (61%), glandular breast tissue (47%, female participants only) and gastric mucosa (33%) (Figure 2-5). Uptake in the pituitary gland in 32 participants was observed as a single spot in the sella turcica (Figure 2). In addition, uptake in the uterus and ovary was observed in four cases (50% of female participants) (Figure 4B). In the myocardium, uptake above blood pool activity was observed in four participants (7%) (Figure 6). In one of these participants, PET/CT was also acquired 2 hours after injection, possibly improving visualization of the myocardial uptake through an increased target-to-background ratio (Figure 7A). In two other participants myocardial uptake was lower than blood pool (example in Figure 7B).

Blood pool activity was observed in all participants. Furthermore, low and equally distributed background activity was seen in liver and spleen, visually comparable or lower than blood pool activity. In the lungs, adipose tissue, skeletal muscles and the brain (other than pituitary gland) no, or very low uptake was observed.

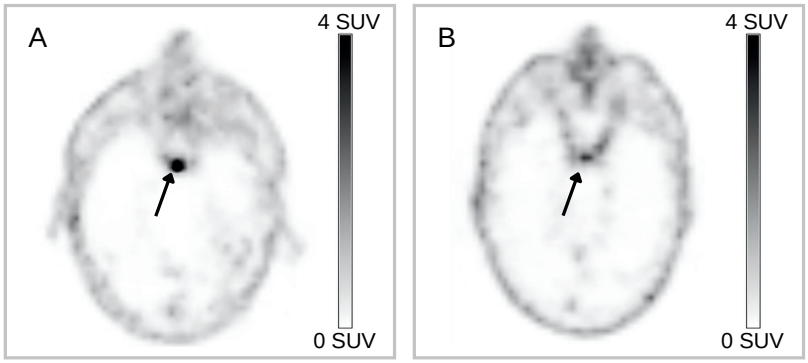


Figure 2. Accumulation in the pituitary varied among participants and other parts of the brain lack accumulation. Accumulation of ^{68}Ga-exendin in the pituitary was observed in 78% of the participants, with vVariable levels of accumulation are shown in two participants. An example of high uptake in 2A ($SUV_{70\%}$=9.1, solid arrow) and moderate uptake in 2B ($SUV_{70\%}$=3.1, solid arrow). No accumulation was observed in other parts of the brain. SUV = standardized uptake value.

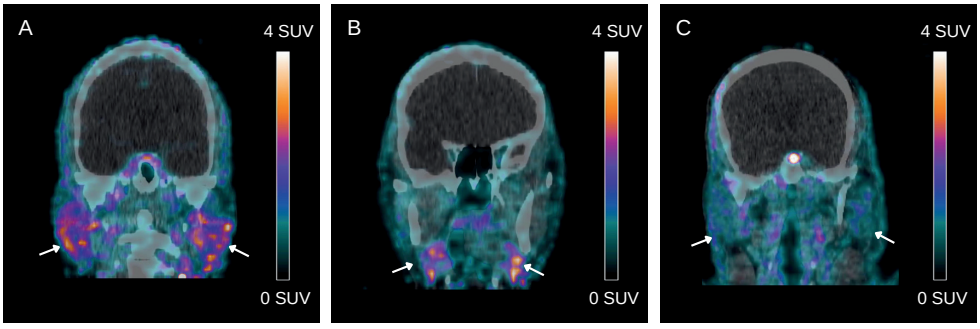


Figure 3. Accumulation in the salivary glands varied in amount and location. In 95% of the participants ^{68}Ga-exendin accumulated in one or more salivary glands. The level of uptake and uptake patterns varied among the participants. Here, examples of a participant with clear uptake in the parotid glands (3A, arrow), with clear uptake in the submandibular glands (3B, dotted arrow) and without clear uptake in the salivary glands (3C, arrow) are shown. SUV = standardized uptake value.

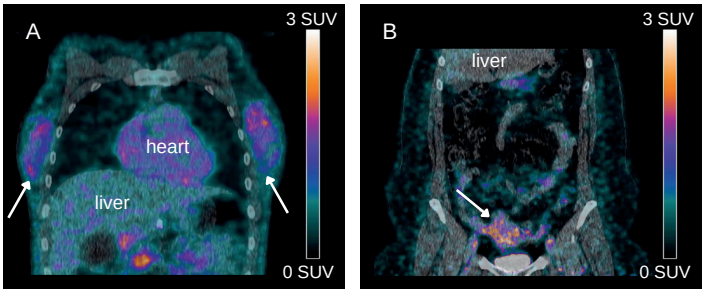


Figure 4. Acumulation of ^{68}Ga-exendin-4 in female organs. Approximately in half of the female participants ^{68}Ga-exendin accumulated in the breast tissue, as shown in Figure 4A (arrow). In 4/8 cases with PET/CT imaging of the pelvic region accumulation was observed in the uterus and ovary, as shown in Figure 4B (arrow).

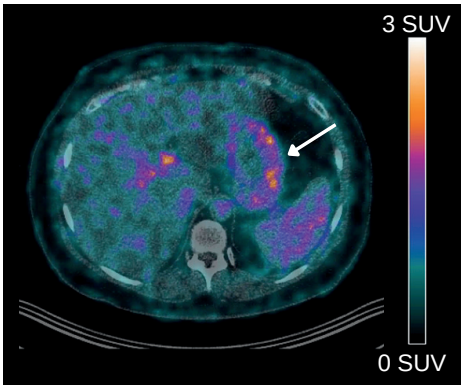


Figure 5. Accumulation of ^{68}Ga-exendin-4 in the gastric wall. In a some of the participants (33%) activity could be observed in the gastric wall, an example is shown in this figure.

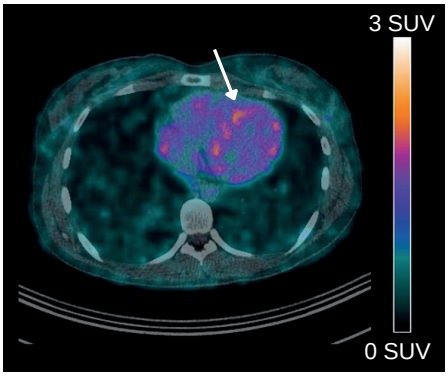


Figure 6. Accumulation of ^{68}Ga-exendin-4 in the heart. In only a few participants activity was observed in myocardium. This figure shows an example of ^{68}Ga-exendin accumulation in the myocardium of the left ventricle (arrow)

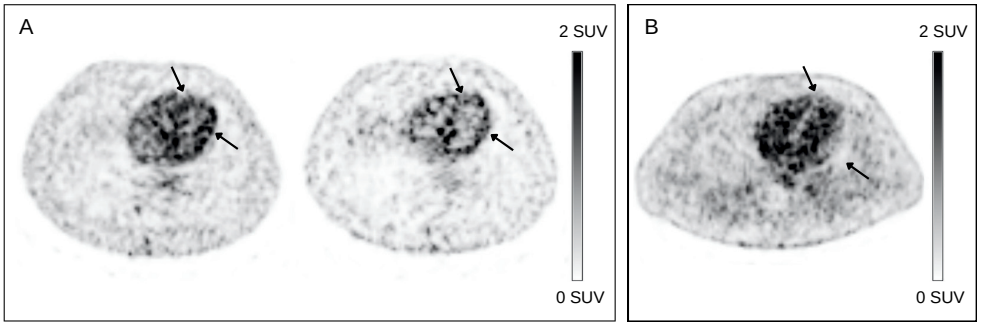


Figure 7. Example of ^{68}Ga-exendin PET of the heart in two participants. In A, ^{68}Ga-exendin accumulation (arrows) was observed in the myocardium of the left ventricle at one (left) and two (right) hours after administration. In B, lack of accumulation of ^{68}Ga-exendin was observed (arrows). PET images were performed without correction for breathing or ECG triggering.

Uptake quantification

Activity quantification as $ACID_{70\%}$, $SUV_{70\%}$ and SUV_{max} in pancreas, duodenum, pituitary and parotid glands of participants with visually assessable uptake in those organs is summarized in table 3. Nonspecific and blood pool activity of all participants is summarized in table 3 as well. Finally, activity concentration ($ACID_{70\%}$) and individual variation in $ACID_{70\%}$ is visualized in Figure 8.

Table 3. Quantification of GLP-1R specific activity in pancreas, duodenum pituitary and parotid glands (in participants with visually observed uptake) and unspecific and blood pool activity in kidneys, aorta, liver and spleen (in all participants).

	N	$ACID_{70\%}$ (Bq/MBq·ml)	$SUV_{70\%}$	SUV_{max}
Pancreas	62	94 ± 30	8.0 ± 2.8	10 ± 3.5
Duodenum	62	94 ± 40	8.0 ± 3.5	9.9 ± 4.3
Pituitary gland	32	31 ± 18	2.9 ± 1.8	3.1 ± 1.8
Parotid glands	32	27 ± 9.3	2.5 ± 0.8	3.1 ± 1.0
Kidneys	62	1506 ± 127	127 ± 27	163 ± 35
Descending thoracic aorta	62	27 ± 8.2	2.4 ± 0.8	2.9 ± 1.0
Liver	62	19 ± 6.2	1.7 ± 0.7	2.1 ± 0.9
Spleen	55*	17 ± 5.7	1.5 ± 0.6	1.8 ± 0.7

Data are shown as mean ± standard deviation. *In seven participants reliable quantification of uptake in the spleen could not be determined due to artefacts. $ACID_{70\%}$ = Average above 70% of the maximum activity concentration corrected for injected dose; $SUV_{70\%}$ = Average above 70% of the maximum standard uptake value; SUV_{max} = maximum standard uptake value

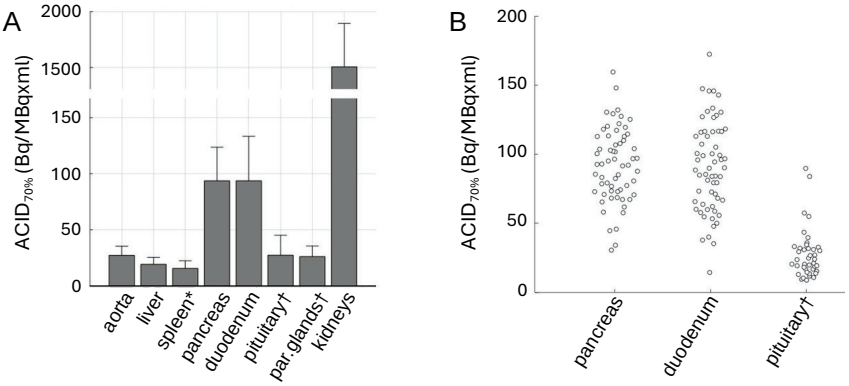


Figure 8. Uptake quantification in organs with clear uptake, blood pool uptake in liver, spleen and aorta and no-receptor specific uptake in the kidneys. Figure 8A shows the quantification of accumulation in multiple organs as average $ACID_{70\%}$ with standard deviation in all available participants (N=62; *N=55 for spleen, due to artefacts and †N=41 for the head). The individual variation in tracer accumulation ($ACID_{70\%}$) in the pancreas, duodenum and pituitary among all participants can be observed in the scatterplots in 8B, showing all individual data points. ACID = activity concentration corrected for injected dose.

Uptake over time

In blood pool (measured in the descending thoracic aorta and left ventricle), decay corrected activity concentration decreased (RC = 0.53; R^2=0.90, 95%CI 0.45-0.61), from one to two hours after administration. As expected, the decay corrected activity in the pancreas increased over time (RC = 1.2 R^2=0.99, 95%CI 1.12-1.24). General linear model analysis showed a significant difference in RC between blood pool and pancreas (interaction p<0.001). Analysis in breast tissue could be performed in seven female participants with RC of 0.84 (R^2=0.99, 95%CI 0.74-0.94), which statistically differed from blood pool (interaction p<0.001). In liver, spleen, skeletal muscle and lung RC were comparable to blood pool: 0.61 (R^2=0.83, 95%CI 0.44-0.78, interaction p=0.41), 0.48 (R^2=0.54, 95%CI 0.22-0.74, interaction p=0.69), 0.48 (R^2=0.86, 95%CI 0.36-0.60, interaction p=0.71) and 0.44 (R^2=0.71, 95%CI 0.27-0.60, interaction p=0.60), respectively. In absolute values, activity concentration in these tissues was lower compared to blood pool (visualized in detail in Figure 9).

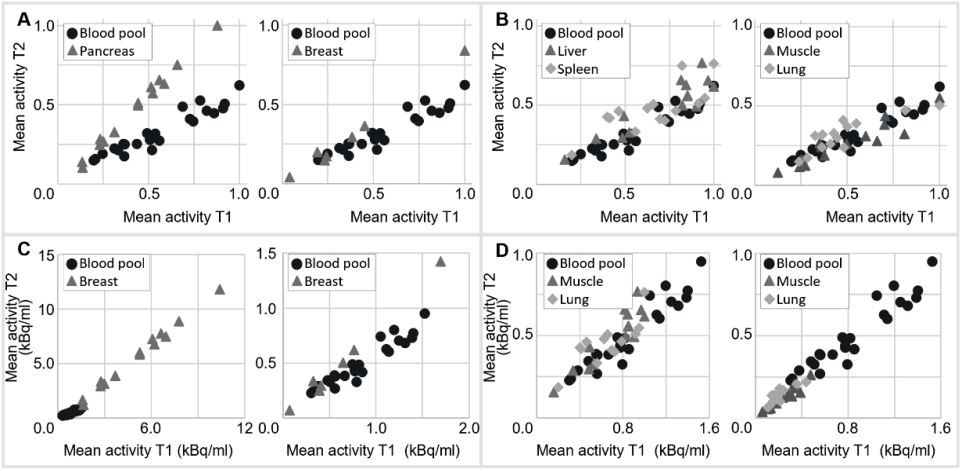


Figure 9. Uptake at one hour vs two hours. Scatterplots of decay corrected and normalized (top row) or unnormalized (bottom row) activity concentrations at one hour (T1) versus two hours (T2) after ^{68}Ga-exendin administration. In all subfigures, organ activity is compared with blood pool activity as measured in the descending thoracic aorta (all participants) and left ventricle (10 participants). The normalized data only shows the slope of the scatterplots, while the unnormalized data also shows the absolute uptake count. The subfigures show: receptor specific uptake in the pancreas in A (N=14) and in glandular breast tissue in B (N=7); non-specific uptake in the liver and spleen in C; and no uptake in skeletal muscle and lung in D (N=14).

Image quality

In 20 PET/CT scans (31%), artefacts surrounding the kidneys were observed. These were photopenic or halo artefacts of variable extent in 16 participants (Figure 10) and spillover artefacts in four participants (Figure 10). Artefacts were mainly observed in participants with obesity, but also in some participants with normal to slightly increased weight. As

a result, uptake values could not be determined in spleen in seven cases and uptake in the small and large intestines, could not reliably be assessed. In the liver, quantification possible in all participants in at least a major part of the organ. In one participant with morbid obesity, a possible artefact appeared as irregular uptake with hotspots in the liver; subsequent ultrasound did not reveal any abnormalities.

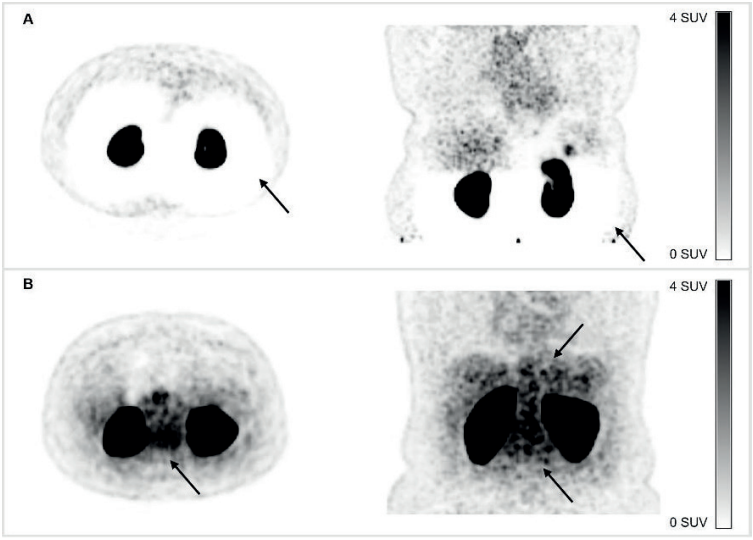


Figure 10. Photopenic and spillover artefact. Especially in participants with larger abdominal size, artefacts (arrows) surrounding the very high uptake in the kidneys (K) occurred. Here, an examples of a halo artefact (A) in one participant and a spillover artefact (B) in another participant are shown in an axial and a coronal view. A halo artefact is shown as area with a lack of activity (A, arrows) and a spillover artefact as area with increased activity (B, arrows).

DISCUSSION

The main finding of this study is that ^{68}Ga-exendin accumulates in several organs outside the pancreas and duodenum in humans, suggesting GLP-1R expression in those organs. These organs include the pituitary gland, salivary glands, gastric mucosa, glandular breast tissue, myocardium, uterus and ovaries. This information may be important to study the extra-pancreatic effects of GLP-1RAs in more detail. Here, we compare these findings with known GLP-1R expression and GLP-1 actions and discuss their significance for further understanding of the physiological actions of GLP-1 and GLP-1RAs.

Our results are in line with earlier findings of ^{68}Ga-exendin imaging and GLP-1R expression assessments in animals and *ex vivo* human tissues (1, 4, 7-9, 15-23). In the pancreas and duodenum, GLP-1R expression resulting in ^{68}Ga-exendin accumulation is well known. The expression of the GLP-1R on the beta cells in the islets of Langerhans forms the basis

for the use of GLP-1RAs and beta cell imaging by ^{68}Ga-exendin PET/CT. Our data confirm previously described pancreas uptake of radiolabeled exendin and interindividual differences, which reflects the natural variability of pancreatic beta cell mass as previously demonstrated by histopathology/immunohistochemistry (24).

In the duodenum, strong ^{68}Ga-exendin accumulation has been attributed to GLP-1R expression in the Brunner glands (15). In this study, accumulation levels in the duodenum were similar to those in the pancreas in all participants, and high interindividual variability in volume and intensity was observed. In view of these results, duodenal GLP-1Rs may have an important physiological role. For example, GLP-1R signaling has been suggested to play a role in regulating the secretion of mucin and other factors that protect the mucosa or to affect gastro-intestinal motility, although the effect of vagal mechanisms may be much larger (25). In view of the high GLP-1R expression levels in the duodenum (comparable to the uptake in the beta cells) and the anticipated important physiological function this observation points to, we should consider to more systematically assess the effects of GLP-1 exerted in the duodenum.

Accumulation in the gastric mucosa was of lower intensity than in the duodenum. Here, GLP-1R expression has been assigned to secretory and parietal cells, potentially regulating gastric acid secretion (17, 25). In line with this, an older study suggested that GLP-1RAs inhibit gastric acid secretion (26). However, the physiological role of GLP-1R signaling in the gastric wall, and how physiological effects are correlated with the rate of receptor expression, are not yet understood. The much less intense gastric accumulation of ^{68}Ga-exendin than duodenal accumulation may indicate towards a more prominent physiological role of GLP-1R signaling in the duodenum. However, we would like to point out that stronger signal amplification may lead to stronger effects than expected based on receptor expression alone.

In the pituitary gland, accumulation of ^{68}Ga-exendin in most participants. This is in line with previous observations of GLP-1R expression in the pituitary gland (7, 18). In other central brain structures known to express GLP-1R, we did not observe any accumulation of the tracer, possibly suggesting that ^{68}Ga-exendin does not pass the blood brain barrier (BBB). Passage of the BBB by other GLP-1Ras has been a matter of debate as well, and an alternative pathway for GLP-1 signaling to the central nervous system (CNS) via the pituitary gland may exist, as we have discussed previously (27). These findings may point towards a pivotal role of the pituitary gland (and possibly surrounding hypothalamic areas) in central GLP-1RA effects (27).

In the myocardium, ^{68}Ga-exendin accumulation was observed in only few participants, but this seems to be in line with previous reports. To date, human cardiac GLP-1R expression has mainly been studied in tissue samples from diseased hearts and GLP-1R expres-

sion has been demonstrated in, for example, the sinus node and cardiac ventricles (8, 16, 20, 28, 29). One of the effects of GLP-1RAs on the heart is increasing the heart rate (1, 4). We did not detect clear tracer accumulation in the sinus node in any of our participants, possibly due to low GLP-1R expression and the small volume of the sinus node in combination with its movement and background activity in the blood. In another study, upregulation of GLP-1R expression in the myocardium has been linked to cardiac failure (20). In line with this, GLP-1RAs seem to have beneficial effects on cardiac function (1, 4). Moreover, in rodents, GLP-1R upregulation was observed after myocardial infarction, which was visualized by increased myocardial accumulation of radiolabeled exendin (30, 31). In the current study, none of the participants had known cardiac disease, infarction or cardiac failure. Upregulation of the GLP-1R due to cardiac failure is therefore not expected, which may explain the relatively low ^{68}Ga-exendin accumulation we observed in only a few individuals. However, the fact that we have been able to identify ^{68}Ga-exendin uptake by *in vivo* PET imaging in those participants with probably low rates of GLP-1R expression, indicates the potential of GLP-1R PET imaging to further elucidate the presence and role of GLP-1R expression in the human myocardium.

In females, ^{68}Ga-exendin accumulation in breast tissue, uterus and ovary corresponds with previous findings, both in normal and malignant tissues (7, 19, 21, 22, 32). In tissue samples and cell lines of ovarian, endometrial and breast cancer, GLP-1RAs attenuated cell growth and high GLP-1R expression was correlated with longer progression-free survival in endometrial cancer (21, 32, 33). However, treatment with GLP-1RAs was not associated with incidence of cancer in breast, ovary or uterus in human (34, 35). In polycystic ovary syndrome, treatment with GLP-1RAs ameliorates metabolic and hormonal parameters (34).

Finally, accumulation of ^{68}Ga-exendin in the salivary glands and, with less intensity, in the nasal mucosa, is to the best of our knowledge one of the first indications of GLP-1R expression in these tissues in humans. GLP-1R expression has been detected in the duct systems of large salivary glands in rats and has been proposed to be expressed in mucinous cells in the tracheal mucosa (23, 36). However, it may be difficult to discriminate GLP-1R expression in these tissues from the presence of GLP-1R expressing macrophages or from nonspecific uptake in these tissues as is known from other radiotracers (37-39).

In few organs where GLP-1R expression has been described, we did not observe accumulation of ^{68}Ga-exendin, including for example, the thyroid gland and lung. Several reasons may explain the lack of accumulation. First, GLP-1R expression may be very low, resulting in undetectable levels of accumulation or volumes that are too small to visualize with PET. However, the radiotracer has a high sensitivity for the GLP-1R, allowing detection of picomolar amounts of the tracer and very low levels of GLP-1R (10). Another reason might be differences between humans and animal models that have been used in the majority

of studies demonstrating GLP-1R expression (18, 40, 41). For example, in the lung, thyroid and exocrine pancreas, it is known that findings from animal studies does not reflect human GLP-1R expression (7, 42, 43).

Altogether, our data suggest that ^{68}Ga-exendin PET/CT is a suitable and valuable technique to assess GLP-1R expression *in vivo* in humans. Radiolabeled exendin-4 has very high specificity and affinity for the GLP-1R, as was demonstrated in pancreatic islets, duodenal Brunner's glands and gastric glandular cells (7, 11-13, 17, 44-48). At low peptide doses, as administered in the current study, self-blocking of the radiotracer is prevented (44). Moreover, our findings on ^{68}Ga-exendin accumulation were highly reproducible among the participants and in line with expected GLP-1R expression and its individual variation in different tissue types, based on GLP-1RA effects and histopathological tissue analyses (11, 24, 44, 47). Therefore, we assume that ^{68}Ga-exendin uptake as measured with PET/CT accurately reflects interindividual variation in tissue-specific GLP-1R expression levels.

Our study has potential limitations that need to be mentioned. First, as the individuals scanned participated in different studies focusing on different areas of the body, we did not obtain images of all examined organs in all individuals. Second, patient inclusion was selective according to the respective study protocol and healthy controls were not included. However, our data still represent the most elaborate analysis of organ-specific GLP-1R expression *in vivo* in humans to date, and provide important insights into the physiological relevance of these organs for GLP-1R signaling. Third, ^{68}Ga-exendin PET/CT was performed at a single time point after administration of the radiotracer, while a dynamic scanning protocol may better reflect GLP-1R expression. However, in a recent clinical study, the quantification of radiolabeled exendin-4 at 55 minutes after administration correlated very well with the modelled uptake rate from a dynamic scanning protocol (44). Finally, when analyzing our data, we have taken into account the limitations of the technique itself (i.e. ^{68}Ga-exendin PET/CT imaging) and how these affect quantification. Radiotracer accumulation is very high in the kidneys, due to non-receptor specific reabsorption and retention of ^{68}Ga-exendin in the proximal tubules via the scavenger receptors cubilin and megalin (14). In combination with increased scattering, mainly due to large waist circumference in individuals with obesity, this resulted in halo- or spill-over artefacts in some individuals. Consequently, accurate visualization and quantification of ^{68}Ga-exendin uptake in the region around the kidneys may be impaired. In order to obtain accurate quantification results, we have tackled this issue by quantification of those regions only that were not affected by such artefacts. In addition to these artefacts, quantification may be inaccurate in small volumes, such as the pituitary, due to partial volume effects which are a common limitation in image quantification in general (49). However, as this is a shortcoming occurring in all analyzed individuals to the same extent, we presume that this effect is leveled out.

The data as presented in this study was not suitable to perform reliable comparison of radiotracer uptake quantification between different groups of patients, mainly due the small sizes of the subgroups and large inter-individual variation. However, this would be of utmost importance in future studies, as is substantiated by recently published data. Jansen et al. showed a lower uptake of 68Ga-exendin-4 in the pancreas in patients with poor-regulated T1D as compared to patients with well-regulated T1D (50). Unpublished own data revealed lower uptake in the pancreas in patients with T2D treated with insulin as compared to patients with T2D treated only with metformin (51). In contrast, no differences were found in pancreas uptake in patients with complete and no remission of T2D after bariatric surgery, nor between patients with post-bariatric hypoglycemia and post-bariatric controls without hypoglycemia or (a history of) diabetes (52, 53). In the pituitary, radiotracer uptake was higher in men than women in participants with T2D and the uptake was not related with good or poor weight loss responses on GLP-1RA therapy (54). These data and the data as presented here demonstrated the possibility to quantify 68Ga-exendin uptake in relevant extrapancreatic tissues.

The use of GLP-1R imaging may have important implications for studying the effects of treatment with GLP-1RAs. Traditionally, research has focused mainly on the (patho) physiological role of GLP-1 and GLP-1RAs in glucose homeostasis and diabetes treatment. More recently, the focus has also shifted to obesity treatment and treatment of other diseases, such as neurodegenerative disorders (2, 5, 55, 56). However, despite the remarkable treatment effects of GLP-1RAs, the exact mechanisms behind its positive effects remain incompletely understood. Therefore, it seems intriguing that ^{68}Ga-exendin PET/CT may help us to better elucidate the pathophysiological mechanisms responsible for successful GLP-1RA treatment by for example comparing treatment effects in specific organs with GLP-1R expression. This may open possibilities to define new or optimize existing therapy regimens. In addition, we may be able to individually predict treatment response or specifically select patients that will respond to treatment. For this purpose and for correct interpretation of uptake patterns in patients, it is also essential to understand baseline radiotracer uptake. Therefore, the inclusion of healthy controls is essential in future studies assessing ^{68}Ga-exendin uptake. The very low effective radiation dose of ^{68}Ga-exendin justifies the inclusion of healthy controls or repeated examinations (47).

CONCLUSION

This study confirms accumulation of ^{68}Ga-exendin in organs with well-known GLP-1R expression, the pancreas and duodenum, but also identifies accumulation in the pituitary gland, salivary glands, glandular breast tissue and myocardium. We suggest that the level of uptake of ^{68}Ga-exendin reflects the physiological importance for GLP-1 effects on the respective organ. ^{68}Ga-exendin PET/CT is therefore a valuable technique to increase our knowledge about physiological GLP-1R signaling and to elucidate pathophysiological mechanisms underlying (variable) treatment responses to GLP-1RAs.

REFERENCES

1. Müller TD, Finan B, Bloom SR, D'Alessio D, Drucker DJ, Flatt PR, Fritsche A, Gribble F, Grill HJ, Habener JF, Holst JJ, Langhans W, Meier JJ, Nauck MA, Perez-Tilve D, Pocai A, Reimann F, Sandoval DA, Schwartz TW, Seeley RJ, Stemmer K, Tang-Christensen M, Woods SC, DiMarchi RD, and Tschöp MH. Glucagon-like peptide 1 (GLP-1). *Mol Metab* 30: 72-130, 2019.
2. Brown E, Heerspink HJL, Cuthbertson DJ, and Wilding JPH. SGLT2 inhibitors and GLP-1 receptor agonists: established and emerging indications. *Lancet* 398: 262-276, 2021.
3. Abu-Hamdah R, Rabiee A, Meneilly GS, Shannon RP, Andersen DK, and Elahi D. Clinical review: The extrapancreatic effects of glucagon-like peptide-1 and related peptides. *J Clin Endocrinol Metab* 94: 1843-1852, 2009.
4. Drucker DJ. The Cardiovascular Biology of Glucagon-like Peptide-1. *Cell Metab* 24: 15-30, 2016.
5. Holscher C. Protective properties of GLP-1 and associated peptide hormones in neurodegenerative disorders. *Br J Pharmacol* 179: 695-714, 2022.
6. Heppner KM, and Perez-Tilve D. GLP-1 based therapeutics: simultaneously combating T2DM and obesity. *Front Neurosci* 9: 92, 2015.
7. Korner M, Stockli M, Waser B, and Reubi JC. GLP-1 receptor expression in human tumors and human normal tissues: potential for in vivo targeting. *J Nucl Med* 48: 736-743, 2007.
8. Pyke C, Heller RS, Kirk RK, Ørskov C, Reedtz-Runge S, Kaastrup P, Hvelplund A, Bardram L, Calatayud D, and Knudsen LB. GLP-1 receptor localization in monkey and human tissue: novel distribution revealed with extensively validated monoclonal antibody. *Endocrinology* 155: 1280-1290, 2014.
9. Manell E, Puuvuori E, Svensson A, Velikyan I, Hulsart-Billstrom G, Hedenqvist P, Holst JJ, Jensen Waern M, and Eriksson O. Exploring the GLP-1-GLP-1R axis in porcine pancreas and gastrointestinal tract in vivo by ex vivo autoradiography. *BMJ Open Diabetes Res Care* 9: 2021.
10. Brom M, Joosten L, Oyen WJ, Gotthardt M, and Boerman OC. Radiolabelled GLP-1 analogues for in vivo targeting of insulinomas. *Contrast Media Mol Imaging* 7: 160-166, 2012.
11. Brom M, Woliner-van der Weg W, Joosten L, Frielink C, Bouckenooghe T, Rijken P, Andralojc K, Göke BJ, de Jong M, Eizirik DL, Béhé M, Lahoutte T, Oyen WJ, Tack CJ, Janssen M, Boerman OC, and Gotthardt M. Non-invasive quantification of the beta cell mass by SPECT with ^{111}In-labelled exendin. *Diabetologia* 57: 950-959, 2014.
12. Jodal A, Lankat-Buttgereit B, Brom M, Schibli R, and Béhé M. A comparison of three (67/68) Ga-labelled exendin-4 derivatives for β-cell imaging on the GLP-1 receptor: the influence of the conjugation site of NODAGA as chelator. *EJNMMI Res* 4: 31, 2014.
13. Selvaraju RK, Velikyan I, Johansson L, Wu Z, Todorov I, Shively J, Kandeel F, Korsgren O, and Eriksson O. In vivo imaging of the glucagonlike peptide 1 receptor in the pancreas with 68Ga-labeled DO3A-exendin-4. *J Nucl Med* 54: 1458-1463, 2013.
14. Gotthardt M, van Eerd-Vismale J, Oyen WJ, de Jong M, Zhang H, Rolleman E, Maecke HR, Béhé M, and Boerman O. Indication for different mechanisms of kidney uptake of radiolabeled peptides. *J Nucl Med* 48: 596-601, 2007.
15. Antwi K, Hepprich M, Müller NA, Reubi JC, Fani M, Rottenburger C, Nicolas G, Kaul F, Christ ER, and Wild D. Pitfalls in the Detection of Insulinomas With Glucagon-Like Peptide-1 Receptor Imaging. *Clin Nucl Med* 45: e386-e392, 2020.
16. Baggio LL, Yusta B, Mulvihill EE, Cao X, Streutker CJ, Butany J, Cappola TP, Margulies KB, and Drucker DJ. GLP-1 Receptor Expression Within the Human Heart. *Endocrinology* 159: 1570-1584, 2018.

17. Broide E, Bloch O, Ben-Yehudah G, Cantrell D, Shirin H, and Rapoport MJ. GLP-1 receptor is expressed in human stomach mucosa: analysis of its cellular association and distribution within gastric glands. *J Histochem Cytochem* 61: 649-658, 2013.
18. Goke R, Larsen PJ, Mikkelsen JD, and Sheikh SP. Identification of specific binding sites for glucagon-like peptide-1 on the posterior lobe of the rat pituitary. *Neuroendocrinology* 62: 130-134, 1995.
19. Hashimoto Takigami N, Kuniyoshi S, Miki Y, Tamaki K, Kamada Y, Uehara K, Tsuchiya S, Terukina S, Iwabuchi E, Kanai A, Miyashita M, Ishida T, Tamaki N, and Sasano H. Breast Cancer, Diabetes Mellitus and Glucagon-Like Peptide-1 Receptor Toward Exploring Their Possible Associations. *Breast Cancer Res Treat* 189: 39-48, 2021.
20. Hattori A, Kawamura I, Yamada Y, Kanamori H, Aoyama T, Ushikoshi H, Kawasaki M, Nishigaki K, Tamemura G, and Minatoguchi S. Elevated plasma GLP-1 levels and enhanced expression of cardiac GLP-1 receptors as markers of left ventricular systolic dysfunction: a cross-sectional study. *BMJ Open* 3: e003201, 2013.
21. Kanda R, Hiraike H, Wada-Hiraike O, Ichinose T, Nagasaka K, Sasajima Y, Ryo E, Fujii T, Osuga Y, and Ayabe T. Expression of the glucagon-like peptide-1 receptor and its role in regulating autophagy in endometrial cancer. *BMC Cancer* 18: 657, 2018.
22. Mao D, Cao H, Shi M, Wang CC, Kwong J, Li JJX, Hou Y, Ming X, Lee HM, Tian XY, Wong CK, Chow E, Kong APS, Lui VWY, Chan PKS, and Chan JCN. Increased co-expression of PSMA2 and GLP-1 receptor in cervical cancer models in type 2 diabetes attenuated by Exendin-4: A translational case-control study. *EBioMedicine* 65: 103242, 2021.
23. Ono R. [GLP-1 receptor expression in rat major salivary glands and the effects of bilateral maxillary molar extraction on its expression]. *Kokubyo Gakkai Zasshi* 81(3)-82(1): 8-14, 2015.
24. Rahier J, Guiot Y, Goebbels RM, Sempoux C, and Henquin JC. Pancreatic beta-cell mass in European subjects with type 2 diabetes. *Diabetes Obes Metab* 10 Suppl 4: 32-42, 2008.
25. Holst JJ, Andersen DB, and Grunddal KV. Actions of glucagon-like peptide-1 receptor ligands in the gut. *Br J Pharmacol* 179: 727-742, 2022.
26. Wettergren A, Wojdemann M, Meisner S, Stadil F, and Holst JJ. The inhibitory effect of glucagon-like peptide-1 (GLP-1) 7-36 amide on gastric acid secretion in humans depends on an intact vagal innervation. *Gut* 40: 597-601, 1997.
27. Deden LN, Booij J, Grandjean J, Homberg JR, Hazebroek EJ, Gotthardt M, and Boss M. Brain Imaging of the GLP-1 Receptor in Obesity Using (68)Ga-NODAGA-Exendin-4 PET. *Brain Sci* 11: 2021.
28. Wallner M, Kolesnik E, Ablasser K, Khafaga M, Wakula P, Ljubojevic S, Thon-Gutschi EM, Sourij H, Kapl M, Edmunds NJ, Kuzmiski JB, Griffith DA, Knez I, Pieske B, and von Lewinski D. Exenatide exerts a PKA-dependent positive inotropic effect in human atrial myocardium: GLP-1R mediated effects in human myocardium. *J Mol Cell Cardiol* 89: 365-375, 2015.
29. Clarke SJ, Giblett JP, Yang LL, Hubsch A, Zhao T, Aetesam-Ur-Rahman M, West NEJ, O'Sullivan M, Figg N, Bennett M, Wewer Albrechtsen NJ, Deacon CF, Cheriyan J, and Hoole SP. GLP-1 Is a Coronary Artery Vasodilator in Humans. *J Am Heart Assoc* 7: e010321, 2018.
30. Gao H, Kiesewetter DO, Zhang X, Huang X, Guo N, Lang L, Hida N, Wang H, Wang H, Cao F, Niu G, and Chen X. PET of glucagonlike peptide receptor upregulation after myocardial ischemia or reperfusion injury. *J Nucl Med* 53: 1960-1968, 2012.
31. Ståhle M, Kytö V, Kiugel M, Liljenbäck H, Metsälä O, Käkelä M, Li XG, Oikonen V, Saukko P, Nuutila P, Knuuti J, Roivainen A, and Saraste A. Glucagon-like peptide-1 receptor expression after myocardial infarction: Imaging study using (68)Ga-NODAGA-exendin-4 positron emission tomography. *J Nucl Cardiol* 27: 2386-2397, 2020.

32. He W, Yu S, Wang L, He M, Cao X, Li Y, and Xiao H. Exendin-4 inhibits growth and augments apoptosis of ovarian cancer cells. *Mol Cell Endocrinol* 436: 240-249, 2016.
33. Tanaka Y, Iwaya C, Kawanami T, Hamaguchi Y, Horikawa T, Shigeoka T, Yanase T, Kawanami D, and Nomiyama T. Combined treatment with glucagon-like peptide-1 receptor agonist exendin-4 and metformin attenuates breast cancer growth. *Diabetol Int* 13: 480-492, 2022.
34. Abdalla MA, Deshmukh H, Atkin S, and Sathyapalan T. The potential role of incretin-based therapies for polycystic ovary syndrome: a narrative review of the current evidence. *Ther Adv Endocrinol Metab* 12: 2042018821989238, 2021.
35. Piccoli GF, Mesquita LA, Stein C, Aziz M, Zoldan M, Degobi NAH, Spiazzi BF, Lopes Junior GL, Colpani V, and Gerchman F. Do GLP-1 Receptor Agonists Increase the Risk of Breast Cancer? A Systematic Review and Meta-analysis. *J Clin Endocrinol Metab* 106: 912-921, 2021.
36. Richter G, Feddersen O, Wagner U, Barth P, Göke R, and Göke B. GLP-1 stimulates secretion of macromolecules from airways and relaxes pulmonary artery. *Am J Physiol* 265: L374-381, 1993.
37. Stahle M, Hellberg S, Virta J, Liljenback H, Metsala O, Jauhiainen M, Saukko P, Yla-Herttuala S, Nuutila P, Knuuti J, Saraste A, and Roivainen A. Positron Emission Tomography Tracer [68ga] Nodaga-Exendin-4 Detects Glucagon-Like Peptide-1 Receptor Expression in Mouse Atherosclerotic Vascular Lesions. *Atherosclerosis* 263: E55-E56, 2017.
38. Buldak L, Machnik G, Buldak RJ, Labuzek K, Boldys A, Belowski D, Basiak M, and Okopien B. Exenatide (a GLP-1 agonist) expresses anti-inflammatory properties in cultured human monocytes/macrophages in a protein kinase A and B/Akt manner. *Pharmacol Rep* 68: 329-337, 2016.
39. Rupp NJ, Umbricht CA, Pizzuto DA, Lenggenhager D, Topfer A, Muller J, Muehlematter UJ, Ferraro DA, Messerli M, Morand GB, Huber GF, Eberli D, Schibli R, Muller C, and Burger IA. First Clinicopathologic Evidence of a Non-PSMA-Related Uptake Mechanism for (68)Ga-PSMA-11 in Salivary Glands. *J Nucl Med* 60: 1270-1276, 2019.
40. Farkas E, Szilvasy-Szabo A, Ruska Y, Sinko R, Rasch MG, Egebjerg T, Pyke C, Gereben B, Knudsen LB, and Fekete C. Distribution and ultrastructural localization of the glucagon-like peptide-1 receptor (GLP-1R) in the rat brain. *Brain Struct Funct* 226: 225-245, 2021.
41. Trapp S, and Brierley DI. Brain GLP-1 and the regulation of food intake: GLP-1 action in the brain and its implications for GLP-1 receptor agonists in obesity treatment. *Br J Pharmacol* 179: 557-570, 2022.
42. Gotthardt M, Joosten L, Jansen TJP, Brom M, Boss M, and Willekens SMA. From Mice to Humans: The Exocrine Pancreas Does Not Matter in Human GLP-1 Receptor Imaging. *J Nucl Med* 62: 745, 2021.
43. Waser B, Blank A, Karamitopoulou E, Perren A, and Reubi JC. Glucagon-like-peptide-1 receptor expression in normal and diseased human thyroid and pancreas. *Mod Pathol* 28: 391-402, 2015.
44. Eriksson O, Velikyan I, Haack T, Bossart M, Laitinen I, Larsen PJ, Berglund JE, Antoni G, Johansson L, Pierrou S, Tillner J, and Wagner M. Glucagonlike Peptide-1 Receptor Imaging in Individuals with Type 2 Diabetes. *J Nucl Med* 63: 794-800, 2022.
45. Hepprich M, Antwi K, Waser B, Reubi JC, Wild D, Christ ER. Brunner's Gland Hyperplasia in a Patient after Roux-Y Gastric Bypass: An Important Pitfall in GLP-1 Receptor Imaging. *Case Rep Endocrinol* 2020: 4510910, 2020.
46. Brom M, Joosten L, Frielink C, Peeters H, Bos D, van Zanten M, Boerman O, and Gotthardt M. Validation of (111)In-Exendin SPECT for the Determination of the beta-Cell Mass in BioBreeding Diabetes-Prone Rats. *Diabetes* 67: 2012-2018, 2018.

47. Boss M, Buitinga M, Jansen TJP, Brom M, Visser EP, and Gotthardt M. PET-Based Human Dosimetry of (68)Ga-NODAGA-Exendin-4, a Tracer for beta-Cell Imaging. *J Nucl Med* 61: 112-116, 2020.
48. Mikkola K, Yim CB, Fagerholm V, Ishizu T, Elomaa VV, Rajander J, Jurttila J, Saanijoki T, Tolvanen T, Tirri M, Gourni E, Behe M, Gotthardt M, Reubi JC, Macke H, Roivainen A, Solin O, and Nuutila P. 64Cu- and 68Ga-labelled [Nle(14),Lys(40)(Ahx-NODAGA)NH2]-exendin-4 for pancreatic beta cell imaging in rats. *Mol Imaging Biol* 16: 255-263, 2014.
49. Soret M, Bacharach SL, and Buvat I. Partial-volume effect in PET tumor imaging. J Nucl Med 48: 932-945, 2007.
50. Jansen TJP, Brom M, Boss M, Buitinga M, Tack CJ, van Meijel LA, de Galan BE, Gotthardt M. Importance of beta cell mass for glycaemic control in people with type 1 diabetes. Diabetologia 66(2):367-75, 2023.
51. Deden L, Boss M, Tokgöz S, de Boer H, Aarts E, van Bon A, Janssen I, Berends F, de Galan B, Hazebroek E, Gotthardt M. Changes in beta cell mass in remission of type 2 diabetes after Roux-en-Y gastric bypass surgery, quantified in vivo by 68Ga-exendin-4 PET/CT. Diabetologia Abstract Volume 60th EASD Annual Meeting, 2024. doi.org/10.1007/s00125-024-06226-0
52. Tokgöz S, Deden LN, Hofboer A, Hazebroek EJ, de Boer H, van Bon AC, Meijer RI, de Galan BE, Tack CJ, Boss M, Gotthardt M. β-Cell Mass in Individuals With and Without Postbariatric Hypoglycemia After Roux-en-Y Gastric Bypass. Diabetes (12):1203-2306, 2015
53. Tokgöz S, Deden LN, Hofboer A, Hazebroek EJ, de Boer H, van Bon AC, Meijer RI, de Galan BE, Tack CJ, Boss M, Gotthardt M. Beta cell function and mass in individuals with and without remission of type 2 diabetes after Roux-en-Y gastric bypass. Diabetologia, preprint, 2025
54. Tokgöz S, Boss M, Jansen TJP, Meijer R, Frielink C, van Bon AC, Tack CJ, de Galan BE, Gotthardt M. Activation of the HPA axis does not explain nonresponsiveness to GLP-1R agonist treatment in individuals with type 2 diabetes. Diabetes 74(2):212-222, 2025
55. Mulvaney CA, Duarte GS, Handley J, Evans DJ, Menon S, Wyse R, and Emsley HC. GLP-1 receptor agonists for Parkinson's disease. Cochrane Database Syst Rev 7: Cd012990, 2020.
56. Iqbal J, Wu HX, Hu N, Zhou YH, Li L, Xiao F, Wang T, Jiang HL, Xu SN, Huang BL, and Zhou HD. Effect of glucagon-like peptide-1 receptor agonists on body weight in adults with obesity without diabetes mellitus-a systematic review and meta-analysis of randomized control trials. Obes Rev 23: e13435, 2022.



6

Brain Imaging of the GLP-1 Receptor in Obesity Using ^{68}Ga-NODAGA-exendin-4 PET

Laura N. Deden[1,2], Jan Booij[1,3], Joanes Grandjean[1,4], Judith R. Homberg[4], Eric J. Hazebroek[2,5], Martin Gotthardt[1], Marti Boss[1]

Brain Sci. 2021, 11(12):1647. doi: 10.3390/brainsci11121647

ABSTRACT

Stimulation of glucagon-like peptide-1 (GLP-1) receptors increases the insulin release in the pancreas during high glucose levels, and also stimulates a feeling of satiety. Likewise, synthetic GLP-1 receptor agonists derived from exendin are used successfully in the treatment of type 2 diabetes mellitus and obesity. Interestingly, preclinical and clinical studies further suggest that GLP-1 receptor agonists may decrease motor, behavioral, and cognitive symptoms in (animal models) Parkinson's disease and Alzheimer's disease and may slow down neurodegeneration. These observations suggest stimulation of GLP-1 receptors in the brain. The GLP-1 positron emission tomography (PET) tracer ^{68}Ga-NODAGA-exendin-4 (^{68}Ga-exendin) has been developed and successfully used for imaging in humans. In an ongoing study on the effects of bariatric surgery on GLP-1 receptor expression, we performed ^{68}Ga-exendin PET/CT in obese subjects. Here we evaluated whether GLP-1 receptor binding could be visualized in the central nervous system in 10 obese subjects (seven woman; body mass index: mean ± SD: 39 ± ± 4.4 kg/m2) before bariatric surgery. Although we observed clear uptake in the pituitary area (mean SUV_{max} 4.3 ± 2.3), we found no significant uptake in other parts of the brain. We conclude that ^{68}Ga-exendin PET/CT cannot be used to analyze GLP-1 receptors in the brain of obese subjects.

INTRODUCTION

Glucagon-like peptide-1 (GLP-1) is predominantly synthesized in enteroendocrine cells of the distal small intestine and secreted in the blood when food enters the duodenum (for a recent review, see Mori et al. [1]). GLP-1 belongs to the incretin family (INtestinal seCRETion of INSulin). Incretins increase the release of insulin in the pancreas during high blood glucose levels, which is named the "incretin effect" [2].

GLP-1 is also synthesized in the brain, and particularly in the nucleus tractus solitarius, which is located in the brainstem [3]. These GLP-1 expressing neurons extend to parts of the hypothalamus, particularly the paraventricular nucleus and arcuate nucleus [4]. GLP-1 secretion stimulates a feeling of saturation, and as such plays a role in the regulation of appetite. Likewise, synthetic GLP-1 receptor agonists are used successfully in the treatment of type 2 diabetes mellitus and to reduce overweight in obesity (for recent reviews, see Nauck and Meier [5] and Hussein et al. [6]).

GLP-1 receptors are, however, not only located in the hypothalamus and nucleus tractus solitarius, but also in the substantia nigra, amygdala, hippocampus as well as in cortical areas such as the lateral prefrontal cortex [4,7–11]. Stimulation of these receptors may induce synaptogenesis/neurogenesis and protect against oxidative stress, neuroinflammation, and apoptosis [12]. Interestingly, in animal models of Parkinson's disease (PD) and Alzheimer's disease (AD), administration of GLP-1 receptor agonists may decrease the amyloid load, slow down dopaminergic degeneration, and improve motor and cognitive functions such as learning and memory [8,12–23].

The half-life of GLP-1 is short (a few minutes) because it is rapidly metabolized by the enzyme dipeptidyl peptidase IV (DDP-IV) [24]. Fortunately, the naturally occurring GLP-1 agonist exendin-4 is resistant to DDP-IV degradation. Exendin-4 has a much longer half-life (approximately 2.4 h) [25] than GLP-1 and is thus suitable for treating type 2 diabetes mellitus by increasing insulin secretion. Several synthetic GLP-1 agonists derived from exendin-4 have been produced successfully [26].

Importantly, a recent randomized, placebo-controlled study showed that administration of the GLP-1 agonist exenatide (a synthetic GLP-1 analog derived from exendin-4) is able to slow down motor progression in patients suffering from PD [27]. Moreover, a smaller, open label study showed significant effects on cognition in PD [28]. Additionally, a small randomized, placebo-controlled study on AD showed that exenatide prevented decline of cerebral glucose metabolism, measured with 18F-FDG positron emission tomography (PET) [29].

PET tracers derived from exendin have been developed successfully, including ^{68}Ga-NODAGA-exendin-4 (for a recent review, see Jansen et al. [30]). In a recent study, we demonstrated the ability of ^{68}Ga-Exendin to visualize GLP-1 receptor expression on pancreatic beta cells [31]. Since GLP-1 receptor agonists are successfully used to reduce body weight and improve insulin resistance in obese subjects, and bariatric surgery may influence GLP-1 levels [32], we recently started a clinical study on the effects of bariatric surgery on GLP-1 binding as measured with ^{68}Ga-Exendin PET.

Although it is undisputed that GLP-1 agonists have central effects, the localization of GLP-1 receptors in the brain in human and mechanisms of GLP-1 agonists to cross the blood–brain barrier (BBB) are debated, especially since several observations do not support that these agonists can cross the BBB by general BBB permeability [4,9,33]. To contribute to this relevant issue, we here evaluated whether ^{68}Ga-exendin PET can be used to visualize and quantify GLP-1 receptors in the central nervous system (CNS). Furthermore, we discuss possible mechanisms of GLP-1 agonists to enter the CNS.

MATERIALS AND METHODS

Participants

Study subjects have been participating in an ongoing clinical study on the effects of bariatric surgery on GLP-1 receptor expression at the Radboud University Medical Center (Radboud UMC, Nijmegen, The Netherlands). Inclusion criteria for participation in this study were obesity (body mass index (BMI) ≥35 kg/m2), age >18 years, scheduled for bariatric surgery, and type 2 diabetes mellitus treated with insulin, sulfonylureas, or metformin. Exclusion criteria included pregnancy or breast feeding, kidney failure, liver failure, treatment with GLP-1 receptor agonists or DDP IV inhibitors, and BMI ≥50 kg/m2. Subjects underwent a medical evaluation, including medical history, physical examination, and blood tests, before study participation.

Participating subjects were eligible for the present analysis if they underwent whole-body ^{68}Ga-exendin PET imaging before surgery. All procedures were approved by the medical ethics committee of the Radboud UMC, and all subjects provided written informed consent in accordance with the Declaration of Helsinki.

Anthropometric Measurements

Demographic and anthropometric parameters were measured and documented by trained medical doctors.

PET/CT Imaging

To measure GLP-1 receptor expression, subjects underwent PET imaging after an overnight fast or fasting for at least four hours. Imaging was performed 60 min after intravenous bolus injection of approximately 100 MBq ^{68}Ga-exendin PET (for details on the synthesis of the radiotracer, see Boss et al. [31]). PET imaging from the skull to pelvis was performed on a Biograph mCT-40 time-of-flight PET-CT scanner (Siemens) located at the Radboudumc.

After acquiring a low-dose CT scan, static images were acquired for 5 min per bed position. Low-dose CT (40 mAs, 130 kV) was obtained without contrast and applied for attenuation correction and anatomical localization. PET was reconstructed using ultra-high definition, time-of-flight, scatter and attenuation correction and post-reconstruction Gaussian filter of 3 mm FWHM settings.

Volume-of-Interest (VOI) Analysis

Specific ^{68}Ga-exendin binding was assessed in the whole brain (exclud-ing the pituitary), pituitary, and pancreas. Blood pool activity was determined in the left ventricle and uptake in liver and subcutaneous adipose tissue was used to assess back-ground activity. Tracer uptake was determined in ellipsoid volumes of interest (VOI) that were representative for the whole organ and quantified using Inveon Research Workplace (version 4.1; Siemens Healthcare). Within the VOIs, the maximum standardized uptake (SUV_{max}) and mean SUV (SUV_{mean}) values were determined. Calculation of SUV was car-ried out as activity concentration (kBq/g)/[injected dose (MBq)/body weight (g)]; corrected for decay and assuming that 1 g tissue is equal to a volume of 1 mL.

Statistical Analysis

Since we analyzed data in 10 subjects with obesity, only descriptive statistics were performed.

RESULTS

Participants

We included 10 subjects (seven woman) with a median age of 55 years and a mean BMI of 39 kg/m^2 (Table 1).

Table 1. Demographic and weight characteristics of the 10 included participants.

Sex woman (%)	7 (70%)
Age (years)	53 ± 5.5
Weight (kg)	113 ± 13
BMI (kg/m^2)	39 ± 4.4

Data are expressed as number of cases (%) or mean ± standard deviation.

3.2. PET Analysis

In the CNS, we observed clear ^{68}Ga-exendin uptake in the pituitary area (Figure 1), which was variable between subjects, with a mean SUV_{mean} of 1.7 ± 0.57 (range: 0.88–2.7) and mean SUV_{max} of 4.3 ± 3.3 (range: 1.4–9.1). However, no ^{68}Ga-exendin uptake was visible in other parts of the brain (mean SUV_{mean}: 0.0010 ± 0.0066 (range: 0.0001–0.21) and SUV_{max} of 0.17 ± 0.095 (range: 0.013–0.32)) (Table 2).

Table 2. Uptake values of 68Ga-exendin (N=10)

	SUV_{mean}	SUV_{max}
Pituitary	1.7 ± 0.6 (0.9-2.7)	4.3 ± 2.3 (1.4-9.1)
Whole brain	0.01 ± 0.01 (0.00-0.02)	0.17 ± 0.10 (0.01-0.32)
Pancreas	5.5 ± 1.8 (2.3-8.1)	10.3 ± 3.0 (5.0-15.5)
Blood pool	1.5 ± 0.2 (1.2-2.0)	3.3 ± 0.6 (2.4-4.4)
Liver	0.67 ± 0.17 (0.26-0.96)	2.1 ± 0.6 (1.3-3.3)
SAT	0.20 ± 0.05 (0.14-0.29)	0.65 ± 0.16 (0.38-0.91)

Data are mean values ± standard deviation (range). SAT = subcutaneous adipose tissue, SUV = standard uptake value.

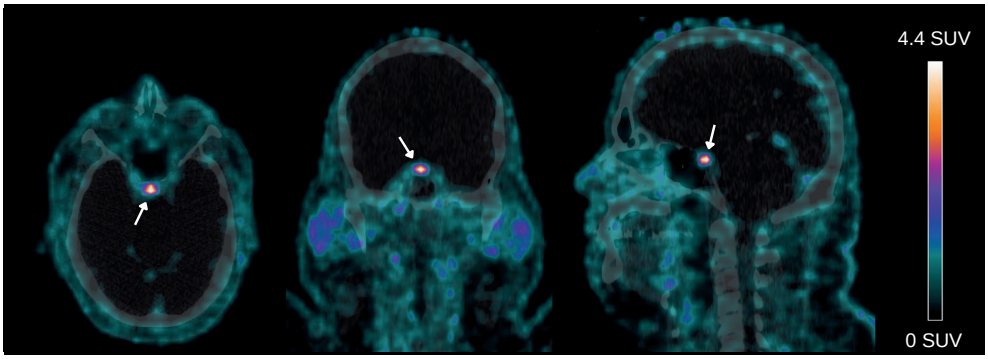


Figure 1. Example of ^{68}Ga-exendin PET/CT scan of the head of one of the participants in a coronal (left), axial (middle) and sagittal (right) view. Note the intense uptake in the pituitary gland (arrow)

In peripheral organs, clear uptake of ^{68}Ga-exendin was visible in the pancreas (Figure 2), with an average SUV_{mean} of 5.5 ± 1.8 (range 2.3–8.1) and SUV_{max} of 10.3 ± 3.0 (range: 5.0–15.5). In the blood pool, average SUV_{mean} was 1.5 ± 0.23 and in back-ground tissues

highest uptake levels were measured in the liver (SUV_{mean}: 0.67 ± 0.17) and lowest in subcutaneous adipose tissue (SUV_{mean}: 0.20 ± 0.054).

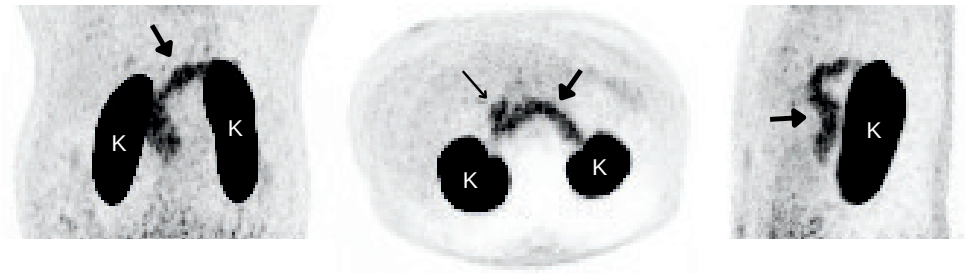


Figure 2. Maximum intensity projections of ^{68}Ga-exendin PET/CT of the abdomen of one of the participants in a coronal (left), axial (middle) and sagittal (right) view. Uptake in the pancreas (closed arrow), duodenum (open arrow) and kidneys (k) can be observed.

DISCUSSION

In this study, we show that there is no significant uptake of ^{68}Ga-exendin in the brain (parts inside the blood–brain barrier; BBB) of sub-jects with obesity, although there is clear uptake in the pituitary. We also reproduce the accumulation of ^{68}Ga-exendin PET in the pancreas [31].

^{68}Ga-exendin Uptake in Peripheral Organs

We have confirmed the ability of ^{68}Ga-exendin to assess GLP-1 binding in the pancreas [31]. In line with this finding, other radiotracers derived from exendin showed the ability to visualize the GLP-1 receptor expression in the pancreas [30,34].

^{68}Ga-exendin Uptake in the Pituitary Area

We can show significant ^{68}Ga-exendin uptake in the pituitary of subjects with obesity. Since earlier studies showed the ability of ^{68}Ga-exendin PET to visualize GLP-1 receptors in beta-cells of the pancreas [31], and the pituitary is located outside the blood–brain barrier (BBB) and expresses GLP-1 receptors extensively in rats and humans, particularly in the neuro-pituitary [35,36], this was an expected finding. As GLP-1 receptors play an important role in appetite and stress regulation), and the pituitary is an essential part of the hypothalamus–pituitary–adrenal gland (HPA)-axis, the GLP-1 receptor expression in the pituitary may play a role in appetite and stress regulation in humans [37–39]. Importantly, GLP-1 receptor tracers such as ^{68}Ga-exendin offer the unique opportunity to test this postulate directly in humans.

The basal part of the hypothalamus is closely located to the pituitary. GLP-1 receptors are expressed in the paraventricular nucleus and arcuate nucleus [4,9], which are both

located in the basal hypothalamus. The median eminence is a small brain area forming both the structural and functional bridge between the hypothalamus and the pituitary [40]. In the basal part of the hypothalamus and the median eminence, the blood–brain barrier (BBB) is not as tight as in other regions of the brain but rather "leaky", due to fenestrated capillaries. The entry of hormones and other compounds into the brain, through fenestrated capillaries may be important for feedback regulation of, amongst others, the HPA-axis [41]. In other words, this special connection between the basal hypothalamus and the (neuro)pituitary may play a crucial role to integrate changes in hormones relevant for metabolism (like GLP-1 in blood) and food intake, with feedback systems within the brain (e.g., feeling of satiety).

In the present study, we were not able to differentiate binding to the pituitary from binding in the basal hypothalamus. Therefore, we cannot exclude that we did not measure only uptake in the pituitary, but also in the basal hypothalamus. In other ongoing studies, by also acquiring magnetic resonance (MR) images for better anatomical referencing, we aim to evaluate this relevant topic.

No Significant Uptake of ^{68}Ga-exendin in the Brain

Apart from uptake in the pituitary, we observed that there is no significant uptake of ^{68}Ga-exendin in other parts of the brain of subjects with obesity. Although expression of GLP-1 receptors is well documented in cortical and subcortical brain areas [4,8–10], the lack of uptake may be explained by the low lipophilicity and/or large molecular weight of the PET tracer. Indeed, other gallium-68-labelled tracers such as ^{68}Ga-dotatate (which binds preferentially to the somatostatin receptor-2) also showed no uptake in the brain (being much smaller than exendin and containing less charges), while these somatostatin receptors are expressed throughout the brain in deep layers of cortical cortex as well as in the cerebellum [42]. If labeling with the radionuclide gallium-68 indeed hinders brain uptake, development of e.g., fluorine-18 labelled PET tracers derived from exendin-4 may allow the visualization of GLP-1 receptors in the brain. Interestingly, recent animal studies using 18F-AlF-NOTA-MAL-Cys39-exendin-4 showed indeed some in-vivo binding to GLP-1 receptors in the brain of rats [43,44]. However, the specific binding in brain was very low, which precluded use of this tracer in brain studies in humans. Finally, a recent study evaluated another fluorine-18 labelled PET tracer derived from ex-endin-4 (18F-FB(ePEG12)12-Exendin-4) in humans; this tracer also did not show any brain uptake [45]. So, it is questionable if this approach will be successful in future human PET studies aiming to visualize GLP-1 receptors in the brain (see also below).

Uptake of GLP-1 Receptor Agonists in the Brain

As already mentioned, administration of GLP-1 analogues induces central effects, which suggests that GLP-1 analogues may pass the BBB. Indeed, several studies suggested that GLP-1 analogues may pass the BBB [46,47]. Also, in a placebo-controlled clinical study

in PD, in which half of the PD patients were treated for almost 1 year with the GLP-1 analogue exenatide [27], exenatide was detectable in the cerebrospinal fluid (CSF). Conversely, a clinical study in type 2 diabetes showed that the transfer from blood to CSF of the GLP-1 analogue liraglutide was only minimal [48].

Successfully developed radiotracers for brain studies in humans are transported actively over the BBB, or diffuse rapidly into the brain [49]. For example, the PET tracer 18F-DOPA is taken up fast by the large neutral amino acid transport carrier-mediated system of the BBB [50]. Alternatively, successful brain PET/SPECT tracers should not be transported rapidly from the brain back to the blood, e.g., by efflux via the P-glycoprotein (PgP) expressed in the BBB [51].

However, whether, and what extent, GLP-1 analogues penetrate the BBB is an important point of discussion in research on the mechanism of action of this class of drugs [9,23]. For example, the GLP-1 analogue liraglutide (which is marketed both for treatment of type 2 diabetes and obesity) was injected intraperitoneally (i.p.) in mice, and later on the levels of this drug were measured in the brain. Interestingly, there were no significant levels of liraglutide found 5 min post-injection in the brains of mice administered with a 2.5, 25 or 250 nmol/kg dose of the peptide. Also, at higher doses (25–250 mg/kg bodyweight), no significant levels of liraglutide were found 5 min post i.p., but only at later timepoints [46]. This may indicate that the passage of GLP-1 analogues (and possibly related radiotracers) via the BBB is not rapid, and probable not by active transport. Moreover, to evaluate the mechanism by which liraglutide is able to reduce body weight, mice were injected subcutaneously with liraglutide labeled with a fluorescent probe [52]. Interestingly, liraglutide labelling was highly abundant within parts of the hypothalamus, including the arcuate nucleus and paraventricular nucleus, as well as the median eminence, but not in other brain areas. No liraglutide signal was observed in the nucleus tractus solitarius, which could indicate that peripheral administration of liraglutide does not directly en-gage the GLP-1 receptor in this brain region.

Interestingly, recent evidence indicates that peripheral administrated peptides (e.g., GLP-1) may enter the brain via transcytosis across so-called tanycytes (which are classified as astroglia). These tanycytes are located around the floor of the third ventricle (in the area of the median eminence and basal hypothalamus), and by transport via these tanycyte peptides can enter the third ventricle (CSF), but also distant brain structures lining the ventricles (for a recent review see Garcia-Caceres et al. [33]). Importantly, a recent study by Gabery and co-workers demonstrated that tanycytes express GLP-1 receptors. They also showed that the GLP-1 analogue semaglutide, when administrated peripheral-ly, do not enter the brain by general BBB permeability, but via the tanycytes [9]. Regarding neuro- PET imaging, if PET tracers derived from exendin-4 may enter the brain also via

transcytosis by tanycytes, this approach may not lead to a successful development of neuro PET tracers.

Final Remarks and Limitations

In sum, we only observed uptake in the brain of ^{68}Ga-exendin in the pituitary area of subjects with obesity and it is becoming more likely that (part) of the mechanism of actions of GLP-1 receptor agonists and PET tracers on brain functions might be due to (slow) uptake by tanycytes, located in the median eminence/basal hypo-thalamus. To shed more light on this topic, it may be relevant to determine whether ^{68}Ga-exendin binds in-vivo in humans only in the pituitary, or also in the median eminence/basal hypothalamus. Additionally, it still cannot be excluded that the central effects of GLP-1 analogues are (partly) induced via peripheral mechanisms and/or by direct uptake via the pituitary/basal hypothalamus.

If the future novel PET tracers derived from exendin-4 do show rapid and intense uptake in the brain, it is unlikely that this brain uptake is only by the tanycytes. If this happens, it is more likely that they pass the BBB by an active mechanism or diffuse rapidly through the BBB. Furthermore, it may be relevant to determine whether tracers derived from exendin-4, like ^{68}Ga-exendin, are a substrate for the efflux transporter PgP.

We only studied ^{68}Ga-exendin in obese subjects. We therefore cannot exclude that it is possible to imagine visualize GLP-1 receptors in the brain in disorders in which the BBB function is severely disrupted. Finally, we only studied a small number of subjects. Therefore, our findings are in need for replication.

CONCLUSION

In conclusion, we have shown that in subjects with obesity there is no significant up-take of ^{68}Ga-exendin in the parts of the brain located within the BBB. Therefore, ^{68}Ga-exendin PET cannot be used to analyze GLP-1 receptors in the brain of people with obesity. However, there is clear uptake of the tracer in the pituitary, which offers the unique opportunity to evaluate the role of GLP-1 receptor expression in the pituitary in health and disease.

REFERENCES

1. Mori, Y.; Matsui, T.; Hirano, T.; Yamagishi, S.-I. GIP as a Potential Therapeutic Target for Atherosclerotic Cardiovascular Disease–A Systematic Review. Int. J. Mol. Sci. 2020, 21, 1509.
2. Drucker, D.J.; A Nauck, M. The incretin system: Glucagon-like peptide-1 receptor agonists and dipeptidyl peptidase-4 inhib-itors in type 2 diabetes. Lancet 2006, 368, 1696–1705.
3. Holt, M.; Llewellyn-Smith, I.J.; Reimann, F.; Gribble, F.; Trapp, S. Serotonergic modulation of the activity of GLP-1 producing neurons in the nucleus of the solitary tract in mouse. Mol. Metab. 2017, 6, 909–921.
4. Heppner, K.M.; Kirigiti, M.; Secher, A.; Paulsen, S.J.; Buckingham, R.; Pyke, C.; Knudsen, L.B.; Vrang, N.; Grove, K.L. Expression and distribution of glucagon-like peptide-1 receptor mRNA, protein and binding in the male nonhuman primate (Macaca mulatta) brain. Endocrinology 2015, 156, 255–67.
5. Nauck, M.A.; Meier, J.J. The incretin effect in healthy individuals and those with type 2 diabetes: Physiology, pathophysiology, and response to therapeutic interventions. Lancet Diabetes Endocrinol. 2016, 4, 525–536.
6. Hussein, H.; Zaccardi, F.; Khunti, K.; Davies, M.J.; Patsko, E.; Dhalwani, N.; Kloecker, D.E.; Ioannidou, E.; Gray, L.J. Efficacy and tolerability of sodium-glucose co-transporter-2 inhibitors and glucagon-like peptide-1 receptor agonists: A systematic review and network meta-analysis. Diabetes Obes. Metab. 2020, 22, 1035–1046.
7. Cork, S.; Richards, J.E.; Holt, M.; Gribble, F.; Reimann, F.; Trapp, S. Distribution and characterisation of Glucagon-like pep-tide-1 receptor expressing cells in the mouse brain. Mol. Metab. 2015, 4, 718–731.
8. Yun, S.P.; Kam, T.-I.; Panicker, N.; Kim, S.; Oh, Y.; Park, J.-S.; Kwon, S.-H.; Park, Y.J.; Karuppagounder, S.S.; Park, H.; et al. Block of A1 astrocyte conversion by microglia is neuroprotective in models of Parkinson's disease. Nat. Med. 2018, 24, 931–938.
9. Gabery, S.; Salinas, C.G.; Paulsen, S.J.; Ahnfelt-Rønne, J.; Alanentalo, T.; Baquero, A.F.; Buckley, S.T.; Farkas, E.; Fekete, C.; Frederiksen, K.S.; et al. Semaglutide lowers body weight in rodents via distributed neural pathways. JCI Insight 2020, 5.
10. Jensen, C.B.; Pyke, C.; Rasch, M.G.; Dahl, A.B.; Knudsen, L.B.; Secher, A. Characterization of the Glucagonlike Peptide-1 Receptor in Male Mouse Brain Using a Novel Antibody and In Situ Hybridization. Endocrinology 2017, 159, 665–675.
11. Mansur, R.B.; Fries, G.R.; Trevizol, A.P.; Subramaniapillai, M.; Lovshin, J.; Lin, K.; Vinberg, M.; Ho, R.; Brietzke, E.; McIntyre, R.S. The effect of body mass index on glucagon-like peptide receptor gene expression in the post mortem brain from indi-viduals with mood and psychotic disorders. Eur. Neuropsychopharmacol. 2019, 29, 137–146.
12. Athauda, D.; Foltynie, T. The glucagon-like peptide 1 (GLP) receptor as a therapeutic target in Parkinson's disease: Mechanisms of action. Drug Discov. Today 2016, 21, 802–818.
13. Badawi, G.A.; El Fattah, M.A.A.; Zaki, H.F.; El Sayed, M.I. Sitagliptin and liraglutide reversed nigrostriatal degeneration of rodent brain in rotenone-induced Parkinson's disease. Inflammopharmacology 2017, 25, 369–382.
14. Bu, L.-L.; Liu, Y.-Q.; Shen, Y.; Fan, Y.; Yu, W.-B.; Jiang, D.-L.; Tang, Y.-L.; Yang, Y.-J.; Wu, P.; Zuo, C.-T.; et al. Neuroprotection of Exendin-4 by Enhanced Autophagy in a Parkinsonian Rat Model of α-Synucleinopathy. Neurotherapy 2021, 18, 962–978.
15. Elbassuoni, E.A.; Ahmed, R.F. Mechanism of the neuroprotective effect of GLP-1 in a rat model of Parkinson's with pre-existing diabetes. Neurochem. Int. 2019, 131, 104583.

16. Feng, P.; Zhang, X.; Li, D.; Ji, C.; Yuan, Z.; Wang, R.; Xue, G.; Li, G.; Hölscher, C. Two novel dual GLP-1/GIP receptor agonists are neuroprotective in the MPTP mouse model of Parkinson's disease. Neuropharmacology 2018, 133, 385–394
17. Hansen, H.H.; Fabricius, K.; Barkholt, P.; Mikkelsen, J.D.; Jelsing, J.; Pyke, C.; Knudsen, L.B.; Vrang, N. Characterization of liraglutide, a glucagon-like peptide-1 (GLP-1) receptor agonist, in rat partial and full nigral 6-hydroxydopamine lesion models of Parkinson's disease. Brain Res. 2016, 1646, 354–365.
18. Li, T.; Tu, L.; Gu, R.; Yang, X.-L.; Liu, X.-J.; Zhang, G.-P.; Wang, Q.; Ren, Y.-P.; Wang, B.-J.; Tian, J.-Y. Neuroprotection of GLP-1/GIP receptor agonist via inhibition of mitochondrial stress by AKT/JNK pathway in a Parkinson's disease model. Life Sci. 2020, 256, 117824.
19. Park, J.-S.; Kam, T.-I.; Lee, S.; Park, H.; Oh, Y.; Kwon, S.-H.; Song, J.-J.; Kim, D.; Kim, H.; Jhaldiyal, A.; et al. Blocking microglial activation of reactive astrocytes is neuroprotective in models of Alzheimer's disease. Acta Neuropathol. Commun. 2021, 9, 1–15.
20. Yuan, Z.; Li, D.; Feng, P.; Xue, G.; Ji, C.; Li, G.; Hölscher, C. A novel GLP-1/GIP dual agonist is more effective than liraglutide in reducing inflammation and enhancing GDNF release in the MPTP mouse model of Parkinson's disease. Eur. J. Pharmacol. 2017, 812, 82–90.
21. Zhang, L.; Zhang, L.; Li, L.; Hölscher, C. Neuroprotective effects of the novel GLP-1 long acting analogue semaglutide in the MPTP Parkinson's disease mouse model. Neuropeptides 2018, 71, 70–80.
22. Zhang, L.; Zhang, L.; Li, L.; Hölscher, C. Semaglutide is Neuroprotective and Reduces α-Synuclein Levels in the Chronic MPTP Mouse Model of Parkinson's Disease. J. Park. Dis. 2019, 9, 157–171.
23. Zhang, Z.Q.; Hölscher, C. GIP has neuroprotective effects in Alzheimer and Parkinson's disease models. Peptides 2020, 125, 170184.
24. Deacon, C.F.; A Nauck, M.; Toft-Nielsen, M.; Pridal, L.; Willms, B.; Holst, J.J. Both Subcutaneously and Intravenously Ad-ministered Glucagon-Like Peptide I Are Rapidly Degraded From the NH2-Terminus in Type II Diabetic Patients and in Healthy Subjects. Diabetes 1995, 44, 1126–1131.
25. National Center for Biotechnology Information, PubChem Compound Summary for CID 53396299, Byetta. 2021. Available online: https://pubchem.ncbi.nlm.nih.gov/compound/Byetta (accessed on 19 October 2021).
26. Mousa, S.A.; Ayoub, B.M. Repositioning of dipeptidyl peptidase-4 inhibitors and glucagon like peptide-1 agonists as potential neuroprotective agents. Neural Regen. Res. 2019, 14, 745–748.
27. Athauda, D.; Maclagan, K.; Skene, S.; Bajwa-Joseph, M.; Letchford, D.; Chowdhury, K.; Hibbert, S.; Budnik, N.; Zampedri, L.; Dickson, J.; et al. Exenatide once weekly versus placebo in Parkinson's disease: A randomised, double-blind, place-bo-controlled trial. Lancet 2017, 390, 1664–1675.
28. Aviles-Olmos, I.; Dickson, J.; Kefalopoulou, Z.; Djamshidian, A.; Ell, P.; Soderlund, T.; Whitton, P.; Wyse, R.; Isaacs, T.; Lees, A.; et al. Exenatide and the treatment of patients with Parkinson's disease. J. Clin. Investig. 2013, 123, 2730–2736.
29. Egejl, M.; Gjedde, A.; Eegefjord, L.; Emøller, A.; Hansen, S.B.; Evang, K.; Rodell, A.B.; Ebraendgaard, H.; Egottrup, H.; Eschacht, A.; et al. In Alzheimer's Disease, 6-Month Treatment with GLP-1 Analog Prevents Decline of Brain Glucose Metabolism: Randomized, Placebo-Controlled, Double-Blind Clinical Trial. Front. Aging Neurosci. 2016, 8, 108.
30. Jansen, T.; van Lith, S.; Boss, M.; Brom, M.; Joosten, L.; Béhé, M.; Buitinga, M.; Gotthardt, M. Exendin-4 analogs in insulinoma theranostics. J. Label. Compd. Radiopharm. 2019, 62, 656–672.

31. Boss, M.; Rottenburger, C.; Brenner, W.; Blankenstein, O.; Prasad, V.; Prasad, S.; de Coppi, P.; Kühnen, P.; Buitinga, M.; Nuutila, P.; et al. ^{68}Ga-NODAGA-exendin-4 PET improves the detection of focal congenital hyperinsulinism. J. Nucl. Med. 2021.
32. Ruze, R.; Xu, Q.; Liu, G.; Li, Y.; Chen, W.; Cheng, Z.; Xiong, Y.; Liu, S.; Zhang, G.; Hu, S.; et al. Central GLP-1 contributes to improved cognitive function and brain glucose uptake after duodenum-jejunum bypass on obese and diabetic rats. Am. J. Physiol. Metab. 2021, 321, E392–E409.
33. García-Cáceres, C.; Balland, E.; Prevot, V.; Luquet, S.; Woods, S.C.; Koch, M.; Horvath, T.L.; Yi, C.-X.; Chowen, J.A.; Verkhratsky, A.; et al. Role of astrocytes, microglia, and tanycytes in brain control of systemic metabolism. Nat. Neurosci. 2019, 22, 7–14.
34. Buitinga, M.; Jansen, T.J.; van der Kroon, I.; van der Weg, W.W.-; Boss, M.; Janssen, M.; Aarntzen, E.; Behe, M.; Wild, D.; Visser, E.; et al. Succinylated Gelatin Improves the Theranostic Potential of Radiolabeled Exendin-4 in Insulinoma Patients. J. Nucl. Med. 2019, 60, 812–816.
35. Göke, R.; Larsen, P.J.; Mikkelsen, J.D.; Sheikh, S.P. Identification of specific binding sites for glucagon-like peptide-1 on the posterior lobe of the rat pituitary. Neuroendocr. 1995, 62, 130–4.
36. Körner, M.; Stöckli, M.; Waser, B.; Reubi, J.C. GLP-1 Receptor Expression in Human Tumors and Human Normal Tissues: Potential for In Vivo Targeting. J. Nucl. Med. 2007, 48, 736–743.
37. Scott, K.A.; Melhorn, S.J.; Sakai, R.R. Effects of Chronic Social Stress on Obesity. Curr. Obes. Rep. 2012, 1, 16–25.
38. Turton, M.D.; O'Shea, D.; Gunn, I.; Beak, S.A.; Edwards, C.M.B.; Meeran, K.; Choi, S.J.; Taylor, G.M.; Heath, M.M.; Lambert, P.D.; et al. A role for glucagon-like peptide-1 in the central regulation of feeding. Nature 1996, 379, 69–72.
39. Van der Valk, E.; Savas, M.; van Rossum, E.F.C. Stress and Obesity: Are There More Susceptible Individuals? Curr. Obes. Rep. 2018, 7, 193–203.
40. Kiss, A. Morphological aspects of the median eminence—Place of accumulation and secretion of regulatory neurohormones and neuropeptides. Gen. Physiol. Biophys. 1997, 16, 301–9.
41. Clarke, I. Hypothalamus as an Endocrine Organ. Comprehensive Physiology 2014, 5, 217–253.
42. Thoss, V.S.; Piwko, C.; Probst, A.; Hoyer, D. Autoradiographic analysis of somatostatin SRIF1 and SRIF2 receptors in the human brain and pituitary. Naunyn-Schmiedebergs Arch. fur Exp. Pathol. und Pharmakol. 1997, 355, 168–176.
43. Liu, Y.; Wang, L.; Pan, D.; Li, M.; Li, Y.; Wang, Y.; Xu, Y.; Wang, X.; Yan, J.; Wu, Q.; et al. PET evaluation of light-induced modulation of microglial activation and GLP-1R expression in depressive rats. Transl. Psychiatry 2021, 11, 1–11.
44. Wang, L.; Liu, Y.; Xu, Y.; Sheng, J.; Pan, D.; Wang, X.; Yan, J.; Yang, R.; Yang, M. Age-related change of GLP-1R expression in rats can be detected by [18F]AlF-NOTA-MAL-Cys39-exendin-4. Brain Res. 2018, 1698, 213–219.
45. Fujimoto, H.; Fujita, N.; Hamamatsu, K.; Murakami, T.; Nakamoto, Y.; Saga, T.; Ishimori, T.; Shimizu, Y.; Watanabe, H.; Sano, K.; et al. First-in-Human Evaluation of Positron Emission Tomography/Computed Tomography With [18F]FB(ePEG12)12-Exendin-4: A Phase 1 Clinical Study Targeting GLP-1 Receptor Expression Cells in Pancreas. Front. En-docrinol. 2021, 12, 717101.
46. Hunter, K.; Hölscher, C. Drugs developed to treat diabetes, liraglutide and lixisenatide, cross the blood brain barrier and enhance neurogenesis. BMC Neurosci. 2012, 13, 33.
47. Kastin, A.J.; Akerstrom, V. Entry of exendin-4 into brain is rapid but may be limited at high doses. Int. J. Obes. 2003, 27, 313–318.

48. Christensen, M.; Sparre-Ulrich, A.H.; Hartmann, B.; Grevstad, U.; Rosenkilde, M.M.; Holst, J.J.; Vilsbøll, T.; Knop, F.K. Transfer of liraglutide from blood to cerebrospinal fluid is minimal in patients with type 2 diabetes. Int. J. Obes. 2015, 39, 1651–1654.
49. Luurtsema, G.; Delange, E.; Lammertsma, A.; Franssen, E. Transport across the blood-brain barrier: Stereoselectivity and PET-tracers. Mol. Imaging Biol. 2004, 6, 306–318.
50. Hammerstad, J.P.; Pate, B.D.; Hewitt, K.A.; Chan, G.L.-Y.; Ruth, T.J.; Calne, D.B. The transport ofL-6-fluorodopa and its me-tabolites from blood to cerebrospinal fluid and brain. Ann. Neurol. 1993, 34, 603–608.
51. Luurtsema, G.; Elsinga, P.; Dierckx, R.; Boellaard, R.; Waarde, A. PET Tracers for Imaging of ABC Transporters at the Blood-Brain Barrier: Principles and Strategies. Curr. Pharm. Des. 2016, 22, 5779–5785.
52. Secher, A.; Jelsing, J.; Baquero, A.F.; Hecksher-Sørensen, J.; Cowley, M.; Dalbøge, L.S.; Hansen, G.; Grove, K.L.; Pyke, C.; Raun, K.; et al. The arcuate nucleus mediates GLP-1 receptor agonist liraglutide-dependent weight loss. J. Clin. Investig. 2014, 124, 4473–4488.



7

General discussion and future perspectives

Glucagon-like peptide-1 (GLP-1) receptor imaging using radiolabeled exendin-4 has been developed for visualizing and quantifying beta cell mass in humans. It was previously shown that pancreatic uptake of radiolabeled exendin-4 is highly specific for GLP-1 receptors and is associated with beta cell mass (1-5). Within the pancreas, GLP-1 receptor expression is found on beta cells and delta cells in the islets of Langerhans. Since the delta cells only form a small part of the islets, GLP-1 receptor mediated uptake of radiolabeled exendin-4 of these cells is not relevant for beta cell imaging (6-8). Therefore, radiolabeled exendin is the most suitable tracer for non-invasive beta cell imaging to date. The value of GLP-1 receptor imaging for detecting beta cells has previously been reported in the diagnosis of insulinoma and the study of beta cells in type 1 diabetes in humans (1-5, 8-12).

In this thesis, GLP-1 receptor imaging was used to assess beta cell mass in T2D and to measure whole-body GLP-1 receptor expression. The first questions to answer were whether beta cell mass changes in people with T2D undergoing gastric bypass surgery and whether there is a difference between people with T2D who do and do not require insulin therapy (Chapter 2). Secondly, we aimed to better understand the effect of artefacts occurring around the kidneys on the quantification of radiotracer uptake in the pancreas. For this purpose, phantom studies were performed on SPECT/CT (Chapter 3) and PET/CT (Chapter 4) using a specially developed pancreas-kidneys phantom. Finally, we assessed how ^{68}Ga-exendin accumulates in organs other than the pancreas and how these accumulation patterns relate to known GLP-1 receptor expression. In Chapter 5 we examined the uptake of the radiotracer in a large part of the body and in Chapter 6 we looked specifically at the uptake of radiolabeled exendin-4 in the brain.

BETA CELL MASS IN T2D BEFORE AND AFTER GASTRIC BYPASS SURGERY

Chapter 2 presents a study investigating beta cell mass using ^{68}Ga-Exendin PET/CT in people with T2D and severe obesity undergoing RYGB surgery. Beta cell mass and function was compared before and one year after surgery in two groups: seven participants treated with metformin alone and six participants requiring insulin therapy. Two main findings of this study were: 1) a lower preoperative beta cell mass in participants who required insulin therapy than in participants using only metformin and 2) participants requiring insulin therapy showed an increase in beta cell mass one year after surgery, while no change was observed in the other group. These observations provide novel insights into beta cell mass in relation to T2D severity and treatment by RYGB surgery in humans. These findings underline the importance of weight loss and improving lifestyle before the onset or in an early disease state of T2D, to preserve beta cell mass.

The participants requiring insulin therapy are assumed to have a more advanced T2D state than the participants using metformin alone. The lower beta cell mass in participants requiring insulin than in participants using metformin alone is in line with the progressive loss of beta cell mass in more advanced T2D, but was never demonstrated in humans non-invasively before. The majority of data on beta cell mass is available from human pancreas specimens and has shown a decline in beta cell mass in T2D ranging from 24% to 65% compared to non-diabetic controls (13). More specifically, Rahier *et al*. showed that there was a greater reduction of beta cell mass in people with T2D for more than 15 years than in people with a more recent diagnosis (14).

The increased pancreas uptake of ^{68}Ga-exendin in participants requiring insulin therapy after RYGB surgery suggests potential beta cell recovery after RYGB-induced weight loss in this group. Similarly, several animal studies have revealed an increase in beta cell mass after RYGB surgery (15-18). In humans, an improved beta cell function and functional mass have been demonstrated, which is in line with our findings (19, 20). In contrast to the insulin group, participants using metformin showed no change in beta cell mass. Probably this reflects an earlier stage of T2D where beta cell mass has not yet declined significantly, or may even be increased in response to the increased body's insulin demand (13). This is in line with the considerable individual variation that we observed among the metformin participants.

A PANCREAS-KIDNEY PHANTOM MIMICKING ANATOMY AND TRACER DISTRIBUTION HELPS TO UNDERSTAND ARTEFACTS AND TO OPTIMIZE QUANTIFICATION IN BETA CELL IMAGING

An important limitation that was observed in the clinical studies applying beta cell imaging, is the appearance of large artefacts surrounding the kidneys, often including part of the pancreas. The occurrence of these artefacts in exendin-based nuclear imaging is very specific for the receptor-mediated tracer distribution of this radiotracer and the very high uptake in the kidneys, causing many scatter events. Due to the anatomical location of the pancreas close to the kidneys, radiotracer quantification in the pancreas may be negatively affected by these artefacts. In the studies in Chapters 2 and 5, artefacts were observed in part of the participants, mainly in those with overweight or obesity. These artefacts can hamper a reliable assessment of radiotracer uptake in the pancreas, since there is a lack of activity within the artefact region. Therefore, data of participants with severe artefacts had to be excluded from analysis in Chapter 2.

The effect of these artefacts on the quantification of pancreas uptake of radiolabeled exendin-4 were examined in this thesis in Chapter 3 for ^{111}In-exendin SPECT/CT and in Chapter 4 for ^{68}Ga-exendin PET/CT. In addition, the effects of several clinically available

acquisition and reconstruction settings on the appearance of these artefacts were explored. Regular phantoms in nuclear medicine, such as the NU2 NEMA phantom (21), cannot mimic this specific anatomy and radiotracer distribution of exendin-based tracers, nor do they represent people having overweight or obesity. Therefore a 3D-printed anatomical phantom representing the human pancreas and kidneys was developed. This pancreas-kidneys phantom was placed in a normal body casing in Chapter 3. Since the artefact mainly appears in people with increased body sizes in PET/CT, the pancreas-kidney phantom was placed in body casings representing normal weight, overweight and severe obesity in Chapter 4. The radiotracer distribution of ^{111}In-exendin and ^{68}Ga-exendin was simulated by filling the organs and background with ^{111}In and ^{68}Ga solutions corresponding to activity concentrations as measured on human SPECT/CT and PET/CT images, respectively.

The phantom study in SPECT/CT (Chapter 3) showed that different software packages and reconstruction methods resulted in relatively large variations in the appearance of artefacts, visualization of pancreas activity and quantification parameters. However, none of the collimator, attenuation and scatter correction methods in these reconstruction packages were able to completely correct for the very large organ-to-background contrast and to resolve the artefacts. We selected Hybrid Recon using OSEM3D reconstruction with 6 iterations and 16 subsets and including scatter, collimator and attenuation correction as the most optimal clinically available reconstruction protocol for ^{111}In-exendin SPECT/CT.

In Chapter 4 it was confirmed that the largest artefacts occurred in the phantom representing severe obesity in ^{68}Ga-exendin PET/CT. Artefacts that were observed included activity spillover from the kidneys and a photopenic region surrounding the kidneys and affected activity recovery in the pancreas. In the presence of a photopenic artefact, the recovery of the activity concentration in the pancreas was significantly reduced and in the presence of a spillover artefact, the recovery of activity was increased. The pancreatic body, which had the largest distance to the kidneys, was least affected by the artefacts and recovery of activity in the larger body cases remained comparable to the smallest phantom without artefacts.

In PET/CT, the size of the artefact in the phantom could be slightly reduced by increasing acquisition time. In the normal weight and overweight phantom, acquisition times longer than 7 minutes did not result in large improvements in the PET images. In the obese phantom, even with acquisition times of 20 minutes, a large photopenic artefact remained. Such long acquisition times are not realistic in human PET/CT, since at least two bed positions are desirable for visualizing the abdomen (containing the pancreas). Thus, in practice, increasing acquisition time can only reduce the artefact appearance to some extent, but cannot resolve it completely. Moreover, prompt gamma correction seemed essential to prevent significant artefacts in the normal- and overweight phantoms but did

not reduce the artefact appearance in the largest phantom. The use of absolute instead of relative scatter scaling did not resolve artefact appearance nor did it improve image quality parameters or quantification of pancreatic activity concentrations.

From these findings, the most optimal settings for ^{68}Ga-exendin PET/CT (PET/CT 1 hour after injection of 100 MBq ^{68}Ga-exendin) to minimize the occurrence of photopenic artefacts should include an acquisition time that is long enough and reconstruction should include prompt gamma correction. The acquisition time depends on the injected activity dose of the tracer and time between injection and acquisition. We simulated PET/CT after a dose of 100 MBq and acquisition one hour after administration and found that acquisition time should be at least 7 minutes. Moreover, most reliable quantification of radiotracer uptake in the pancreas in the presence of a photopenic artefact should include only parts of the pancreas that are minimally overlapped by the artefact, but one should be aware that quantification might be unreliable in these cases. These settings were applied for the analysis in Chapter 2.

Although the reconstruction of activity in PET/CT is better than in SPECT/CT, ^{68}Ga-exendin PET/CT suffers from photopenic artefacts surrounding the high uptake in the kidneys. Similar artefacts occur surrounding very high organ uptake when using other PET-radiopeptides. This happens because the scatter correction methods in PET reconstruction protocols are not optimized for high organ-to-background ratios, which occur frequently when using radiopeptides (22-24). The appearance of artefacts is further exacerbated by larger body sizes, because the available scatter information from outside the body that is used for scatter correction is reduced (22-24). With the increasing availability of new PET-radiopeptides and the increasing prevalence of obesity, there is a clear need to optimize PET/CT reconstruction protocols for these applications. Importantly, these improved reconstruction protocols should be validated and become available on clinical PET/CT systems.

The findings from the phantom studies in this thesis (Chapter 3 and 4) demonstrated that the SPECT/CT and PET/CT images of the customized and case-specific phantom we developed were very similar to human ^{111}In-exendin SPECT/CT and ^{68}Ga-exendin PET/CT, including the appearance of the artefacts surrounding the kidneys. Several other reports demonstrated the added value of customized anthropomorphic phantoms in nuclear medicine as well, especially to understand the occurrence of artefacts and investigate activity reconstruction using new, non-FDG radiotracers (25-28). Altogether this showed that case-specific phantoms can mimic exendin-based, or other radiopeptide-based, PET/CT and SPECT/CT and are of additional value to understand the appearance of artefacts and their effect on quantification and to develop and validate improved reconstruction protocols.

Using ^{68}Ga-exendin PET/CT to assess GLP-1 receptor expression

The use of ^{68}Ga-exendin PET/CT also provides an opportunity to measure whole body GLP-1 receptor expression in humans. We performed two studies to assess extra-pancreatic ^{68}Ga-exendin accumulation in humans. In the first study (Chapter 5) we showed accumulation of ^{68}Ga-exendin in the pancreas, duodenum, pituitary gland, salivary glands, gastric mucosa, glandular breast tissue, myocardium, uterus and ovaries. We were able to link the accumulation in these organs to existing data on GLP-1 receptor expression, supporting GLP-1 receptor specific ^{68}Ga-exendin accumulation in these tissues. The ability to non-invasively visualize GLP-1 receptor density makes exendin-based imaging an important tool for studying the role of GLP-1 receptor expression and its dynamics in diseases and GLP-1-based pharmacotherapy in humans.

In several other tissues where GLP-1 receptor expression is suggested, we were not able to detect ^{68}Ga-exendin accumulation, for example, in the thyroid gland, lungs, adipose tissue or endothelial cells (29-33). There are various potential explanations for this discrepancy. Interspecies differences can explain the lack of accumulation in thyroid gland and lungs in humans (29, 31, 33-35). In the kidneys and endothelial cells, receptor-specific accumulation may be hidden by much higher non-specific accumulation in blood and kidneys. In other tissues, the lack of radiotracer accumulation probably suggests lack of GLP-1 receptor expression, since radiolabeled exendin is highly specific and sensitive for the GLP-1 receptor (36).

In line with GLP-1 receptor expression in the human neuro-pituitary, we observed clear accumulation of ^{68}Ga-exendin in the pituitary in the majority of human ^{68}Ga-exendin PET/CT scans (33, 37, 38). To the contrary, a lack of uptake was observed in other parts of the brain, including areas in which GLP-1 receptor expression is expected (38-41). The distribution pattern of ^{68}Ga-exendin in the brain was more specifically examined and discussed in people with T2D and severe obesity in Chapter 6. The blood-brain-barrier may explain the lack of uptake in regions protected by the BBB, since the ability of GLP-1 and GLP-1 receptor agonists to cross the healthy BBB is questionable (42-46). However, GLP-1 receptor expression has previously also been shown in several circumventricular organs that are not protected by the BBB, such as the area postrema, subfornical organ and median eminence (38, 39, 41, 43). In our study, we were not able to detect any radiotracer in these brain areas in humans. Again, interspecies differences may occur, since previous studies on brain tissues were performed in animal models. Another explanation might be that the sensitivity of ^{68}Ga-exendin in combination with the relatively limited spatial resolution of PET/CT scanners is not sufficient to visualize relatively low receptor densities in these very small areas. The fact that we only observed ^{68}Ga-exendin uptake in the pituitary may point towards a role for the pituitary in exerting central effects of GLP-1 and GLP-1 receptor agonists. Although, other signaling routes (such as the autonomous

nervous system) cannot be excluded and future studies are required to confirm these findings and to further understand their implications for clinical practice.

FUTURE PERSPECTIVES

Using ^{68}Ga-exendin PET/CT to assess beta cell mass and GLP-1 receptor expression in people with T2D and obesity was studied in this thesis. To date, many questions regarding the role of the beta cell mass in T2D and the relation between GLP-1 receptor expression and T2D and obesity (and several other diseases) and the results of GLP-1 receptor agonist treatment are unanswered. Imaging with ^{68}Ga-exendin PET/CT enables the ability to measure beta cell mass *in vivo* and multiple times. This is possible since radiation exposure of ^{68}Ga-labeled exendin is low and the imaging protocol is simple: one PET/CT one hour after radiotracer admission (47, 48). This enables research into changes in beta cell mass or GLP-1 receptor expression over the course of a disease.

The possibility for repeated measurements was used in Chapter 2, where people with T2D underwent ^{68}Ga-exendin PET/CT before and after RYGB. We demonstrated differences in beta cell mass linked to different T2D progression states and we observed an increase in beta cell mass in people with T2D after RYGB surgery. Future studies are warranted to confirm these findings, preferably including larger sample sizes because interindividual variation is large (which is in line with the results of Rahier and co-workers) (14). It would also be interesting to apply repeated ^{68}Ga-exendin PET/CT to measure beta cell mass during the development and progression of T2D, while including multiple T2D subtypes and disease phases, because T2D is a heterogeneous disease (49). By combining these measurements with measures of beta cell function and insulin sensitivity, this may improve our understanding of the underlying processes in T2D and, for example, may answer the question of why some people with severe obesity develop T2D and others do not. Besides people with T2D, it would be interesting to include non-diabetic controls with varying body weight, to give insight into a normal range of beta cell mass.

Other applications of repeated ^{68}Ga-exendin PET/CT may include monitoring the effects of treatment strategies aimed at preserving or restoring beta cell mass. Finally, GLP-1 receptor expression can be monitored over time to gain insight into receptor dynamics during disease onset, progression or treatment. This knowledge seems essential to understand the future role of GLP-1 receptor-targeted therapy. For example, exendin-based nuclear imaging demonstrated that GLP-1 receptor expression increased in the myocardial tissue after inducing myocardial infarction in mice (50, 51).

In this thesis we were unable to find an association between measurements of beta cell mass and beta cell function, nor was an increase in beta cell mass related to improve-

ments in blood glucose regulation or T2D remission after RYGB. This might be explained by the method for measuring beta cell function by arginine stimulation, which is an estimate for first phase insulin secretion (52, 53). Another possible explanation is the intricate relationship between beta cell function and beta cell mass, where a certain reduction in beta cell mass may not result in a similar decline in beta cell function (13, 14). Currently, it is incompletely understood how beta cell mass relates to beta cell function, insulin sensitivity and glycemic control in T2D. To further examine these relationships, future studies are warranted to include more extensive measurements of beta cell function, insulin sensitivity and glycemic control.

Applying ^{68}Ga-exendin PET/CT for assessing GLP-1 receptor expression in humans showed novel aspects of the extra-pancreatic radiotracer distribution. This may provide a basis for future discussions on the role of GLP-1 receptors in health and disease in humans. Importantly, future studies should be performed to confirm the findings in this thesis, since comparable studies using GLP-1 receptor imaging have not yet been performed.

It would be interesting to use GLP-1 receptor imaging to assess GLP-1 receptor density in humans for further understanding of the role of GLP-1 receptor signaling in diseases such as T2D and obesity. For example, prospective studies may compare GLP-1 receptor expression between people with T2D or obesity and healthy controls. In the current studies, we were unable to compare ^{68}Ga-exendin distribution between people with different medical histories. In addition, the relationship between GLP-1 receptor expression and the various effects of GLP-1 receptor agonists, including effects on glycemic control, weight loss, cardiac function and the central nervous system, and the interindividual variations in treatment response may be examined using (repeated) GLP-1 receptor imaging. This is especially of interest in the light of newly developed and introduced GLP-1 receptor agonists resulting in weight loss results between 10 and 20% and may help in more patient-specific treatment (54).

An important aspect that should be taken into consideration when determining beta cell mass or GLP-1 receptor density by ^{68}Ga-exendin PET/CT/GLP-1 receptor imaging, is that the GLP-1 receptor expression can be dynamic. For example, in mice persistent hyperglycemia reduced GLP-1 receptor expression on beta cells, which can be restored after returning blood glucose levels to normal (55, 56). The use of medication or dietary intake may also affect GLP-1 receptor expression (57). Until now, data on the dynamics of GLP-1 receptors is limited. The use of GLP-1 receptor imaging may simplify and accelerate studying GLP-1 receptor dynamics in humans.

Before applying ^{68}Ga-exendin PET/CT in people with obesity in larger studies, scatter correction methods for this purpose should be improved to prevent photopenic artefacts. In the phantom studies in this thesis, we were unable to resolve scatter-related artefacts.

Future strategies to reduce or prevent the these artefacts may include improvements in scatter correction methods in PET/CT reconstruction protocols. As was reported by others, reducing the maximum scatter fraction and applying improved methods for scatter correction and scaling by accounting for targeted radiotracer uptake, smaller scatter tails and prompt gamma emission, have shown beneficial effects in reducing or even preventing the occurrence of photopenic artefacts in ^{68}Ga-based radiopeptides in PET/MRI (22, 24, 58-60). Likely, such improvements have beneficial effects in PET/CT and may also lead to improved image reconstruction in regular patient care.

The occurrence of photopenic artefacts in PET/CT is positively related to the organ-to-background ratio (58). Therefore, other strategies to reduce or prevent the occurrence of scatter-related artefacts surrounding the kidneys, should include the reduction of renal radiotracer accumulation. Several approaches to reduce renal accumulation have already been reported. For example, co-injection of Gelofusine reduced renal accumulation (61-65). However, it was not yet investigated if these approaches also improve the quantification of total pancreas uptake in ^{68}Ga-exendin PET/CT. The specific pancreas-kidney phantoms are a valuable tool to examine the effect of lower kidney activity concentration on artefact appearance and recovery of pancreas activity concentrations. Moreover, the minimum required decrease of renal accumulation to be relevant for measuring beta cell mass can be defined.

Taken together, the findings presented in this thesis indicated the potential of GLP-1 receptor imaging using ^{68}Ga-labeled exendin for studying the role of the beta cell mass in T2D, but also for understanding the radiotracer biodistribution in relation to whole-body GLP-1 receptor expression. The phantom studies form the basis for further improvements in imaging acquisition and reconstruction, to be able to improve reliable measurements of radiotracer uptake in the pancreas in people with increased body sizes. Hopefully, this thesis will represent a starting point for further investigation of the role of beta cell mass in type 2 diabetes and of GLP-1 receptor expression and signaling in humans, especially aimed to improve treatment and prevention of obesity and related diseases.

REFERENCES

1. Brom M, Joosten L, Frielink C, Boerman O, Gotthardt M. (111)In-exendin uptake in the pancreas correlates with the beta-cell mass and not with the alpha-cell mass. Diabetes. 2015;64(4):1324-8.
2. Brom M, Joosten L, Frielink C, Peeters H, Bos D, van Zanten M, et al. Validation of (111)In-Exendin SPECT for the Determination of the beta-Cell Mass in BioBreeding Diabetes-Prone Rats. Diabetes. 2018;67(10):2012-8.
3. Brom M, Woliner-van der Weg W, Joosten L, Frielink C, Bouckenooghe T, Rijken P, et al. Non-invasive quantification of the beta cell mass by SPECT with ^{111}In-labelled exendin. Diabetologia. 2014;57(5):950-9.
4. Gotthardt M, Eizirik DL, Cnop M, Brom M. Beta cell imaging - a key tool in optimized diabetes prevention and treatment. Trends Endocrinol Metab. 2014;25(8):375-7.
5. Joosten L, Brom M, Peeters H, Bos D, Himpe E, Bouwens L, et al. Measuring the Pancreatic beta Cell Mass in Vivo with Exendin SPECT during Hyperglycemia and Severe Insulitis. Mol Pharm. 2019;16(9):4024-30.
6. Arrojo EDR, Jacob S, Garcia-Prieto CF, Zheng X, Fukuda M, Nhu HTT, et al. Structural basis for delta cell paracrine regulation in pancreatic islets. Nat Commun. 2019;10(1):3700.
7. Segerstolpe A, Palasantza A, Eliasson P, Andersson EM, Andreasson AC, Sun X, et al. Single-Cell Transcriptome Profiling of Human Pancreatic Islets in Health and Type 2 Diabetes. Cell Metab. 2016;24(4):593-607.
8. Da Silva Xavier G. The Cells of the Islets of Langerhans. J Clin Med. 2018;7(3).
9. Boss M, Eriksson O, Mikkola K, Eek A, Brom M, Buitinga M, et al. Improved Localization of Insulinomas Using (68)Ga-NODAGA-Exendin-4 PET/CT. J Nucl Med. 2024;65(12):1959-64.
10. Boss M, Rottenburger C, Brenner W, Blankenstein O, Prasad V, Prasad S, et al. (68)Ga-NODAGA-exendin-4 PET improves the detection of focal congenital hyperinsulinism. J Nucl Med. 2021.
11. Jansen TJP, Brom M, Boss M, Buitinga M, Tack CJ, van Meijel LA, et al. Importance of beta cell mass for glycaemic control in people with type 1 diabetes. Diabetologia. 2023;66(2):367-75.
12. Jansen TJP, Buitinga M, Boss M, Nijhoff MF, Brom M, de Galan BE, et al. Monitoring beta-Cell Survival After Intrahepatic Islet Transplantation Using Dynamic Exendin PET Imaging: A Proof-of-Concept Study in Individuals With Type 1 Diabetes. Diabetes. 2023;72(7):898-907.
13. Chen C, Cohrs CM, Stertmann J, Bozsak R, Speier S. Human beta cell mass and function in diabetes: Recent advances in knowledge and technologies to understand disease pathogenesis. Mol Metab. 2017;6(9):943-57.
14. Rahier J, Guiot Y, Goebbels RM, Sempoux C, Henquin JC. Pancreatic beta-cell mass in European subjects with type 2 diabetes. Diabetes Obes Metab. 2008;10 Suppl 4:32-42.
15. Li Z, Zhang HY, Lv LX, Li DF, Dai JX, Sha O, et al. Roux-en-Y gastric bypass promotes expression of PDX-1 and regeneration of beta-cells in Goto-Kakizaki rats. World J Gastroenterol. 2010;16(18):2244-51.
16. Lindqvist A, Spegel P, Ekelund M, Garcia Vaz E, Pierzynowski S, Gomez MF, et al. Gastric bypass improves beta-cell function and increases beta-cell mass in a porcine model. Diabetes. 2014;63(5):1665-71.
17. Zhang S, Guo W, Wu J, Gong L, Li Q, Xiao X, et al. Increased beta-Cell Mass in Obese Rats after Gastric Bypass: A Potential Mechanism for Improving Glycemic Control. Med Sci Monit. 2017;23:2151-8.
18. Zhou X, Qian B, Ji N, Lui C, Liu Z, Li B, et al. Pancreatic hyperplasia after gastric bypass surgery in a GK rat model of non-obese type 2 diabetes. J Endocrinol. 2016;228(1):13-23.

19. Guldstrand M, Ahren B, Adamson U. Improved beta-cell function after standardized weight reduction in severely obese subjects. Am J Physiol Endocrinol Metab. 2003;284(3):E557-65.
20. Martinussen C, Bojsen-Moller KN, Dirksen C, Jacobsen SH, Jorgensen NB, Kristiansen VB, et al. Immediate enhancement of first-phase insulin secretion and unchanged glucose effectiveness in patients with type 2 diabetes after Roux-en-Y gastric bypass. Am J Physiol Endocrinol Metab. 2015;308(6):E535-44.
21. (NEMA) NEMA. NEMA Standards Publication NU 2-2007: Performance Measurements of Positron Emission Tomographs. 2007.
22. Bal H, Kiser JW, Conti M, Bowen SL. Comparison of maximum likelihood and conventional PET scatter scaling methods for (18) F-FDG and (68) Ga-DOTATATE PET/CT. Med Phys. 2021;48(8):4218-28.
23. Conti M, Eriksson L. Physics of pure and non-pure positron emitters for PET: a review and a discussion. EJNMMI Phys. 2016;3(1):8.
24. Lindemann ME, Guberina N, Wetter A, Fendler WP, Jakoby B, Quick HH. Improving (68)Ga-PSMA PET/MRI of the Prostate with Unrenormalized Absolute Scatter Correction. J Nucl Med. 2019;60(11):1642-8.
25. Bieniosek MF, Lee BJ, Levin CS. Technical Note: Characterization of custom 3D printed multimodality imaging phantoms. Med Phys. 2015;42(10):5913-8.
26. Driscoll B, Keller H, Coolens C. Development of a dynamic flow imaging phantom for dynamic contrast-enhanced CT. Med Phys. 2011;38(8):4866-80.
27. Gear JI, Long C, Rushforth D, Chittenden SJ, Cummings C, Flux GD. Development of patient-specific molecular imaging phantoms using a 3D printer. Med Phys. 2014;41(8):082502.
28. Mayer R, Liacouras P, Thomas A, Kang M, Lin L, Simone CB, 2nd. 3D printer generated thorax phantom with mobile tumor for radiation dosimetry. Rev Sci Instrum. 2015;86(7):074301.
29. Abu-Hamdah R, Rabiee A, Meneilly GS, Shannon RP, Andersen DK, Elahi D. Clinical review: The extrapancreatic effects of glucagon-like peptide-1 and related peptides. J Clin Endocrinol Metab. 2009;94(6):1843-52.
30. Drucker DJ. The Cardiovascular Biology of Glucagon-like Peptide-1. Cell Metab. 2016;24(1):15-30.
31. Korner M, Stockli M, Waser B, Reubi JC. GLP-1 receptor expression in human tumors and human normal tissues: potential for in vivo targeting. J Nucl Med. 2007;48(5):736-43.
32. Manell E, Puuvuori E, Svensson A, Velikyan I, Hulsart-Billstrom G, Hedenqvist P, et al. Exploring the GLP-1-GLP-1R axis in porcine pancreas and gastrointestinal tract in vivo by ex vivo autoradiography. BMJ Open Diabetes Res Care. 2021;9(1).
33. Pyke C, Heller RS, Kirk RK, Ørskov C, Reedtz-Runge S, Kaastrup P, et al. GLP-1 receptor localization in monkey and human tissue: novel distribution revealed with extensively validated monoclonal antibody. Endocrinology. 2014;155(4):1280-90.
34. Gotthardt M, Joosten L, Jansen TJP, Brom M, Boss M, Willekens SMA. From Mice to Humans: The Exocrine Pancreas Does Not Matter in Human GLP-1 Receptor Imaging. J Nucl Med. 2021;62(5):745.
35. Waser B, Blank A, Karamitopoulou E, Perren A, Reubi JC. Glucagon-like-peptide-1 receptor expression in normal and diseased human thyroid and pancreas. Mod Pathol. 2015;28(3):391-402.
36. Eriksson O, Laughlin M, Brom M, Nuutila P, Roden M, Hwa A, et al. In vivo imaging of beta cells with radiotracers: state of the art, prospects and recommendations for development and use. Diabetologia. 2016;59(7):1340-9.

37. Goke R, Larsen PJ, Mikkelsen JD, Sheikh SP. Identification of specific binding sites for glucagon-like peptide-1 on the posterior lobe of the rat pituitary. Neuroendocrinology. 1995;62(2):130-4.
38. Heppner KM, Kirigiti M, Secher A, Paulsen SJ, Buckingham R, Pyke C, et al. Expression and distribution of glucagon-like peptide-1 receptor mRNA, protein and binding in the male nonhuman primate (Macaca mulatta) brain. Endocrinology. 2015;156(1):255-67.
39. Jensen CB, Pyke C, Rasch MG, Dahl AB, Knudsen LB, Secher A. Characterization of the Glucagonlike Peptide-1 Receptor in Male Mouse Brain Using a Novel Antibody and In Situ Hybridization. Endocrinology. 2018;159(2):665-75.
40. Gabery S, Salinas CG, Paulsen SJ, Ahnfelt-Rønne J, Alanentalo T, Baquero AF, et al. Semaglutide lowers body weight in rodents via distributed neural pathways. JCI Insight. 2020;5(6).
41. Yun SP, Kam TI, Panicker N, Kim S, Oh Y, Park JS, et al. Block of A1 astrocyte conversion by microglia is neuroprotective in models of Parkinson's disease. Nat Med. 2018;24(7):931-8.
42. Christensen M, Sparre-Ulrich AH, Hartmann B, Grevstad U, Rosenkilde MM, Holst JJ, et al. Transfer of liraglutide from blood to cerebrospinal fluid is minimal in patients with type 2 diabetes. Int J Obes (Lond). 2015;39(11):1651-4.
43. Gabery S, Salinas CG, Paulsen SJ, Ahnfelt-Ronne J, Alanentalo T, Baquero AF, et al. Semaglutide lowers body weight in rodents via distributed neural pathways. JCI Insight. 2020;5(6).
44. Hunter K, Holscher C. Drugs developed to treat diabetes, liraglutide and lixisenatide, cross the blood brain barrier and enhance neurogenesis. BMC Neurosci. 2012;13:33.
45. Secher A, Jelsing J, Baquero AF, Hecksher-Sorensen J, Cowley MA, Dalboge LS, et al. The arcuate nucleus mediates GLP-1 receptor agonist liraglutide-dependent weight loss. J Clin Invest. 2014;124(10):4473-88.
46. Zhang ZQ, Holscher C. GIP has neuroprotective effects in Alzheimer and Parkinson's disease models. Peptides. 2020;125:170184.
47. Boss M, Buitinga M, Jansen TJP, Brom M, Visser EP, Gotthardt M. PET-Based Human Dosimetry of (68)Ga-NODAGA-Exendin-4, a Tracer for beta-Cell Imaging. J Nucl Med. 2020;61(1):112-6.
48. Eriksson O, Velikyan I, Haack T, Bossart M, Laitinen I, Larsen PJ, et al. Glucagonlike Peptide-1 Receptor Imaging in Individuals with Type 2 Diabetes. J Nucl Med. 2022;63(5):794-800.
49. Ahlqvist E, Storm P, Karajamaki A, Martinell M, Dorkhan M, Carlsson A, et al. Novel subgroups of adult-onset diabetes and their association with outcomes: a data-driven cluster analysis of six variables. Lancet Diabetes Endocrinol. 2018;6(5):361-9.
50. Gao H, Kiesewetter DO, Zhang X, Huang X, Guo N, Lang L, et al. PET of glucagonlike peptide receptor upregulation after myocardial ischemia or reperfusion injury. J Nucl Med. 2012;53(12):1960-8.
51. Ståhle M, Kytö V, Kiugel M, Liljenbäck H, Metsälä O, Käkelä M, et al. Glucagon-like peptide-1 receptor expression after myocardial infarction: Imaging study using (68)Ga-NODAGA-exendin-4 positron emission tomography. J Nucl Cardiol. 2020;27(6):2386-97.
52. Robertson RP. AIRarg and AIRgluc as predictors of insulin secretory reserve. Transplant Proc. 2004;36(4):1040-1.
53. Sjöstrand M, Carlson K, Arnqvist HJ, Gudbjörnsdottir S, Landin-Olsson M, Lindmark S, et al. Assessment of beta-cell function in young patients with type 2 diabetes: arginine-stimulated insulin secretion may reflect beta-cell reserve. Journal of Internal Medicine. 2013;275(1):39-48.
54. van Rossum EFC, Boon MR. Farmacotherapie voor obesitas. Huisarts en Wetenschap. 2024;67(9):28-33.

55. Buitinga M, Cohrs CM, Eter WA, Claessens-Joosten L, Frielink C, Bos D, et al. Noninvasive Monitoring of Glycemia-Induced Regulation of GLP-1R Expression in Murine and Human Islets of Langerhans. Diabetes. 2020;69(11):2246-52.
56. Xu G, Kaneto H, Laybutt DR, Duvivier-Kali VF, Trivedi N, Suzuma K, et al. Downregulation of GLP-1 and GIP receptor expression by hyperglycemia: possible contribution to impaired incretin effects in diabetes. Diabetes. 2007;56(6):1551-8.
57. Natalicchio A, Biondi G, Marrano N, Labarbuta R, Tortosa F, Spagnuolo R, et al. Long-Term Exposure of Pancreatic beta-Cells to Palmitate Results in SREBP-1C-Dependent Decreases in GLP-1 Receptor Signaling via CREB and AKT and Insulin Secretory Response. Endocrinology. 2016;157(6):2243-58.
58. Heusser T, Mann P, Rank CM, Schafer M, Dimitrakopoulou-Strauss A, Schlemmer HP, et al. Investigation of the halo-artifact in 68Ga-PSMA-11-PET/MRI. PLoS One. 2017;12(8):e0183329.
59. Overbeck N, Ahangari S, Conti M, Panin V, Azam A, Kurbegovic S, et al. Improved Positron Emission Tomography Quantification: Evaluation of a Maximum-Likelihood Scatter Scaling Algorithm. Diagnostics (Basel). 2024;14(11).
60. Wangerin KA, Baratto L, Khalighi MM, Hope TA, Gulaka PK, Deller TW, et al. Clinical Evaluation of (68)Ga-PSMA-II and (68)Ga-RM2 PET Images Reconstructed With an Improved Scatter Correction Algorithm. AJR Am J Roentgenol. 2018;211(3):655-60.
61. Buitinga M, Jansen T, van der Kroon I, Woliner-van der Weg W, Boss M, Janssen M, et al. Succinylated Gelatin Improves the Theranostic Potential of Radiolabeled Exendin-4 in Insulinoma Patients. J Nucl Med. 2019;60(6):812-6.
62. Gotthardt M, van Eerd-Vismale J, Oyen WJ, de Jong M, Zhang H, Rolleman E, et al. Indication for different mechanisms of kidney uptake of radiolabeled peptides. J Nucl Med. 2007;48(4):596-601.
63. Joosten L, Frielink C, Jansen TJP, Lobeek D, Andreae F, Konijnenberg M, et al. New Radiolabeled Exendin Analogues Show Reduced Renal Retention. Mol Pharm. 2023;20(7):3519-28.
64. Vegt E, Eek A, Oyen WJ, de Jong M, Gotthardt M, Boerman OC. Albumin-derived peptides efficiently reduce renal uptake of radiolabelled peptides. Eur J Nucl Med Mol Imaging. 2010;37(2):226-34.
65. Vegt E, van Eerd JE, Eek A, Oyen WJ, Wetzels JF, de Jong M, et al. Reducing renal uptake of radiolabeled peptides using albumin fragments. J Nucl Med. 2008;49(9):1506-11.





English summary
Nederlandse samenvatting
Research data management
Dankwoord
PhD portfolio
List of publications
About the author

ENGLISH SUMMARY

Obesity and type 2 diabetes

Obesity and type 2 diabetes (T2D) are closely linked and represent a growing global health problem. Obesity significantly increases the risk of T2D. Type 2 diabetes is characterized by reduced insulin sensitivity and impaired insulin secretion by the beta cells in the pancreas. The treatment of obesity and type 2 diabetes (T2D) involves weight loss and lifestyle modifications. These interventions have been demonstrated to yield health benefits and can even lead to the remission of T2D. While lifestyle interventions serve as primary interventions, additional interventions are often necessary. Bariatric surgery is currently the most effective treatment for severe obesity and T2D. Among these procedures, the Roux-en-Y gastric bypass (RYGB) is one of the most commonly used methods. This surgical intervention results in substantial weight reduction and, in many cases, in the remission of T2D.

In addition to bariatric surgery, GLP-1 receptor agonists have emerged as a central component in the pharmacological treatment of T2D and, subsequently, obesity. Glucagon-like peptide-1 (GLP-1) is a hormone that stimulates insulin secretion, reduces appetite, and slows gastric emptying. As a result, GLP-1 receptor agonists enhance glucose regulation and body weight management. These medications exert their effects via the GLP-1 receptor. The expression of this receptor is predominantly on the beta cells of the pancreas. In addition, the GLP-1 receptor is also expressed in other organs.

GLP-1 receptor imaging

Visualization of the GLP-1 receptor facilitates noninvasive studies of GLP-1 receptor expression and beta cell mass. This technique makes use of radioactively labeled Exendin-4, which is a GLP-1 receptor agonist. The uptake of this radiotracer is visualized using nuclear imaging techniques, such as PET/CT or SPECT/CT. To date, research has demonstrated the value of this imaging technique in 1) detecting insulinomas and 2) studying beta cells in (type 1) diabetes. This dissertation describes the application of Exendin-4 imaging to determine beta cell mass in patients with T2D and to evaluate the expression of GLP-1 receptors in regions beyond the pancreas.

In addition to reduced insulin sensitivity and a (relative) insulin deficiency, T2D is also associated with reduced beta cell mass. Following RYGB surgery, this beta cell mass may restore. However, to date, knowledge about beta cell mass in humans and its temporal dynamics remains limited.

Beta cell mass in type 2 diabetes and obesity

In **Chapter 2**, we describe a prospective clinical study in which we used ^{68}Ga-exendin PET/CT imaging to assess beta cell mass in individuals with T2D and obesity who under-

went RYGB surgery. Beta cell mass and beta cell function were measured before and one year after surgery. We distinguished between individuals who required insulin to regulate their blood glucose levels and those who used only metformin for this purpose. This study revealed that individuals using insulin had lower beta cell mass and beta cell function prior to surgery in comparison to those using only metformin. After RYGB surgery, we observed an increase in beta cell mass in people who used insulin and no change in those who used only metformin.

In **Chapters 3 and 4**, we describe the use of a 3D-printed pancreas-kidney phantom to investigate and reduce artifacts in GLP-1 receptor imaging. These artifacts arise from high radiotracer uptake in the kidneys and impeding the accurate quantification of uptake in the pancreas. **Chapter 3** describes the phantom's design. The phantom was applied to investigate the effect of different reconstruction methods on artefacts in ^{111}In-exendin-4 SPECT/CT. In **Chapter 4**, the presence of halo artifacts in ^{68}Ga-exendin-4 PET/CT was investigated, along with the effect of these artifacts on the quantification of radiotracer uptake in the pancreas. These artifacts occur particularly in individuals with larger body sizes. Therefore, phantoms simulating different body sizes were developed. The findings of both studies demonstrated that the pancreas-kidney phantom realistically simulated Exendin-4 imaging in humans. In **Chapter 3**, the optimal reconstruction parameters for SPECT/CT were selected. In **Chapter 4**, we found that severe halo artifacts hinder reliable quantification of uptake in the pancreas. Increasing the acquisition time and adjustments to the reconstruction model slightly reduced the size of the artifact, but did not prevent severe artifacts in cases of severe obesity. Consequently, reliable quantification is then not possible, or is only possible in parts of the pancreas that lie outside the artifact region.

GLP-1 receptor imaging beyond the pancreas

The uptake of ^{68}Ga-exendin-4 outside the pancreas has not been described in detail previously, but is of interest for two reasons. First, it is important for understanding the normal distribution of the radiotracer. Second, it is expected that this technique enables studying the expression of GLP-1 receptors noninvasively, which remains not yet fully understood in humans. In **Chapter 5**, we describe the uptake of ^{68}Ga-exendin-4 on PET/CT in participants from various clinical studies. The uptake of the radiotracer was observed in organs and tissues with known expression of GLP-1 receptors, including the pancreas and duodenum. Furthermore, radiotracer uptake was observed in organs in which the expression of GLP-1 receptors is less well understood, such as the heart and the pituitary gland. In **Chapter 6**, we examine the uptake of ^{68}Ga-exendin-4 in the brains of people with obesity and T2D. The uptake of the radiotracer in the pituitary gland was notably evident, while no uptake was observed in other parts of the brain. These two chapters demonstrate the potential of ^{68}Ga-exendin-4 PET/CT for studying the expression of GLP-1 receptors in humans.

NEDERLANDSE SAMENVATTING

Obesitas en type 2 diabetes

Obesitas en type 2 diabetes (T2D) zijn nauw met elkaar verbonden en vormen een groeiend wereldwijd gezondheidsprobleem. Obesitas verhoogt het risico op T2D aanzienlijk. Type 2 diabetes wordt gekenmerkt door een verminderde insulinegevoeligheid en een gestoorde insulineafgifte door de bètacellen in het pancreas. Gewichtsverlies en leefstijlverandering zijn belangrijk bij de behandeling van zowel obesitas als T2D. Het leidt tot gezondheidswinst en kan ook leiden tot remissie van T2D. Hoewel leefstijlinterventies hiervoor de basis vormen, zijn aanvullende interventies vaak noodzakelijk. Bariatrische chirurgie is momenteel de meest effectieve behandeling voor ernstige obesitas en T2D. Hierbij is Roux-en-Y gastric bypass (RYGB) is een van de meest toegepaste methoden. Deze operatie leidt tot aanzienlijk gewichtsverlies en vaak tot remissie van T2D.

Naast bariatrische chirurgie hebben GLP-1-receptoragonisten de laatste jaren een centrale rol gekregen in de farmacologisch behandeling van eerst T2D en later ook obesitas. Glucagon-like peptide-1 (GLP-1) is een hormoon dat de insulineafgifte stimuleert, en ook de eetlust vermindert en de maaglediging vertraagt. Hierdoor verbeteren GLP-1-receptoragonisten de glucoseregulatie en het lichaamsgewicht. De werking van deze medicijnen verloopt via de GLP-1 receptor. Deze receptor komt vooral tot expressie op de bètacellen van het pancreas. Daarnaast komt de GLP-1 receptor ook in andere organen tot expressie.

Beeldvorming van GLP-1 receptoren

Beeldvorming van GLP-1 receptoren maakt het mogelijk om de expressie van GLP-1 receptoren en bètacelmassa niet-invasief te bestuderen. Deze techniek maakt gebruik van het radioactief gelabelde Exendin-4 (een GLP-1-receptoragonist). De opname van deze radiotracer wordt in beeld gebracht met nucleaire beeldvorming (PET/CT of SPECT/CT). Beeldvorming van GLP-1 receptoren maakt het mogelijk om de bètacelmassa in het pancreas zichtbaar te maken. Tot nu heeft onderzoek de waarde van deze beeldvorming bewezen bij de detectie van insulinoom en het bestuderen van bètacellen bij type 1 diabetes. In dit proefschrift wordt de toepassing van Exendin-4 beeldvorming voor het bepalen van de bètacelmassa bij T2D en voor het beoordelen van de expressie van GLP-1 receptoren buiten het pancreas beschreven.

Bètacelmassa in type 2 diabetes en obesitas

Naast verminderde insulinegevoeligheid en een (relatief) tekort aan insuline, wordt T2D ook geassocieerd met een verminderde bètacelmassa. Mogelijk is er bij remissie van T2D na RYGB chirurgie herstel van deze bètacelmassa. Echter, tot nu is de kennis over bètacelmassa bij mensen en veranderingen is de tijd beperkt.

In **hoofdstuk 2** beschrijven we een prospectieve klinische studie waarin we met ^{68}Ga-exendin PET/CT beeldvorming de bètacelmassa hebben bepaald in mensen met T2D en obesitas die een RYGB operatie ondergaan. De bètacelmassa en bètacelfunctie werden gemeten voor en één jaar na de operatie. We maakten hierbij onderscheid tussen mensen die insuline nodig hadden voor de regulatie van hun bloedsuikerwaardes en mensen die hiervoor alleen metformine gebruikten. In deze studie vonden we voor de operatie een lagere bètacelmassa en bètacelfunctie in mensen die insuline gebruikten dan bij de mensen die alleen metformine gebruikten. Na de RYGB operatie zagen we een toename van bètacelmassa bij mensen die insuline gebruikten en geen verschil bij mensen die alleen metformine gebruikten.

In **hoofdstuk 3 en 4** beschrijven we het gebruik van een 3D-geprint pancreas-nierenfantoom om artefacten bij beeldvorming van GLP-1 receptoren te onderzoeken en te verminderen. Deze artefacten ontstaan door de hoge radiotraceropname in de nieren en belemmeren de kwantificatie van opname in het pancreas. **Hoofdstuk 3** beschrijft het ontwerp van het fantoom en focust op ^{111}In-exendin-4 SPECT/CT. Het effect van verschillende reconstructiemethoden op de artefacten werden onderzocht. In **hoofdstuk 4** werden halo-artefacten in ^{68}Ga-exendin-4 PET/CT onderzocht en het effect van deze artefacten op de kwantificatie van radiotraceropname in het pancreas. Deze artefacten treden vooral op bij een grotere lichaamsomvang. Daarom werden fantomen gebruikt die verschillende lichaamsmaten nabootsten. Beide studies toonden aan dat het pancreas-nierenfantoom Exendin-4 beeldvorming in mensen realistisch nabootste. In **hoofdstuk 3** werden voor SPECT/CT de meest optimale reconstructies parameters geselecteerd. In **hoofdstuk 4** vonden we dat ernstige halo artefacten een betrouwbare kwantificatie van opname in het pancreas belemmeren. Verhogen van acquisitietijd en aanpassingen in het reconstructiemodel konden de grootte van het artefact enigszins verkleinen, maar voorkwamen een ernstig artefact niet bij ernstige obesitas. Betrouwbare kwantificatie is dan niet mogelijk of alleen in delen van het pancreas die buiten het artefactgebied liggen.

Beeldvorming van GLP-1 receptoren buiten het pancreas

De opname van ^{68}Ga-exendin-4 is buiten het pancreas is niet eerder uitgebreid beschreven. De opname buiten het pancreas is om twee redenen interessant. Ten eerste is dit is van belang om de normale verdeling van de radiotracer te begrijpen. Daarnaast is dit naar verwachting waardevol voor het bestuderen van de expressie van GLP-1 receptoren, welke nog onvolledig bekend is bij de mens. In **hoofdstuk 5** beschrijven we de opname van ^{68}Ga-exendin-4 op PET/CT in deelnemers van diverse klinische studies. We toonden aan dat er opname is in organen en weefsels met bekende expressie van GLP-1 receptoren, waaronder pancreas en duodenum. Ook zagen we opname in organen waar de expressie van GLP-1 receptoren minder bekend is, zoals in het hart en de hypofyse. In **hoofdstuk 6** gaan we dieper in op de opname van ^{68}Ga-exendin-4 in de hersenen van

mensen met obesitas en T2D. Er was duidelijke opname van de radiotracer in de hypofyse. In andere delen van de hersenen werd geen opname gezien. Deze twee hoofdstukken laten de potentie zien van ^{68}Ga-exendin-4 PET/CT om de expressie van GLP-1 receptoren in mensen te bestuderen.

RESEARCH DATA MANAGEMENT

Ethics and privacy

Chapters 2, 5 and 6 of this thesis are based on studies involving human participants. These studies were performed in accordance with relevant national and international legislation and regulation, guidelines, codes of conduct and Radboudumc policy. The recognized Medical Ethics Review Committee 'METC Oost-Nederland' has given approval to conduct these studies (Clinicaltrial.gov numbers: NCT03189953, NCT02542059, NCT03182231, NCT03182192, NCT03923114, NCT03785275)

Informed consent was obtained from all study participants to collect and process their data for this research project. Consent was not obtained for sharing and reuse of the data for future research.

According to Dutch legislation, data collection from electronic patient files was performed by personnel with a treatment relationship with the patient and by researchers upon consent by the study participant. The privacy of the study participants was warranted by the use of pseudonymization. The pseudonymization key is stored on a secured network drive in Radboudumc or Rijnstate that is only accessible to members of the project who needed access because of their role within the project. The pseudonymization key is stored separately from the research data.

Data collection and storage

The medical data for chapter 2, 5 and 6 was collected through (electronic) Case Report Forms (eCRF) of a prospective data collection in Castor EDC. Data were converged from Castor EDC to SPSS (SPSS Inc., Chicago, Illinois, USA). Quantification data was derived from Inveon Research Workplace software version 4.1 (Siemens Healthcare, Erlangen, Germany) and converged to csv files. For chapter 5, additional visual assessments of the PET/CT images were performed, the findings were added to the database for analysis. Remaining data consists of raw PET/CT data.

All data from these studies were stored and analyzed on the department server at Rijnstate and Radboudumc or in Castor EDC. The data were only accessible by project members working at Rijnstate or Radboudumc. These storage options safeguard the availability, integrity and confidentially of the data. All paper data (i.e. informed consent forms and CRF) are stored in cabinets on the department at Rijnstate or Radboudumc, depending on the location where participants were included.

Data for chapter 3 and 4 were obtained from phantom studies and did not include any human data. Data from these chapters were stored and analyzed on the department server.

Data sharing according to the FAIR principles

Chapters 3 and 6 are published open access. The data used for these chapters are not findable via a data repository, because publication of these chapters was (prepared) before the current Radboud RDM policy was in place in 2021. The data underlying chapter 3 can be requested via the department of nuclear medicine, Radboudumc. The data underlying chapter 6 is not suitable for reuse, because consent for reuse was not provided.

Chapters 5 have been submitted for publication (open access) and is currently under review. Chapter 2 and 4 are not yet published. Chapter 5 is based on results obtained from existing PET/CT scans from several other clinical studies (including the study reported in Chapter 2). These PET/CT data were available from the department of Medical Imaging – Nuclear Medicine. The unpublished data from Chapter 2, 4 and 5 are archived at the department server. The data underlying chapter 2, and 5 are not suitable for reuse because consent for reuse was not provided. These data will be archived with closed access for 15 years in a data acquisition collection (DAC) of the Radboud Data Repository after termination of the studies (DOI 10.34973/ptjs-n197 and DOI 10.34973/cfye-6g83). The data underlying chapter 4 will be archived in a data sharing collection (DSC) of the Radboud Data Repository via restricted access for 15 years after publication of the study (DOI 10.34973/kztz-3d74). Requests for access will be checked by the PI or data steward. Statements on data sharing will be included in publications.

DANKWOORD

En daar was eens een proefschrift! Na wat meer jaren te spenderen aan mijn promotie-onderzoek dan gedacht is het zo ver. Gelukkig bleef ik, met ups en downs, gemotiveerd om dit onderzoek af te maken. Het heeft daarbij zeker geholpen dat ik in de tussentijd aan veel nieuwe dingen heb kunnen werken binnen Rijnstate. Dit proefschrift had ik niet alleen kunnen schrijven, maar is het resultaat van vele samenwerkingen en inhoudelijke bijdragen, motivatie en steun van anderen. Met zo veel fijne mensen waar ik mee samen mocht werken is het bijna niet mogelijk iedereen bij naam te noemen. Ik probeer het toch, al ben ik vrij zeker dat ik minstens één iemand vergeet te noemen. En daarom voor iedereen die heeft bijgedragen aan dit proefschrift: Graag wil ik je bedanken voor hetgene je voor mij gedaan hebt om dit proefschrift te kunnen schrijven.

Als eerste wil ik alle deelnemers aan de studies opgenomen in dit proefschrift (en daarbuiten) enorm bedanken voor hun deelname. Door jullie deelname hebben we nieuwe inzichten op kunnen doen over de rol van bètacellen en GLP-1 receptoren bij type 2 diabetes en obesitas. Vrijwillig hebben jullie tijd vrijgemaakt voor testen en scans, en daarmee dit onderzoek mogelijk gemaakt.

Martin, mede dankzij jou kon ik aan dit onderzoek starten in Arnhem en Nijmegen. Bedankt voor je begeleiding en vertrouwen tot aan het einde van mijn promotietijd (en dat was een behoorlijke periode). Ik heb veel geleerd in deze tijd van onze gesprekken over eerst betacelmassa, maar later steeds meer over de GLP-1 receptor, brainstorms, en hoe dit alles te verwoorden (of niet te noemen) op papier. Ik heb jouw altijd kritische blik, out-of-the-box ideeën, maar ook het brengen van focus op de juiste momenten gewaardeerd. Ik ben benieuwd wat de Exendin radiotracer nog gaat brengen in de toekomst.

Marti, voor het eerst hebben onze paden gekruist bij onze sollicitatie op dezelfde (jouw) promotieplek. Wat fijn dat we uiteindelijk beide onderzoek hebben gedaan naar GLP-1 receptor imaging! Het was heel waardevol om de studies rondom bariatrische chirurgie samen op te zetten, waarbij jij veel van de taken die in het Radboudumc moesten gebeuren op je nam. Uiteindelijk heb jij mij als co-promotor geholpen focus te brengen in de onderzoeken voor mijn proefschrift. En last, but not least, heb jij mij ook de basics van het skiën bijgebracht.

Eric, toen jij startte in Rijnstate, was ik al een eind op weg met mijn promotie-onderzoek. Het was fijn (weer) iemand vanuit Rijnstate te hebben die meekeek naar de stukken. We hebben vooral veel samengewerkt voor het onderzoeksteam van Vitalys. Ik heb hierin mogen leren van jouw kunde, rust en brede blik bij de begeleiding van anderen en het leiden van een team of project. Bedankt voor de fijne samenwerking in de afgelopen jaren.

Edo, Frits en Ignace, bedankt voor jullie belangrijke rol in de eerste en meest intensieve jaren van mijn promotie-onderzoek. Zonder jullie was dit onderzoek nooit gestart en van de grond gekomen. Jullie namen mij aan als eerste technisch geneeskundige in een team van arts-onderzoekers en chirurgen. Als deel van dit team heb ik veel geleerd over de klinische zaken rondom obesitaszorg en bariatrische chirurgie. De vrijheid die jullie gaven, jullie vele ideeën en de gesprekken over het doen van onderzoek, maar vooral ook over de skills daaromheen, heb ik als erg waardevol ervaren. Dit bleek na een aantal jaar een goede basis om Edo op te volgen als onderzoekscoördinator bij Vitalys.

Hans en Arianne, bedankt voor jullie enthousiasme en het delen van jullie endocrinologische kennis en visie in mijn promotie-onderzoek. Hans, vanaf het begin ben jij betrokken geweest bij mijn onderzoeken. Jij had altijd vele praktische tips en was een bron van nieuwe ideeën. Daar heb ik veel van kunnen leren. Arianne, na het vertrek van Hans, heb jij met veel enthousiasme deze rol overgenomen.

Graag bedank ik alle co-auteurs, en overige collega's waarmee ik heb samengewerkt, voor jullie bijdragen aan de publicaties in dit proefschrift. Prof. dr. Bastiaan de Galan bedankt voor de fijne samenwerking en je altijd snelle, uitgebreide en kritische feedback op stukken. Ik heb veel geleerd over (type 2) diabetes en glucoseregulatie, en welke hypotheses aannemelijk zijn en welke niet. Prof. dr. Jan Booij, bedankt voor de samenwerking en het initiëren van de studie naar Exendin uptake in de hersenen. Dr Ivo Rausch and Prof Dr Thomas Beyer, thank you for the additional PET reconstructions and your contribution to the paper of the ^{68}Ga-Exendin PET phantom study.

De leden van mijn manuscriptcommissie, prof. dr. Maria Hopman, prof. dr. Ronald Boellaard en dr. Mark Smits, wil ik graag bedanken voor het beoordelen van mijn proefschrift.

Lieve onderzoeks-collega's bij Vitalys en in Rijnstate, bedankt voor de fijne, leerzame en leuke jaren op het 'Barrie-eiland' en in diverse Europese steden tijdens congressen. Bark, Jens en Wendy, jullie waren het team waar ik als eerste TG-er in startte, en jullie mij snel onderdeel van lieten zijn. Jullie hebben mij veel bijgebracht over de obesitas- en bariatrische zorg, maar ook de zorg in het ziekenhuis in het algemeen, zoals het draaien van een poli. Wendy, we hebben heel wat infusen weer 'lopend' gekregen. Bedankt voor je hulp bij de glucosetesten. Mellody, Abel, Debby, Laura, Sophie, Yonta, Claudia, Sietske, Emma, Mitchell, Nadia, Tessa en Adrianne, Suzanne en Daphne met jullie was werken ook gezellig. Termen als 'promoveren kun je leren', 'bariavaatjes', 'powerpaint' en 'de Augurkenparty' zullen altijd bijblijven. Mellody, Tessa en Adrianne, zonder jullie hulp had ik nooit alle patiënten kunnen includeren en de glucosetesten kunnen uitvoeren. Laura, na al een tijdje samen gewerkt te hebben, heb jij het stokje helemaal van mij overgenomen om de onderzoeksgroep te coördineren. Dat gaat je goed af, en ik wens je heel veel succes voor de toekomst!

Lieve Kristy, we hebben zo goed als dezelfde periode gewerkt bij Vitalys. Als manager heb je me als onderzoeker altijd gesteund en gaf je vertrouwen. Met alles kon ik bij jou terecht. En natuurlijk ook bedankt voor de gezelligheid tijdens congressen en uitjes.

Lief Vitalys-team, zonder jullie was onderzoek doen niet mogelijk en werken een stuk minder leuk. Wat een fijn team. Bedankt voor jullie betrokkenheid, gezelligheid, planningen, informatie, helpen bij inclusies en alles wat nodig was bij het uitvoeren van onderzoeken, eerst in Velp (o.a. Nadine, Gül, Linda, Annemieke, Sander, Lysbert, Brigit, Ada, Anja, Caroline, Ellen, Frieda, Peggy) en later, flink gegroeid, in Elst. Gelukkig kom ik jullie zo af en toe nog tegen bij het halen van een kop thee. Alle chirurgen, Theo, Bart, Wouter, Willem, bedankt voor jullie interesse in en medewerking aan de 'denk-tank'.

Onderzoek doen in Rijnstate was niet mogelijk geweest zonder ondersteuning vanuit het wetenschapsbureau, het trial-lab en de trial-apotheek. Esther, bedankt voor de beoordeling en nuttige feedback van alle onderzoeksprotocollen. Lian, bedankt voor jouw adviezen wat betreft epidemiologie en statistiek. Alle collega's van het trial-lab en de trial-apotheek, bedankt voor het altijd op tijd klaarmaken van alle benodigdheden voor de testen.

In het Radboudumc wil ik iedereen van de afdeling nucleaire geneeskunde bedanken voor jullie hulp, interesse en gezelligheid. Wietske, mijn promotie-onderzoek begon achteraf gezien eigenlijk al tijdens een stage bij jou, wat leidde tot het eerste artikel van mijn proefschrift. Bedankt voor jouw enthousiasme en de fijne samenwerking. Eric en Antoi, zonder jullie hulp waren de fantoomstudies niet mogelijk geweest. Bedankt voor het delen van jullie kennis over PET en SPECT reconstructies en de praktische hulp bij de experimenten, zoals het vullen van fantomen en maken van PET-scans. Het maken van de ^{68}Ga-Exendin PET/CT scans bij studie-deelnemers had nog al eens de nodige uitdagingen, maar jullie kregen het altijd weer opgelost. Maichel, Natascha, Danny, Peter, Michel, Judith, Peter, en alle andere collega's uit het Hotlab, laboranten en artsen, veel dank voor het labelen, plannen, organiseren, toedienen, scannen en beoordelen van ^{68}Ga-exendin scans. Mijke, Annemarie, Tom, Lieke, en alle andere onderzoekers en ondersteuners die ik tegen ben gekomen, bedankt voor de gezelligheid op mijn 'Radboud-werkplek' en het meedenken bij de onderzoeken. Sevilay, met jouw hulp hebben we de bariatriestudies af kunnen ronden. Bedankt voor je fijne samenwerking in de afgelopen paar jaar!

Lieve Daphne en Adrianne, wat fijn dat jullie mijn paranimfen zijn. Adrianne, jij was een grote steun bij het afronden van de studies met jouw hulp bij inclusies en glucosetesten voor de bètacelstudies. Jij had altijd alles perfect op orde, vond het nooit een punt om nog iets te doen en bovenal waren het gezellige ochtenden. Daphne, al vanaf onze studentenperiode trekken we samen op. Tijdens mijn promotie werkte jij ook in het Radboud, wat erg gezellig was, maar ook tot een fijne samenwerking heeft geleid voor een van de artikelen in dit proefschrift. En al lopen we de deur niet plat bij elkaar, we zien elkaar nog steeds regelmatig, werkgerelateerd, en ook voor gezelligheid buiten werk.

Al een tijd 'rond ik mijn proefschrift af' naast mijn werk in Rijnstate. Gelukkig heb ik altijd steun en interesse ervaren van mijn collega's en heeft mijn werk me, ondanks het tijdgebrek, altijd gemotiveerd en energie gegeven om dit proefschrift af te ronden. Ik wil daarom alle collega's van de Radiologie en Nucleaire Geneeskunde en het team Robotics & 3D centrum hiervoor bedanken. En in het bijzonder Frank en Milan, voor jullie vertrouwen bij het opzetten van mijn functie als technisch geneeskundige en onderzoeker bij de vakgroep RNG.

Lieve TG chicks, jullie mogen hier niet ontbreken. Sinds onze eerste dag in Enschede zijn we vriendinnen en intussen is deze groep flink uitgebreid! De gezellige momenten hebben geholpen om naast de vele uurtjes schrijven, ook te ontspannen. En intussen heb ik gebruik kunnen maken van alle tips & tricks van de chicks die mij voor zijn gegaan. En Anniek, een heuse schrijfweek en 'Good luck chick' was een hele goede duw voor het 'laatste' schrijfwerk.

Lieve pap, mam en Bren. Zonder jullie was het me niet gelukt dit proefschrift te schrijven. Naast de praktische hulp om de laatste jaren wat schrijftijd vrij te maken, was jullie liefde, aandacht en vertrouwen voor dit werk en voor het (blijven) doen waar ik gelukkig van wordt een hele belangrijke bijdrage. Bedankt voor het er altijd en onvoorwaardelijk zijn.

Lieve Pat, Jurre en Jinte. Pat, jij weet als geen ander hoeveel uren, energie en soms frustratie er in dit proefschrift zit. Jouw geduld en vertrouwen in dit proces heeft een hele belangrijke rol gespeeld bij het afronden. Ik ben dankbaar voor alles wat we samen hebben meegemaakt en alle jaren dat we samen zijn. Lieve Jurre en Jinte, jullie liefde heeft mij extra gemotiveerd het schrijfwerk echt af te ronden. Bedankt voor alle slaapjes waarin ik nog even achter mijn laptop kon kruipen. Nu mijn promotietraject afgerond is, komen deze uren vrij om samen te zijn. Ik kijk uit naar een lange toekomst samen en een 'happily ever after'.

PHD PORTFOLIO

Department: Medical Imaging
PhD period: 2014-10-01 – 2026-10-22

PhD Supervisor(s):
prof. dr. M. Gotthardt
prof. dr. E.J. Hazebroek

PhD Co-supervisor(s):
dr. M. Boss

Training activities	Hours
Courses	
Good Clinical Practice (2014)	14.00
Medical Data Analysis with MATLAB (2016)	3.00
Workshop Persoonlijk Businessplan (2016)	4.00
Radiation safety laboratory (2017)	1.00
Privacy legislation General Data Protection Regulation (GDPR) (2018)	2.00
Low literacy (2018)	2.00
GCP re-registration (2018)	3.00
Workshop 'making a Vlog' (2019)	3.00
TechMed Summerschool (2021)	22.00
Workshop writing without stress (2022)	2.00
Workshop presenting (1/2) (2022)	3.00
GCP re-registration (2022)	3.00
The Art of Presenting Science (2022)	36.00
RU - Effective Writing Strategies (2023)	75.00
Workshop presenting (2/2) (2023)	3.00
Re-registration GCP (2025)	3.00
Coursera MOOC - INTEGRITY Responsible Conduct of Research (2026)	8.00
Conferences	
NVvTG Congress (2015)	6.00
DSMBS congress (2015)	4.00
IFSO congress 2015 (2015)#	15.00
DSMBS congress (2016) #,#	5.00
European Obesity Summit (2016) #,^	21.00
Symposium Quantification and Standardisation in Medical Imaging (MIC) (2016)^	14.00
EANM congress (2016) #	22.00
Obesity Days (2016)	11.00
Dutch Endocrine Meeting (2017) #	15.00
DSMBS congress (2017) #	5.00
IFSO congress (2017) #,^,^,^	15.00

Annual Dutch Diabetes Research Meeting (2017) #	10.00
TOPIM on Imaging Metabolism (2018)^	15.00
Technical Innovations In Medicine Congress 2018 (2018) #	5.00
DSMBS congress (2018) #	5.00
Scientific meeting NVNG (2018) #	5.00
Dutch Endocrine Meeting (2019) #	12.00
DSMBS congress (2019)*,* (best poster pitch award)	5.00
IFSO congress 2019 (2019) #,#,#	15.00
Annual Dutch Diabetes Research Meeting 2020 (2020) #	3.00
NASO spring meeting (2021) #	6.00
EASD congress (2021) #	14.00
IFSO congress (2021) #,#	12.00
DSMBS congress (2022)#,*	5.00
IFSO congress ZoomForward (2022)#	20.00
Dutch Endocrine Meeting (2023) #	12.00
DSMBS congress (2023)	5.00
IFSO congress (2023) #	14.00
Annual Dutch Diabetes Research Meeting (2023) #	10.00
EASD congress (2024) #,*	10.00
Teaching	
Supervision Internship Technical Medicine student (Master 2) (2015)	12.00
Presentation radiology and nuclear medicine (Rijnstate) (2016)	1.00
Supervision Internship Technical Medicine student (Master 2) (2016)	12.00
Supervision Internship Technical Medicine student (Master 2) (2016)	12.00
Supervision Internship Technical Medicine student (Master 2) (2016)	12.00
Presentation nuclear medicine (Rijnstate) (2016)	1.00
Supervision graduation project Technical Medicine (Master 3) (2017)	40.00
Supervision Internship Technical Medicine student (Master 2) (2018)	12.00
Supervision Internship Technical Medicine student (Master 2) (2019)	12.00
Supervision Internship Technical Medicine student (Master 2) (2019)	12.00
Supervision Internship Technical Medicine student (Master 2) (2020)	12.00
Supervision Internship Technical Medicine student (Master 2) (2021)	12.00
Supervision internship master Nutrition and Health (WUR) (2022)	30.00
Supervision graduation project Technical Medicine (Master 3) (2022)	45.00
Other	
Presentatation at research meeting Medical Imaging (2015)	1.00
Research Meeting Medical Imaging (2017)	15.00
Research Meeting Nuclear Imaging (Radboudumc) (2021)	30.00
Presentation at Rijnstate Research Rounds (2022)	1.00
PhD meeting Rijnstate (PRO) (2023)	10.00
Research Meeting Bariatric surgery (Vitalys, Rijnstate) (2023)	160.00
Total hours	945.00

[#] Oral presentation, [^] Poster presentation, [*] Poster pitch/short oral presentation

LIST OF PUBLICATIONS

Jansen AS, Berends C, Garssen SH, **Deden LN**, Kooij L, van Harten WH, Hazebroek EJ, Doggen CJM. The value of Continuous Remote Monitoring in Clinical Decision Making After Same-day Discharge Metabolic Bariatric Surgery. Obes Surg. 2026 Jul;36(7):3521-3534

Yamazaki H, Tokgöz S, Tauchi S, Nakamura F, Dohke M, Hanawa N, Kodama Y, Katanuma A, Yamamoto Y, Fukuhara S, Prystupa K, Hummel J, **Deden L**, Boss M, Gotthardt M, Wagner R, Heni M. Structural determinants of beta-cell failure in type 2 diabetes: a multimodality imaging study. Metabolism. 2026 Aug;181:156631

Tokgöz S, Boss M, Meijer RI, Jansen TJP, **Deden LN**, Tack CJ, de Galan BE, Gotthardt M. Sex Differences in [(68)Ga]Ga-NODAGA-Exendin-4 Uptake in the Pituitary of Individuals With Type 2 Diabetes. Diabetes Obes Metab. 2026 May;28(5):4387-4390

Tokgöz S, **Deden LN**, Hofboer A, Meijer RI, Hazebroek EJ, van Bon AC, de Galan BE, Tack CJ, Boss M, Gotthardt M. Beta cell function and mass in individuals with and without remission of type 2 diabetes after Roux-en-Y gastric bypass. Diabetologia. 2026 May;69(5):1295-1300

Krol JP, Duteweert RJ, **Deden LN**, Bernsen ML, Smeets L, Slump CH, Oyen WJ. Combining 4DCT and [18F]choline PET/CT as first-line imaging in primary hyperparathyroidism patients a one-stop shop. Q J Nucl Med Mol Imaging. 2025 Dec;69(4):308-314

Deden LN, Tokgöz S, Hofboer A, Hazebroek EJ, de Boer H, van Bon AC, Meijer RI, de Galan BE, Tack CJ, Boss M, Gotthardt M. β-Cell Mass in Individuals With and Without Postbariatric Hypoglycemia After Roux-en-Y Gastric Bypass. Diabetes. 2025 Dec;174(12):2301-2306 (S.T. and L.N.D. share first authorship)

Krol JP, Duteweert RJA, **Deden LN**, Bernsen MLE, Slump CH, Oyen WJG. Four-dimensional Computed Tomography Imaging in Primary Hyperparathyroidism: Multireader Multicase Study of Both Neuroradiologists and General Radiologists of Imaging Approaches With Less Phases. J Comput Assist Tomogr. 2026 Mar;0150(2):331-338

Krol JP, Veerbeek T, **Deden LN**, Joosten FBM, Bernsen MLE, Slump CH, Oyen WJG. Limited additional value of dual-layer spectral 4DCT compared with conventional 4DCT for preoperative localization in primary hyperparathyroidism. Eur J Radiol Open. 2025 Jun; 2415:100669

Botros N, Czymoniewicz-Klippel MT, van de Scheur V, **Deden LN**, van den Berg EM, Hazebroek EJ. How well does it fit? Process evaluation of a multidisciplinary pre- and

postoperative metabolic bariatric surgery support programme: A patients' perspective. Clin Obes. 2025 Aug;15(4):e70006

Botros N, **Deden LN**, van den Berg EM, Hazebroek EJ. Preoperative Mental Disorders and Hospital Healthcare Use in the First Year After Metabolic Bariatric Surgery: A Retrospective Study. Obes Surg. 2025 Apr;35(4):1423-1430

van der Meeren MMD, Boers T, de Graaf P, Duvivier KM, Dreijerink KMA, **Deden LN**, Veendrick P, Cernohorsky P, Joosten FBM, Savelberg ABMC, Braak SJ, Roerink SHPP, Versluis M, Manohar S, Oyen WJG. Radiofrequency Ablation for Thyroid Nodules (RATED Study)-Analysis of a Learning Curve and Predictors of Success. J Clin Endocrinol Metab. 2025 Oct;16110(11):3201-3209

Zino L, Qing Chen R, **Deden L**, Hazebroek E, Richel O, Colbers A, Burger DM DATO Research Group. Efficacy and Safety of Bariatric Surgery in Dutch People Living with HIV: a Retrospective Matched Cohort Analysis. Obes Surg. 2024 May;34(5):1584-1589

van Leeuwen KG, Schalekamp S, Rutten MJCM, Huisman M, Schaefer-Prokop CM, de Rooij M, van Ginneken B, Maresch B, Geurts BHJ, van Dijke CF, Laupman-Koedam E, Hulleman EV, Verhoeff EL, Meys EMJ, Mohamed Hoesein FAA, Ter Brugge FM, van Hoorn F, van der Wel F, van den Berk IAH, Luyendijk JM, Meakin J, Habets J, Verbeke JIML, Nederend J, Meys KME, **Deden LN**, Langezaal LCM, Nasrollah M, Meij M, Boomsma MF, Vermeulen M, Vestering MM, Vijlbrief O, Algra P, Algra S, Bollen SM, Samson T, von Brucken Fock YHG Project AIR Working Group. Comparison of Commercial AI Software Performance for Radiograph Lung Nodule Detection and Bone Age Prediction. Radiology. 2024 Jan;310(1):e230981

Heusschen L, Berendsen AAM, Balvers MGJ, **Deden LN**, de Vries JHM, Hazebroek EJ. Changes in nutrient composition and diet quality in the first 6 months following bariatric surgery: An observational cohort study. J Hum Nutr Diet. 2024 Feb;37(1):365-376

Jacobs A, Al Nawas M, **Deden LN**, Dijksman LM, Boerma EG, Demirkiran A, Hazebroek EJ, Wiezer MRJ, Derksen WJM, Monpellier VM. Preoperative Weight Gain Is Not Related to Lower Postoperative Weight Loss, But to Lower Total Weight Loss up to 3 Years After Bariatric-Metabolic Surgery. Obes Surg. 2023 Dec;33(12):3746-3754

van der Meeren MMD, Joosten FBM, Roerink SHPP, **Deden LN**, Oyen WJG. Radiofrequency ablation for autonomously functioning nodules as treatment for hyperthyroidism: subgroup analysis of toxic adenoma and multinodular goitre and predictors for treatment success. Eur J Nucl Med Mol Imaging. 2023 Oct;50(12):3675-3683

Krol JP, Veerbeek T, **Deden LN**, Joosten FBM, Slump CH, Oyen WJG. Preoperative imaging in primary hyperparathyroidism patients using 4DCT subtraction maps, a report of three cases. Radiol Case Rep. 2023 Jun;818(8):2814-2822

Campschroer T, Van Balken MR, **Deden LN**, Hazebroek EJ, De Boer H. Effect of preoperative metabolic profiling to reduce the risk of kidney stones after bariatric surgery in patients with a history of stone formation. Surg Obes Relat Dis. 2023 Jun;19(6):633-639

Heusschen L, Berendsen AAM, **Deden LN**, Hazebroek EJ, Aarts EO. Nutritional Deficiencies 3 Years After Sleeve Gastrectomy Can Be Limited by a Specialized Multivitamin Supplement. Obes Surg. 2022 Nov;32(11):3561-3570

Heusschen L, Berendsen AA, Balvers MG, **Deden LN**, de Vries JH, Hazebroek EJ. Relative validity of a short screener to assess diet quality in patients with severe obesity before and after bariatric surgery. Public Health Nutr. 2022 Oct;25(10):2731-2741

Deden LN, Booij J, Grandjean J, Homberg JR, Hazebroek EJ, Gotthardt M, Boss M. Brain Imaging of the GLP-1 Receptor in Obesity Using (68)Ga-NODAGA-Exendin-4 PET. Brain Sci. 2021 Dec;1511(12):1647

Heusschen L, Berendsen AAM, Cooiman MI, **Deden LN**, Hazebroek EJ, Aarts EO. Optimizing Multivitamin Supplementation for Sleeve Gastrectomy Patients. Obes Surg. 2021 Jun;31(6):2520-2528

Heusschen L, Krabbendam I, van der Velde JM, **Deden LN**, Aarts EO, Merién AER, Emous M, Bleumink GS, Lutgers HL, Hazebroek EJ. A Matter of Timing-Pregnancy After Bariatric Surgery. Obes Surg. 2021 May;31(5):2072-2079

Burger PM, Monpellier VM, **Deden LN**, Kooiman LBR, Liem RSL, Hazebroek EJ, Janssen IMC, Westerink J. Standardized reporting of co-morbidity outcome after bariatric surgery: low compliance with the ASMBS outcome reporting standards despite ease of use. Surg Obes Relat Dis. 2020 Nov;16(11):1673-1682

Heusschen L, Schijns W, Ploeger N, **Deden LN**, Hazebroek EJ, Berends FJ, Aarts EO. The True Story on Deficiencies After Sleeve Gastrectomy: Results of a Double-Blind RCT. Obes Surg. 2020 Apr;30(4):1280-1290

van Veldhuisen SL, Arslan I, **Deden LN**, Aarts EO, Hazebroek EJ. Safety of Continuous Postoperative Pulse Oximetry Monitoring Without Obstructive Sleep Apnea Screening in > 5000 Patients Undergoing Bariatric Surgery. Obes Surg. 2020 Mar;30(3):1079-1085

Daemen JHT, **Deden LN**, van den Ende A, Pijl MEJ, Slump CH, Berends FJ, Aarts EO. A novel abdominal wall entry suction device to increase Veress needle safety: A prospective cohort pilot study. Ann Med Surg (Lond). 2019 Oct;747:70-74

Kuin C, den Ouden F, Brandts H, **Deden L**, Hazebroek E, van Borren M, de Boer H. Treatment of Severe Protein Malnutrition After Bariatric Surgery. Obes Surg. 2019 Oct;29(10):3095-3102

Vreeken D, Wiesmann M, **Deden LN**, Arnoldussen IAC, Aarts E, Kessels RPC, Kleemann R, Hazebroek EJ, Aarts EO, Kiliaan AJ. Study rationale and protocol of the BARICO study: a longitudinal, prospective, observational study to evaluate the effects of weight loss on brain function and structure after bariatric surgery. BMJ Open. 2019 Jan;99(1):e025464

Zoon HFA, de Bruijn SEM, Jager G, Smeets PAM, de Graaf C, Janssen IMC, Schijns W, **Deden L**, Boesveldt S. Altered neural inhibition responses to food cues after Roux-en-Y Gastric Bypass. Biol Psychol. 2018 Sep;137:34-41

Klop C, **Deden LN**, Aarts EO, Janssen IMC, Pijl MEJ, van den Ende A, Witteman BPL, de Jong GM, Aufenacker TJ, Slump CH, Berends FJ. Diagnosing Internal Herniation After Roux-en-Y Gastric Bypass Surgery: Literature Overview, Cadaver Study and the Added Value of 3D CT Angiography. Obes Surg. 2018 Jul;28(7):1822-1830

Deden LN, Aarts EO, Aelfers SCW, van Borren MMGJ, Janssen IMC, Berends FJ, de Boer H. Risk of Metformin-Associated Lactic Acidosis (MALA) in Patients After Gastric Bypass Surgery. Obes Surg. 2018 Apr;28(4):1080-1085

Deden LN, Cooiman MI, Aarts EO, Janssen IMC, Gotthardt M, Hendrickx BW, Berends FJ. Gastric pouch emptying of solid food in patients with successful and unsuccessful weight loss after Roux-en-Y gastric bypass surgery. Surg Obes Relat Dis. 2017 Nov;13(11):1840-1846

Woliner-van der Weg W, **Deden LN**, Meeuwis AP, Koenrades M, Peeters LH, Kuipers H, Laanstra GJ, Gotthardt M, Slump CH, Visser EP. A 3D-printed anatomical pancreas and kidney phantom for optimizing SPECT/CT reconstruction settings in beta cell imaging using (111)In-exendin. EJNMMI Phys. 2016 Dec;3(1):29

ABOUT THE AUTHOR



Laura Deden was born on 27th January 1989 in Hilversum, the Netherlands. Following her graduating from the Roland Holst College in Hilversum (VWO), she started her academic path at the University of Twente in 2007, studying technical medicine. During her study she contributed to the organization of multiple events for both the rowing association Euros and the study association Paradoks. In 2010, she successfully completed her Bachelor of Science degree and started the master program 'medical imaging and intervention' of Technical Medicine. The medical internships were performed at the Department of Surgery (NKI-AvL), the Department of Orthopaedics (UMC Utrecht), the Department of Nuclear Medicine (Radboudumc) and the Department of Ear, Nose and Throat (UMC Groningen). The final master's internship was undertaken at the Department of Surgery (NKI-AvL), with graduation in August 2014 (cum laude).

After her graduation, Laura initiated her doctoral research, focusing on beta cell imaging in type 2 diabetes and obesity. This project was a collaboration between the department of bariatric surgery at Vitalys, Rijnstate, and the department of Nuclear Medicine at Radboudumc. The project included clinical using the radiotracer ^{68}Ga-exendin in patients undergoing bariatric surgery and phantom studies. The findings of part of this project are described in this thesis. Besides, Laura performed and contributed to clinical studies on the topic of bariatric surgery and of medical imaging, and she was involved in outpatient care.

Since January 2018, Laura has been employed on a full-time basis as a senior researcher and technical physician at Rijnstate, which she combined with continuing her PhD research. From January 2018 until September 2024 Laura was appointed as senior researcher at Vitalys. In this role, she focused on set up research initiatives in the domains of medical imaging, medical technology and nutrition and obesity. Furthermore she supervised PhD and MSc students. Currently, Laura works as a technical physician at the department of Radiology and Nuclear Medicine (since January 2018) and the department Innovation (since October 2024). In radiology and nuclear medicine, her tasks involve the supervision of PhD and MSc students, performing and coordinating scientific research and coordinating medical technical projects, including the implementation of artificial intelligence within radiology. At the department of Innovation, Laura is involved in the 3D center and the implementation of technical medical innovations at Rijnstate.



Rijnstate

Radboudumc
university medical center

IN·DEI·NOMINE·FELICITER

Radboud University